Pontifícia Universidade Católica
do Rio de Janeiro

Alessandra Pazini

Synthesis and characterization of fluorescent silica nanoparticles with potential application in transport and adsorption studies in porous medium

Tese de doutorado

Thesis presented to the Programa de Pós-graduação em Química of PUC-Rio in partial fullfilment of the requirements for the degree of Doutor em Química.

Advisor: Prof. Aurora Pérez Gramatges
Co-advisor: Dr. Luis Maqueira Espinosa

Rio de Janeiro
June 2023

Pontifícia Universidade Católica
do Rio de Janeiro

Alessandra Pazini

Synthesis and characterization of fluorescent silica nanoparticles with potential application in transport and adsorption studies in porous medium

Thesis presented to the Programa de Pós-graduação em Química of PUC-Rio in partial fullfilment of the requirements for the degree of Doutor em Química. Approved by the undersigned Examination Committee.

Prof. Aurora Pérez Gramatges
Advisor
Departamento de Química – PUC-Rio

Dr. Luis Maqueira Espinosa
Co-advidor
Departamento de Química – PUC-Rio

Prof. Koiti Araki
Instituto de química – USP

Prof. Fabiano Rodembusch
Instituto de química – UFRGS

Prof. Elizabeth R. Lachter
Instituto de química – UFRJ

Prof. Volodymyr Zaitsev
Departamento de Química – PUC-Rio

Rio de Janeiro, 27th June 2023

Alessandra Pazini

PhD candidate in the Chemistry Graduate Program at Pontifícia Universidade Católica do Rio de Janeiro (PUC-Rio). Master's degree in Organic Chemistry concluded at Pontifícia Universidade Católica do Rio de Janeiro (2019). Bachelor's in chemical engineering at Universidade Federal do Rio Grande do Sul (2017).

Bibliographic data

Pazini, Alessandra

Synthesis and characterization of fluorescent silica nanoparticles with potential application in transport and adsorption studies in porous medium / Alessandra Pazini ; advisor: Aurora Pérez Gramatges ; co-advisor: Luis Maqueira Espinosa. – 2023.

133 f. : il. color. ; 30 cm

Tese (doutorado) – Pontifícia Universidade Católica do Rio de Janeiro, Departamento de Química, 2023.

Inclui bibliografia

1. Química – Teses. 2. . Nanopartículas fluorescentes. 3. Sílica. 4. Síntese microemulsão. 5. Síntese Stöber. 6. Meios porosos. I. Pérez Gramatges, Aurora. II. Pontifícia Universidade Católica do Rio de Janeiro. Departamento de Química. III. Título.

CDD: 540

Para J. L.

Acknowledgements

LASURF, especially Professor Aurora Pérez Gramatges and researcher Luis Maqueira, for the opportunity to learn and grow in an excellent laboratory.

PUC-Rio and the Vice-Rector's Office, for support throughout the entire period of conducting this work. This study was financed in part by the Coordenação de Aperfeiçoamento de Pessoal de Nível Superior - Brasil (CAPES) - Finance Code 001. I also thank the partnership of LASURF with the R&D project of ANP No. 20358-8 (PUC-Rio/Shell Brasil/ANP), funded by Shell Brasil, for the support and resources provided.

Family, friends, and lab colleagues who became friends.

Finally, I would like to express my gratitude to myself, as even in the face of challenges posed by a pandemic that shook even the strongest of psyches and a government that discredited and undermined science in Brazil, I managed to complete this thesis.

Abstract

Pazini, Alessandra; Pérez Gramatges, Aurora. **Synthesis and characterization of fluorescent silica nanoparticles with potential application in transport and adsorption studies in porous medium**. Rio de Janeiro, 2023. 133 p. Tese de Doutorado - Departamento de Química, Pontifícia Universidade Católica do Rio de Janeiro.

Silica nanoparticles (SiNPs) are widely used in various fields, and they form nanofluids with exceptional properties when they are suspended in a base fluid. However, the transport and quantification of SiNPs in porous media pose significant challenges. To address this, fluorescence spectroscopy is a promising technique for this task. In this study, a series of core-shell silica-based fluorescent nanoparticles (FSiNPs) with similar cores but different surface groups were synthesized using the Stöber and WORM synthesis methods. These hybrid FSiNPs were designed and presented the same colloidal behavior as commercial SiNPs widely applied in the form of nanofluids. The presence of primary amino groups was confirmed in positive-FSiNPs, and a posterior characterization supported the presence of organic matter in nanoparticles confirming the insertion of fluorescent molecules in all FSiNPs. Comparative analyses revealed that the WORM method produced more homogeneous nanoparticles with consistent form and size distribution. The N_2 adsorption/desorption analysis demonstrated similarities between the synthesized FSiNPs and commercial SiNPs, validating their suitability for transport experiments focusing on colloidal behavior. Both WORM-FSiNPs were successfully quantified in the effluent after flowing through the glass bead column. The SiNP-containing aminopropyl surface groups showed the greatest stability and lowest adsorption compared with those grafted with silanol groups. It was attributed to the effect of stronger attractive interactions between the NPs and anionic surfactant molecules. The potential of these fluorescent NPs as sensitive tracers for transport and adsorption studies in nanofluids containing surfactants was demonstrated.

Keywords

Fluorescent nanoparticles; silica; microemulsion synthesis; Stöber synthesis; porous media; colloidal

Resumo

Pazini, Alessandra; Pérez Gramatges, Aurora. **Síntese e caracterização de nanopartículas de sílica fluorescentes com potencial aplicação em estudos de transporte e adsorção em meio poroso.** Rio de Janeiro, 2023. 133 p. Tese de Doutorado - Departamento de Química, Pontifícia Universidade Católica do Rio de Janeiro.

As nanopartículas de sílica (SiNPs) são amplamente utilizadas em diversas áreas e formam nanofluidos com propriedades excepcionais quando suspensas em um fluido base. No entanto, o transporte e a quantificação de SiNPs em meios porosos representam desafios significativos. Para resolver isso, a espectroscopia de fluorescência é uma técnica promissora para essa tarefa. Neste estudo, uma série de nanopartículas core-shell fluorescentes à base de sílica (FSiNPs) com núcleos semelhantes, mas diferentes grupos de superfície foram sintetizadas usando os métodos de síntese de Stöber e WORM. Essas FSiNPs híbridas foram projetadas e apresentaram o mesmo comportamento coloidal que as SiNPs comerciais amplamente aplicadas na forma de nanofluidos. A presença de grupos amino primários foi confirmada nas FSiNPs positivas, caracterizações posteriores corroboraram a presença de matéria orgânica confirmando a inserção de moléculas fluorescentes em todas as FSiNPs. Análises comparativas revelaram que o método WORM produziu nanopartículas mais homogêneas tanto no quesito formato quanto na distribuição de tamanho. A análise de adsorção/dessorção de N_2 demonstrou semelhanças entre os FSiNPs sintetizados e as SiNPs comerciais, validando sua adequação para experimentos de transporte com foco no comportamento coloidal. Ambas as WORM-FSiNPs foram quantificadas com sucesso no efluente após fluir através da coluna de esferas de vidro. A SiNP contendo grupos de superfície aminopropil mostraram a maior estabilidade e menor adsorção em comparação com aqueles enxertados com grupos silanol. Isso foi atribuído ao efeito de interações atrativas mais fortes entre as NPs e as moléculas do surfactante aniônico. Por fim, foi demonstrado o potencial dessas NPs fluorescentes como marcadores sensíveis para estudos de transporte e adsorção em nanofluidos contendo surfactantes.

Palavras-chave

Nanopartículas fluorescentes; sílica; síntese microemulsão; síntese Stöber; meios porosos; coloidal

Table of contents

List of abbreviations and acronyms

ζ-potential: Zeta potential

I_0: Initial NP suspension fluorescence intensity at working wavelength

C_0: Initial NP concentration

(S): Denomination for nanoparticles synthesized by the Stöber method

(W): Denomination for nanoparticles synthesized by the WORM method

AF4: Asymmetric flow field fractioning technique

APTES: (3-Aminopropyl) triethoxysilane

APTMS: (3-Aminopropyl) trimethoxysilane

BC: Breakthrough curve

BET: Brunauer–Emmett–Teller

BJH: Barrett–Joyner–Halenda

CH_3: Methyl groups

CHN: Elemental analysis

DLS: Dynamic light scattering

DLVO: Derjaguin–Landau–Verwey–Overbeek

DW: Deionized water

EC: Elution curve

EDL: Electric double layer

EDXRF: Energy-dispersive X-ray fluorescence

EOR: Enhanced Oil Recovery

FITC: Fluorescein isothiocyanate

FL: Fluorescent

FSiNPs: Fluorescent silica nanoparticles

FSiNP *(S)*: FSiNPs synthesized via the Stöber method

FSiNP *(W)*: FSiNPs synthesized via the WORM method

FSiNP-NH_2-F*(S)*: Noncore-shell FSiNPs synthesized via Stöber

FSiNP-NH_2 *(S)*: Amino-functionalized FSiNPs synthesized via Stöber

FSiNP-NH_2 *(W)*: Amino-functionalized FSiNPs synthesized via WORM

FTIR-ATR: Fourier-transform infrared spectroscopy with attenuated total reflection

HPAM: Hydrolyzed Polyacrylamide

ICP-MS: Inductively coupled plasma mass spectrometer

ICP-OES: Inductively Coupled Plasma – Optical Emission Spectrometry

IEP: Isoelectric point

IFT: Interfacial tension

N=C=S: Isothiocyanate group

NF: Nanofluid

NPs: Nanoparticles

OH: Hydroxyl group

PEG: polyethylene glycol

PV: Pore volume

RCF: Relative centrifugal force

RF: Response factor

RH: Hydrodynamic radius

RITC: Rhodamine B isothiocyanate

R-NH_2: Primary amino groups

SDS: Sodium dodecyl sulfate

SEM: Scanning Electron Microscopy

SiNP: Commercial silica nanoparticle

SiNP-NH_2: Amino-functionalized SiNPs

SiNPs: Silica nanoparticles in general

Si-OH: Silanol groups

Si-O-Si: Siloxane groups

SSA_{BET}: Specific surface area from BET model

ST: Salt tolerant

STED: Stimulated Emission Depletion microscopy

Stöber-FSiNPs: Fluorescent SiNPs produced by the Stöber method

SW: Seawater

TEM: Transmission Electron Microscopy

TEOS: Tetraethyl orthosilicate

Triton X-100: t-octylnonylphenol polyethoxylate ether

UV-Vis: Ultraviolet-visible

vdW: Van der Waals

WCA: Water contact angle

WORM: Water in oil reverse microemulsion

WORM-FSiNPs: FSiNPs produced by the WORM method

List of figures

List of tables

1 Introduction

Silica nanoparticles (SiNPs) have gained significant attention in various industries due to their unique properties and wide range of applications. They have proven beneficial in fields such as the food industry, water treatment, biomedicine, electronics, energy, and environmental remediation. SiNPs form nanofluids that possess exceptional properties suitable for diverse uses when suspended in a base fluid and their effectiveness in enhancing oil recovery (EOR) has been extensively studied.[1–6] However, the fate of SiNPs, along with surfactants during the injection process remains unclear. Retention mechanisms such as adsorption in porous media and aggregation can lead to pore clogging causing the loss of SiNPs. Furthermore, complete recovery of nanoparticles (NPs) is not achieved when used for objectives like wettability alteration, foam stability enhancement, or interfacial tension reduction. Therefore, understanding the behavior and transport of NPs in porous media is crucial to prevent such losses.

Despite the increasing use of nanofluids combining SiNPs and surfactants in EOR, the challenge that persists is investigating the transport of these nanomaterials in porous media. Most studies rely on quantifying the surfactant to infer the behavior of SiNPs in porous media, but only a few describe the detection and quantification of NPs in eluted fluids. One possible reason for this is the difficulty of consistently detecting low concentrations of SiNPs in aqueous fluids. Many studies have utilized detection techniques such as turbidimetry and UV-vis absorption spectroscopy to quantify SiNPs. However, the potential interference caused by nanoparticle aggregation can compromise accurate determination at the low concentration levels required for EOR applications. Direct quantification of SiNPs can be achieved through inductively coupled plasma optical emission spectrometry (ICP-OES) and stimulated emission depletion

(STED) microscopy, but these methods are costly and more challenging to implement in the field.

Overall, in all fields of SiNPs applications, accurate detection, and quantification in nanofluids are essential for evaluating their concentration, efficacy, and safety. This quantification enables precise assessment of SiNPs' performance, safety, and environmental implications, ensuring their appropriate utilization and understanding across different media. In this context, the detection and quantification of hybrid SiNPs by fluorescence spectroscopy is a promising alternative, as this technique has high selectivity and sensitivity, a low detection limit, ease of measurement, low cost, and the potential to be adapted for real-time monitoring. In addition, fluorescent SiNPs (FSiNPs) with different characteristics can be synthesized using tailored combinations of a silanizing agent, linker, and organic fluorophore. FSiNPs have shown great potential as tracers for transport and retention studies in porous media for environmental applications, but there are few reports of their use in the petroleum industry.

In this study, we synthesized and analyzed four FSiNPs with similar core but different surface groups resembling typical SiNPs used for adsorption and transport studies in porous media of nanofluids containing surfactants. Two synthesis methods, sol-gel (Stöber) and water-in-oil reverse microemulsion (WORM) were applied to obtain NPs with a core-shell architecture in which the fluorophore resides in the nanoparticle core to protect from environmental factors, while the functional groups on the external shell employ distinct strategies, resulting in different surface charges in aqueous solutions. This design allowed us to achieve different degrees of interaction with the anionic surfactant used in the nanofluids. The FSiNPs' structure, morphology, and colloidal stability were compared to those of commercial SiNPs, both in the absence and presence of SDS and the fluorescence response of the nanofluids was evaluated. Finally, the suitability of nanofluids containing fluorescent SiNPs and surfactants as tracers for transport studies was assessed by injecting them into a column packed with glass beads.

While procedures for producing FSiNPs with various applications exist in the literature, to our knowledge, no previous studies have focused on

obtaining FSiNPs with an opposite charge for quantifying NPs transport in porous media in nanofluids containing surfactants. Our research focused on characterizing the FSiNPs not only in terms of their structure, size, and surface area (commonly studied parameters for NPs), but also in terms of their colloidal properties in surfactant solutions to mimic the behavior of commercial SiNPs used in nanofluids. This represents a novel aspect of this work, as previous studies on nanoparticle tracers (such as fluorescent or magnetic) for transport studies in porous media did not consider potential differences in behavior due to functionalization or synthesis methods, therefore, the conclusions drawn from those works cannot be generalized. Moreover, the presence of the anionic surfactant, despite displaying different interactions with each nanoparticle, did not affect the quantification of NPs at low concentration levels, setting our research apart from previous reports.

In conclusion, accurate detection of SiNPs in nanofluids is crucial for assessing their concentration, efficacy, and safety across various fields and fluorescence spectroscopy offers a promising method for this purpose. Through the synthesis and analysis of FSiNPs, we aimed to understand their behavior and colloidal properties in the presence of surfactants, particularly in the context of transport studies in porous media. This research contributes to the knowledge of SiNPs' behavior and paves the way for their effective utilization in diverse applications, including oil recovery and environmental remediation. Figure 1 provides a schematic of the results and discussion.

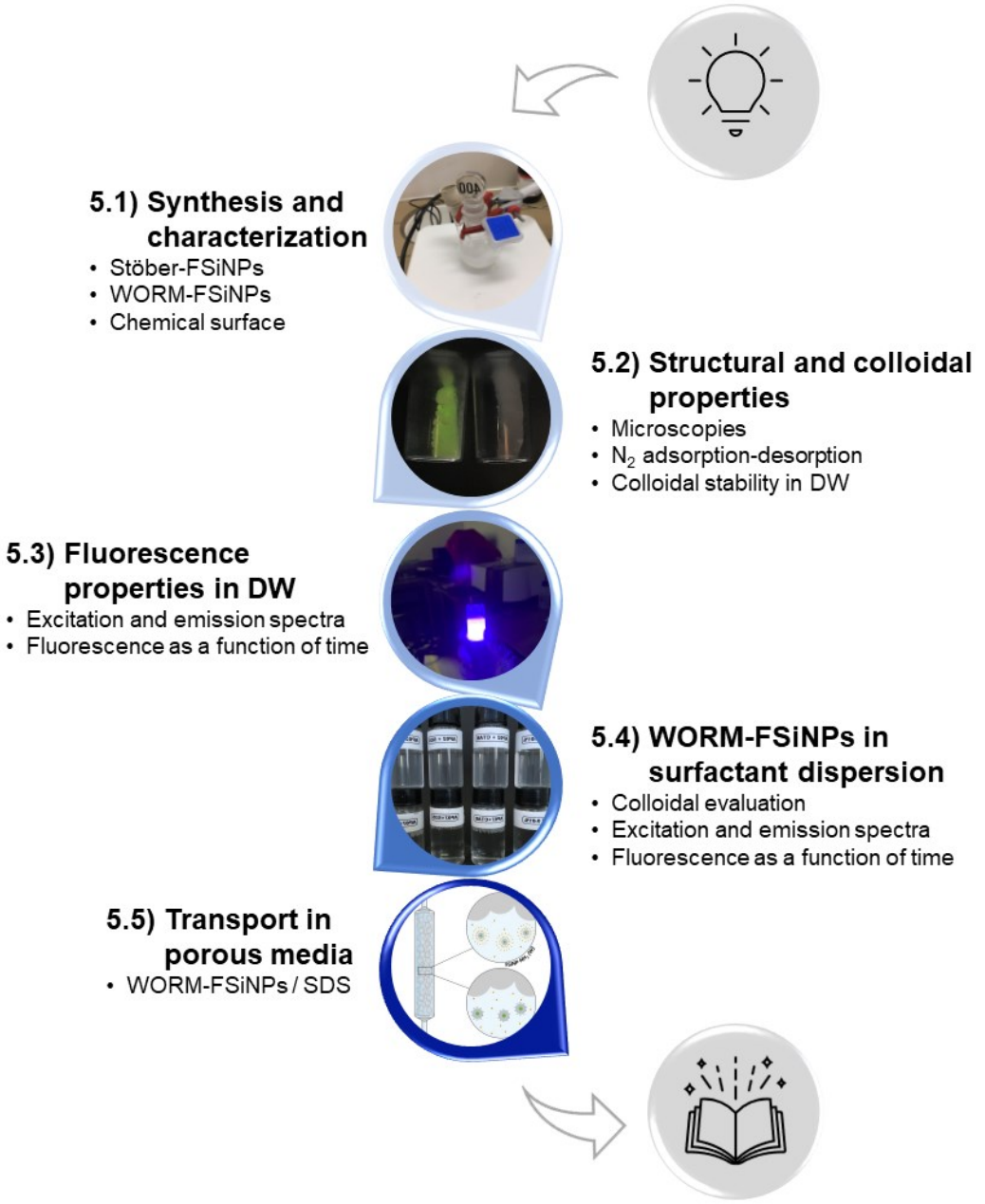

Figure 1: Overview of Chapter 5 that is divided into five parts, each of which outlines the primary objective and the key steps taken to achieve it.

2 Objectives

Synthesize fluorescent core-shell silica nanoparticles with different functional surface groups and high colloidal stability for their detection and quantification in adsorption and transport studies of nanofluids in porous media.

Specific objectives:

• Synthesize and characterize core-shell silica nanoparticles with fluorescent properties and different functional surface groups, using sol-gel and reverse microemulsion methods.

• Evaluate the colloidal stability of synthesized fluorescent nanoparticles in presence and absence of surfactant.

• Evaluate the detection and quantification of nanoparticles in aqueous nanofluids using fluorescence, in presence and absence of surfactant.

• Study the adsorption and transport behavior of the nanoparticles through a glass bead packed column, simulating the flow of nanofluids in porous media.

3 Bibliographical review

3.1. SiNP-based nanofluids

According to Shang and coauthors' review[7], nanomaterials research and applications are being explored at an unprecedented rate, with most of the materials produced and tested on empirical data rather than reliable analytical measurements. Thus, the quantity of nanomaterials is not necessarily a priority in research. In this context, there is a necessity for a universal method that is simple and adaptable with diverse NP sizes, compositions, and structural shapes. One of these materials is silica nanoparticles (SiNPs) and they are more frequent in our daily lives than we realize.

The extensive employment of SiNPs is due to their many benefits, including low cost, low toxicity, high commercial availability in a range of sizes, and a wide range of modification options. They can also be modified from the perspective of interface properties and adsorption, as well as their functional groups, resulting in greater versatility. The modification can occur both superficially and in encapsulated form depending on the purpose of its application.[1,2] Nanomedicine[3,4], catalysis[5,6], and optoelectronics[8,9] use nanoscale-modified silica chemistry with highly functionalized organic or inorganic portions. SiNPs are used in the food industry as additives[10] and potential alternatives to replace plastic packaging materials[11]. Accurate detection and quantification of SiNPs in food nanofluids are crucial for assessing their potential health risks, optimizing their dosage[12], and ensuring compliance with regulatory guidelines[13]. Also, they have shown promise as new possibilities for agro-waste management and valorization[14], and contaminant removal[15], therefore, monitoring the presence and concentration of SiNPs in nanofluids used in diverse fields is vital for evaluating their efficiency, stability, and potential environmental impacts.

3.1.1. Nanomaterials in EOR

EOR shifts oil by altering oil flow and rock-liquid interactions. However, there are some challenges in EOR to be overcome such as the high cost due to its sophistication, the toxicity of the fluids inserted, and how to recover them.[16–18] The pre-salt does not have the characteristics typical for extraction, for instance, the carbonate rocks present in the Brazilian pre-salt fields are composed mostly of calcite, dolomite, and clay. Carbonate reservoirs are porous, permeable rocks that hold hydrocarbons with complex and heterogeneous physical and geological properties.[19] This type of rock has small channels and pores where the largest volume of oil is stored. Generally, the presence of wettability by oil, in some cases mixed, requires the need to have an inversion of this property for wet by water through surfactants or nanofluids, facilitating the displacement of oil.[20,21] This process of changing the wettability of rocks is one of the most efficient EOR methods, especially for carbonate reservoirs.[22] As mentioned, most oil is present in small channels and pores, microscopically retained by capillary forces, and traditional oil displacement methods act macroscopically. EOR methods seek to reduce capillary forces and increase sweep efficiency by adding chemicals to injection fluids.[23]

The nanofluids (NF) can be created by adding NPs to various base fluids, the most common being water.[23] NPs' stability and dispersion depend on their surface functionality and activity. They have unique properties due to their small size (1-100 nm), greater surface area per volume, and ability to manipulate behavior and structure. NPs can also circulate through narrow channels of porous subsurface media without blocking them, improving oil recovery. These characteristics allow for the enhancement of the properties of fluids injected into a reservoir. Examples of NF EOR applications include altering rock wettability[24], reducing interfacial tension (IFT) to reduce surfactant adsorption in reservoir porous walls[20,25], and stabilizing foams[26].

3.1.2. Silica nanoparticles in EOR

SiNPs are one of the most promising systems for reservoir applications. According to Ogolo et al.[27], SiNPs are more effective at oil extraction from rocks than AlO_3, TiO_2, ZnO, and FeO_3. SiNPs can be applied (i) as bare SiNP directly,[28,29] (ii) by modifying the available commercial ones,[30,31] or (iii) synthesized SiNP[32,33]. Table 1 lists more EOR research using SiNPs.

Table 1: Summary of the most recent studies using SiNPs for EOR purposes

Source	Nanofluid	Goal
Rattanaudom et al., 2023[34]	Hydrophobic and hydrophilic NPs with a binary surfactant system	Micro-emulsion, viscosity, and adsorption behaviors of nanofluids
Tang et al., 2023[35]	Modified NPs with cationic, anionic, and nonionic surfactants	Synergy between the NPs and surfactant in lowering the water-phase contact angle of a crude oil droplet on calcite
Ma et al., 2022[36]	Hydrophilic NPs with cationic surfactants	The effects of the chain length of the surfactants and their adsorption on the NP surface on emulsion stability
Li et al., 2021[37]	SiNPs	Visualize and quantify wetness change using complementary contact angle techniques
Zhou et al., 2020[38]	SiNP-NH_2	High-temperature and salinity stability testing
Du et al., 2020[39]	SiNPs	Parameter screening to optimize CO_2 foam static properties

The operation of SiNPs and how they interact is not completely understood. However, the occurrence of disjunction pressure is one of the mechanisms that is well-established in the literature. The process is illustrated in Figure 2, showing that a thin layer of SiNPs adsorption on the surface of the rock creates pressure on the oil phase, changing the way the rock can be wet and causing oil droplets to come off the surface. According to Keykhosravi and Simjoo[28], the process starts with the adsorption of the SiNPs forming a wedge-shaped film that puts extra pressure on oil droplets, called the disjoining pressure. By increasing the contact time between the

silica NPs and the rock surface or by increasing the concentration of SiNPs in the aqueous phase and, therefore, the disjoining pressure, a thin layer of silica NPs covers the rock surface to facilitate the release of oil droplets on the surface of the rock.

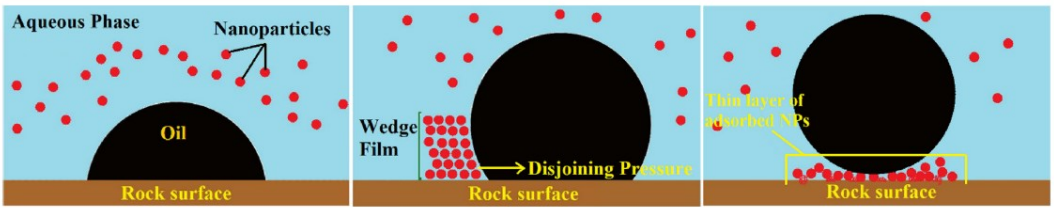

Figure 2: SiNPs' role in the change of wettability through adsorption on the rock surface (adapted from Keykhosravi and Simjoo, 2019)[28].

3.2. SiNPs colloidal stability

One of the most critical concerns for two-phase systems, such as nanofluids, is their ability to maintain colloidal stability, i.e., they must have no or a low rate of NPs agglomeration. Agglomeration can cause microchannels to become blocked, impeding NPs transport and reservoir fluid displacement. The NPs must therefore remain distributed to move in porous media. Electrostatic stabilization, pH variation[40], use of a stabilizing/surface-acting fluid[41], and/or surface functionalization of NPs[29] are the main strategies used to increase the stability of nanofluids.

The forces involved in this phenomenon are the van der Wall's (vdW) force of attraction and the repulsive force through the electrical double layer (EDL). Considering the density and polarizability of the interacting materials, the vdW force is proportional to the Hamaker constant. Typically, the induced dipole-induced dipole or dispersion force is dominant and produces a powerful attraction. However, because this force is inversely proportional to the sixth power of the distance from the particle, it is only meaningful over short distances. Normally, electrostatic repulsion tends to prevail over vdW attraction due to the extended range of the EDL in the solution. This results in the particles being repelled before they can approach each other closely enough for the attractive vdW forces to become significant. The merger of vdW force and electrostatic force is a widely adopted practice that has

resulted in a fundamental theory connected to the stability of particles. A classical theory for determining the interaction is based on the Derjaguin-Landau-Verwey-Overbeek (DLVO) theory, which states that the resulting sum of these forces indicates whether or not there is colloidal stability.[42,43]

In principle, there are three mechanisms (see Figure 3) to stabilize particles against colloidal instability in the liquid state: surface charge-induced electrostatic stabilization, steric stabilization by adsorption of macromolecules, and electrosteric stabilization by adsorption of charged molecules, which combines electrostatic and steric contributions. If size-dependent attractive forces are not inhibited, the relative motion of particles toward each other causes coagulation.[44]

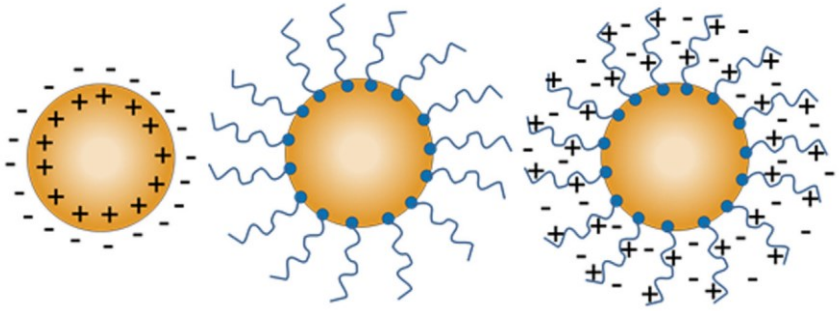

Figure 3: Diverse stabilization mechanisms for particles: electrostatic, steric, and electrosteric stabilization (Peukert & Romeis, 2020)[44].

If electrostatics is the main driving force, there is a practical rule: the higher the zeta potential in the module, the greater the electrostatic repulsion between the particles, which reduces the tendency to aggregate and provides stability. So, samples with a zeta potential between −30 mV and +30 mV tend to aggregate, whereas when estheric stabilization is the main factor, the value of the zeta potential is no longer important. Even when the zeta potential is close to zero, the particles can still be stable. The estheric interaction in these situations keeps the particles from aggregating.[45] However, the surface charge is a crucial parameter for assessing colloidal stability because it affects how NPs interact with the medium and with one another. In addition to other measurements like the hydrodynamic radius, the zeta potential of the nanoparticles, which is an

indirect measure of the surface charge, is typically used to analyze the stability of colloids.[23]

Understanding the forces involved and how colloidal stability is measured experimentally, then the composition, surface structure, and related molecules that define the features of the region near the surface, i.e., the medium in which the NPs meet, will now determine which force will be predominant. The typical groups at the SiNPs surface are demonstrated in Figure 4. The silanol groups (Si-OH) on their surface are responsible for the particle's hydrophilicity, as silanols function as hydrogen bonding sites. If there is no surface modification, the protonation ($Si\text{-}OH^{+}_{2}$) and deprotonation ($Si–O^{-}$) of the silanol groups define the surface charge of the SiNPs and the extent of the repulsive energy that keeps them distributed in the solution.[29] In the meantime, the siloxane groups (Si-O-Si) impart hydrophobic character to the surface of SiNPs and are responsible for Van Der Walls' force of attraction.

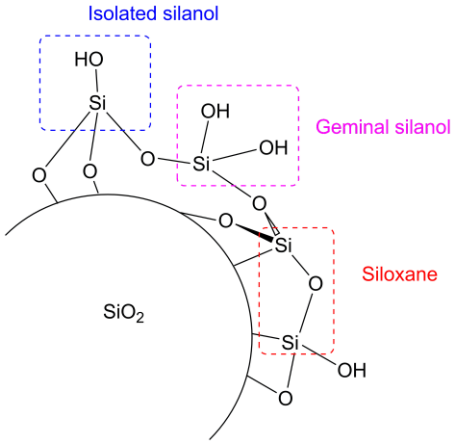

Figure 4: Illustration of the main groups present on the surface of SiNPs.

As an example, Metin et al.[46] used a ζ-potential technique to assess the stability of SiNPs (25 nm) as a function of pH. As most silanols are deprotonated between pH 10 and 7, the zeta potential of the SiNPs in deionized water (DW), shown in Figure 5, demonstrates that the surface charge remains around −45 mV in this pH range. The surface charge moves towards neutral when the pH is lowered because the silanol groups are no longer deprotonated.

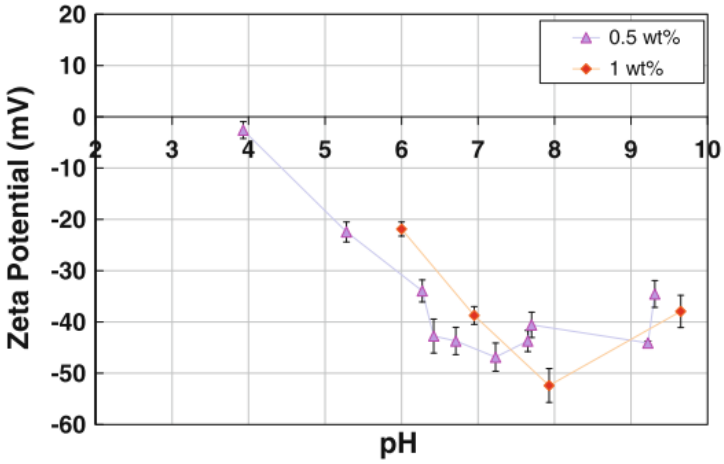

Figure 5: Zeta potential of the SiNP dispersions in DW at concentrations of 0.5 and 1.0 wt% based on pH (Metin et al., 2011)[46].

Although SiNPs have demonstrated excellent performance in modifying wettability and enhancing oil recovery, bare particles have a natural tendency to aggregate and sediment in aqueous fluids, particularly when used at the high temperatures and salinities typical of EOR applications. The combination of nanoparticles with surfactants has been shown to mitigate this effect in nanofluids, where surfactants can act as stabilizers and/or synergistic enhancement agents for oil recovery. Zhou et al.[38] developed a nanofluid by integrating positively charged amino-modified silica nanoparticles (SiNP-NH_2) with a negatively charged anionic surfactant (Soloterra 964) via electrostatic force (see Figure 6). The resultant nanofluid not only showed improved stability at high salinities and temperatures but also great potential for use as a promising new material for EOR.

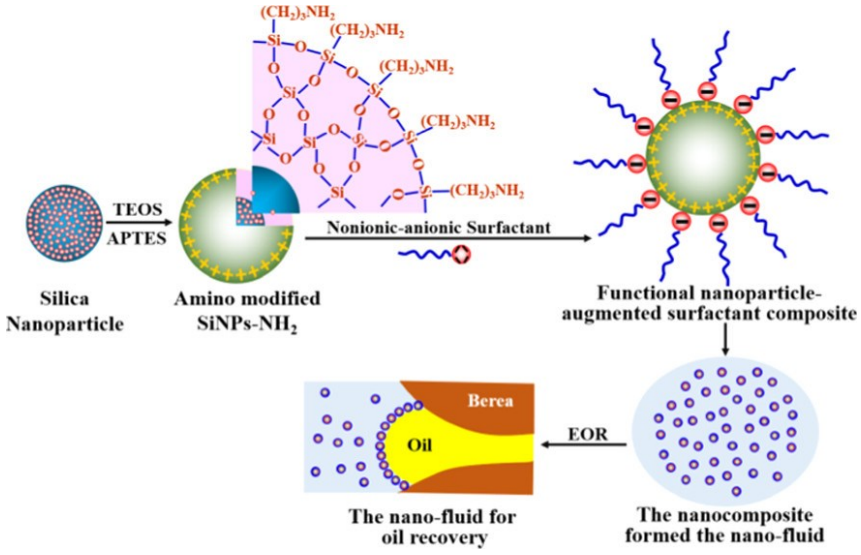

Figure 6: Illustration of modified SiNP-NH_2 with electrostatically adsorption surfactant molecules (adapted from Zhou et al., 2019)[38].

In addition, SiNPs have been reported to reduce surfactant adsorption in porous media. Different mechanisms have been proposed to explain this behavior based on interactions among NPs, surfactants, and porous media.[36,47–49] Wu et al.[50] showed that SiNP effectively reduced the dynamic adsorption of sodium dodecyl sulfate (SDS) on sandstone and that the nanofluid could improve oil recovery. The reduced SDS adsorption was attributed to the retention of surfactant molecules on the SiNP surface instead of on sand, and the collision and friction effects between the SiNP and sand grains lead to the removal of the adsorbed surfactant molecules from the rock during transport in porous media.

Venancio et al.[51] studied the effect of alkyl-modified SiNPs on the dynamic adsorption of SDS using an unconsolidated sand pack as a porous medium. The authors showed that there was an increase in surfactant recovery after the nanofluid injection, and the alkyl-modified nanoparticles could decrease the surfactant loss by 50% compared to using only an SDS slug as shown in Figure 7. More recently, Sun et al.[52] studied the use of SiNPs/SDS nanofluids for foam formation in porous media. The authors reported that there was almost no plugging or viscosity increase when the nanofluids flowed through the porous media and that the mechanical trapping of nanoparticles was not strong because the surface charge of SiNPs matched that of the medium.

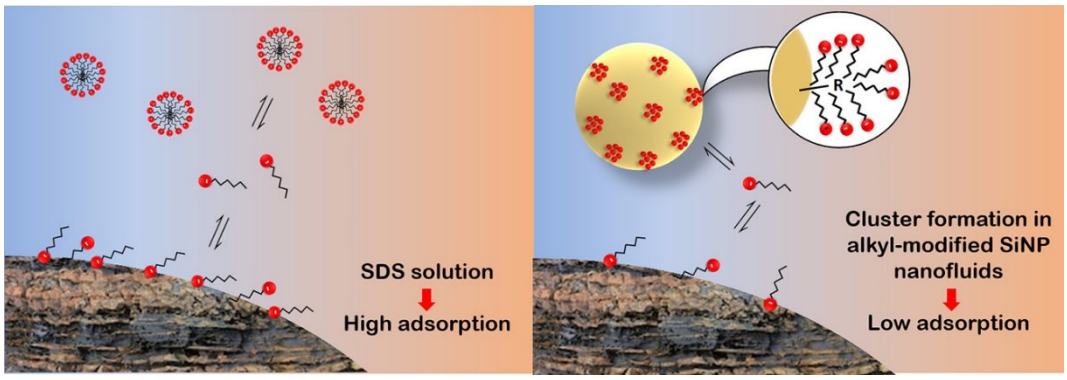

Figure 7: Schematic of surfactant loss in the reservoir rock due to adsorption from (left) micellar solutions and (right) nanofluids containing alkyl-modified silica nanoparticles (Venâncio et al., 2020)[51].

One of the most commonly used and investigated surfactants in EOR is SDS. This anionic surfactant belongs to the alkyl sulfate group, and according to the research, this surfactant is a good partner for nanoparticles when injected as part of an EOR process.[53] As demonstrated in the preceding examples, the SiNP/SDS system is frequently used as the subject of EOR research. Many researchers have evaluated the positive effect of SDS on the stability, interfacial tension, wettability alteration, or foam stability of modified and unmodified SiNP in diverse media.

3.3. SiNP-based nanofluids detection and quantification

This section presents current research on the detection and/or quantification of SiNPs in their various applications, discussing the advantages and disadvantages of the techniques used in subsequent studies involving the quantification of SiNPs, followed by a review of how fluorescent SiNPs have been applied with an emphasis on their detection, colloidal behavior, and emission performance in different environmental conditions.

3.3.1. SiNPs quantification

As an example, the quantification of SiNPs (anticaking agent E551) contained in a commercial high-fat coffee cream was performed by Li et al.[54] using the asymmetric flow field fractioning technique (AF4) in conjunction

with an inductively coupled plasma mass spectrometer (ICP-MS). This is a sophisticated technology and not suitable for certain applications due to its time-consuming nature and viability. Previous investigations have employed ICP-OES[55,56], UV-Vis[56–64], turbidimetry[65–67], DLS[68], refractive index[58] or advanced techniques[64–68] for SiNPs quantification.

Nonetheless, the application of SiNP in EOR is the main topic of this thesis. Table 2 below lists the research projects as well as the approach utilized for SiNP quantification. In porous media transportation experiments where adsorption, interactions, or mechanisms between fluid and rock are evaluated, quantification/detection is typically used. The absorption spectroscopy approach stands out since it is practical and simple to use for conducting measurements, obtaining data, and it is a non-destructive technique. The analysis and comments on a few of the works mentioned in the table are provided below.

Zhang et al.[58] tested how SiNPs moved through porous environments, with flow rate, types, concentrations of nanoparticles (from 0.1 to 5%), and properties of the porous medium used as variables. The types of each NPs tested were with polyethylene glycol (PEG), fluorescent (FL), and salt tolerant (ST) modifications all provided by 3M Company. When high concentrations of NPs were used, the concentration in the effluent was measured using the refraction index. A line ultraviolet detector was used in experiments with low concentrations of NPs probably because the absorption of the SiNPs at certain concentrations is above the range that the technique can offer.

Hamouda et al.[62] filtered the supernatant of each sample through a 0.22 μm filter after passing through the porous media, which allowed nanoparticles but not larger calcite mineral particles to pass through. The absorbance of the nanoparticles in UV/Vis determined their remaining concentration in the supernatant. However, while filtering before measuring can remove agglomerates larger than 200 nm, it does not quantify all the NPs that were not adsorbed.

Table 2: Publications that utilize different approaches for quantifying SiNPs in the context of EOR

Title	Technique
Experimental insight into the SiNPs transport in dolomite rocks: Spotlight on DLVO theory and permeability impairment (2022)[64]	UV-Vis
The impact of NPs adsorption on transport and wettability alteration in water-wet Berea-Sandstone: An experimental study (2019)[61]	UV-Vis
Effect of salinity on SiNPs adsorption kinetics and mechanisms for fluid/rock interaction with calcite (2019)[62]	UV-Vis
Effect of SiNPs on fluid/rock interactions during low salinity water flooding of chalk reservoirs (2018)[56]	UV-Vis (SW) ICPOES (DW)
Stability and flooding analysis of nanosilica/ NaCl /HPAM/SDS solution for enhanced heavy oil recovery (2018)[65]	Turbidimetry
High-temperature stability and low adsorption of sub-100 nm magnetite NPs grafted with sulfonated copolymers on Berea sandstone in high salinity brine (2017)[60]	UV-Vis
Adsorption of SiNPs onto calcite: Equilibrium, kinetic, thermodynamic and DLVO analysis (2015)[59]	UV-Vis
Investigation of NPs adsorption during transport in porous media (2015)[58]	Refractive index and UV-Vis
Transport and retention of engineered Al_2O_3, TiO_2 and SiO_2 nanoparticles through various sedimentary rocks (2015)[57]	UV-Vis
Synergy between Nanoparticles and Surfactants in Stabilizing Foams for Oil Recovery (2015)[74]	ICP-OES

Abhishek et al.[56] evaluated the static and dynamic adsorption of the dispersed SiNPs in DW and seawater (SW). In addition to salinity, the effect of the increase in NPs concentrations was evaluated, as observed in Figure 8A. The authors chose to use ICP-OES to determine the concentration of NPs in the effluent during transport through the porous medium when

injected with DW. However, they chose the spectroscopic technique in the UV-Vis region to quantify SiNPs during high- and low-salinity adsorption tests probably because the ions present in the brine would interfere with the measurement in ICPOES. MEV integrated with a dispersive-energy X-ray fluorescence analyzer (EDXRF) was used to visualize the adsorption of SiNPs in calcite samples (Figure 8B), showing that the dynamic adsorption of NPs in calcite proved irreversible in high salinity, while desorption was observed in conditions of low salinity. Also, MEV images showed no porous channel blockage despite the NPs' attraction to rock surfaces. The authors considered points along the horizontally sectioned core and since they are small portions of the whole, they may not statistically reflect the reality of others.

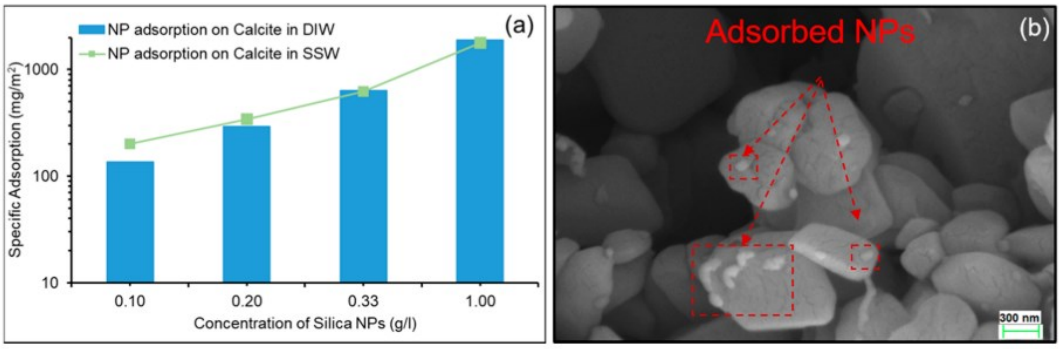

Figure 8: Adsorption of SiNPs onto the surface of calcite via dynamic and static adsorption (A). MEV image showing SiNPs adsorbed in calcite (B) (Abhishek et al., 2018)[56].

UV-Vis spectroscopy is a versatile and practical technique, but one of its limitations is that any particle can absorb or spread radiation. This error can be minimized with the realization of the blank measured, however, during transport in the porous medium, the fluid as a whole in the effluent may be modified in relation to its absorption in the reference spectrum due to its interaction with the medium, whereby particle detachment from the pore medium may occur, another material that may affect the absorptive reading through the spread of radiation.

For more details, such as concentrations and the working wavelength used, as well as the media features see Table 3 which shows absorption spectroscopy research on SiNPs since 2015 aimed at their quantification.

Although most research involves rocks and reservoir conditions, Ghosh and collaborators[63] systematically evaluated the effects of various physicochemical parameters such as pH, ionic force, and the presence of humic acid on the transport and retention of SiNPs in porous media saturated with various types of water (tapwater, a well, a recreational lake, and a river). The authors hypothesized that nanomaterials could carry heavy metals in SiNPs, and thus their quantification is important.

Table 3: List of works in which SiNPs were quantified by a UV-Vis technique

Source	Commercial SiNPs and size[1]	Concentration (wt%)	λ_{abs} (nm)	Dispersion features
[63] (2022)	Lab-made Unmodified (47 nm by TEM)	0.005 a 0.03	265	Quartz /Water
[64] (2022)	Unmodified (14 nm)	0.1 e 0.5	400	Dolomite /DW
[61] (2019)	Unmodified: solid (7 nm), colloidal (18 nm). Alkyl (7 nm)	0.05 a 0.5	-[5]	Berea Sandstone DW/SW
[62] (2019)	Unmodified (5 nm)	0.1 e 0.15	240	Calcite /DW/SW
[56] (2018)	PEG[2] (20 nm)	0.1	240	Calcite /DW/SW
[58] (2015)	PEG[2], FL[3] and ST[4] (10-30 nm)	0.1 a 5	-[5]	Boise /DW/ NaCl
[59] (2015)	Unmodified (10-15 nm)	0.08 a 1	-[5]	Calcite /DW/ NaCl
[57] (2015)	Unmodified (20 nm)	0.005	400	Quartz, limestone and dolomite/DW

[1] Nominal size by the manufacturer

[2] PEG – polyethylene glycol; [3] FL – fluorescent; [4] ST – salt tolerant

[5] Not provided by the authors

λ_{abs}: Wavelength at which the SiNPmeasurements were performed

Table 3 also highlights that the quantification of SiNPs is a topic of current interest but there are still many discrepancies in how this quantification is performed. Due to the lack of information regarding the quantification procedure, some of the presented works do not mention the absorption maximum wavelength at which the analytical curve was produced. Of these eight works, only one (Ghosh et al.[63]) showed the data, the linear regression equation, and the standard deviation of each point, as shown in Figure 9. Another issue to be highlighted is when the curve is not sensitive enough to low concentrations. As described by Shidong and coauthors[61], the transport profile with 0.2 and 0.5 wt% of colloidal SiNPs in the effluent can be measured by UV-Vis. However, at the lowest concentration (0.05% by weight), measurement was not possible due to a weak response signal. These findings point to a shortage of techniques to detect low concentrations of SiNPs.

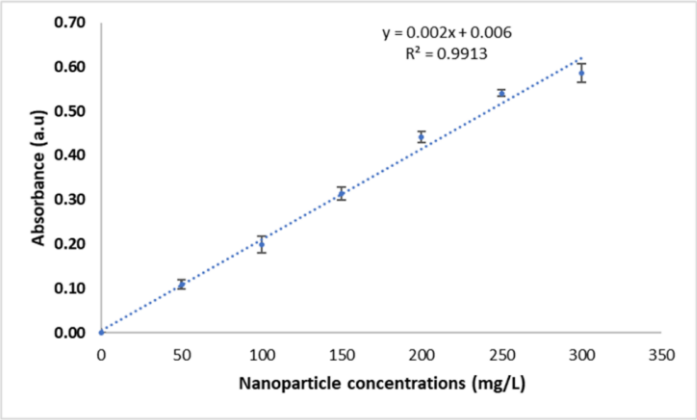

Figure 9: Analytical SiNPs calibration curve by Ghosh and collaborators[63] using UV-Vis technique to measure the amount of SiNPs after they pass through a porous medium.

Keykhosravi and coworkers[64] examined SiNP transport at 0.1 wt% (NF1) and 0.5 wt% (NF6) concentrations (Table 3). Figure 10 shows the displacement profile for each nanofluid during transportation through the porous medium. The authors defined 0.1 wt% of the SiNP nanofluid (NF1) profile as a reference, which can make it difficult to discuss the results. The best option would be to choose an inert material as a reference. This gradual reduction in the effluent during the post-washing (after 5 pore volume, PV)

stage is known as the "long tail" of the curve, indicating the detachment of the adsorbed NPs on the porous surfaces. The authors point out that both reversible and irreversible adsorption of NPs can occur during NPs transportation and the particles that detach can be attributed to the reversible form. A similar trend occurred for the injection of 0.5% (NF6), however, there was a delay in the breakthrough curve (BC) and not at the end as in NF1, probably due to the higher amount of silica NPs retained. Consequently, it took longer to reach the stationary state phase for NF6 and the plateau level was lower, meaning greater retention of NPs in the dolomite rock. During the elution curve (EC), the concentration of effluent also decreased similarly to the reference, but the "tail" was shorter, which may mean a lower degree of detachment from the rock surface. An important point is that the effluent concentration never reached the injection concentration, possibly because NP retention is still occurring during its transportation in the plateau region. As the normalized effluent concentration did not tend to increase towards the unit, the authors suggested continuous particle retention under the experimental conditions.

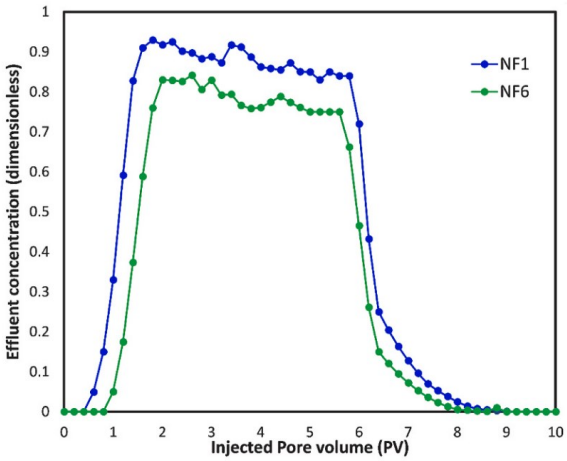

Figure 10: SiNPs displacement profile in DW at different concentrations NF1 (0.1 wt%) and NF6 (0.5 wt%) in a porous medium (dolomite) (Keykhosravi et al., 2022)[64].

Turbidimetry, in which turbidity instead of absorbance is employed to evaluate a suspension's stability and quantify the NPs, is another flexible and practical method. The salinity of a body of water plays a significant role in determining how clear a suspension is when measuring turbidity.[75] For

SiNPs suspension, this was demonstrated by Awan et al. (2007)[66], who found that the turbidity decreased with increasing salinity, even when the initial concentration and NP materials were the same. Since NaCl salt induced the aggregation of the colloids present in the continuous phase (NPs), it increases the rate of sedimentation (also known as settling speed) of the suspended NPs, which in turn has a significant effect on turbidity measurements. This drawback could be overcome by developing a tool that can be used to read the concentration without the aggregation effect, especially in reservoirs with high salinity. The same work[66] evaluated four commercially available NPs (Al_2O_3, SiO_2, MgO, and ZrO_2) for potential use in a proppant fluid. As can be seen in Figure 11, turbidity increases with increasing concentration during the analytical curve-fitting process. The average particle size and physicochemical properties of the various NPs varied leading to a wide range of turbidity values at constant mass concentrations. This demonstrates that, in contrast to other methods, turbidimetry necessitates much attention to detail with regard to the regularity and homogeneity of the shape and size of the NPs used to prevent errors in turbidity measurements.

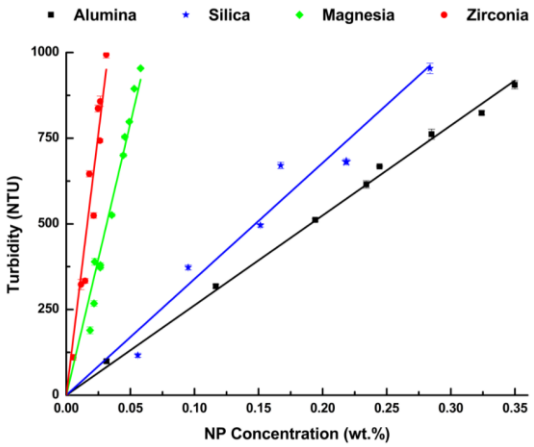

Figure 11: Analytical calibration curves obtained from turbidimetric observations with several unmodified NPs in DW (Awan et al., 2007)[66].

All the strategies discussed in this section have benefits and drawbacks. In addition to the high cost of the analysis, the measurements in ICPOES must be highly diluted to minimize interference from other ions at higher concentrations. Optical analysis-based detection methods are

sensitive in both pure water and thoroughly cleaned porous media. In natural media, such as soil, however, high background signals can hinder detection. Many studies have used turbidimetry and UV-vis absorption spectroscopy as detection techniques to quantify SiNPs. In these methods, NPs are indirectly quantified by measuring the level of light scattering in aqueous suspensions. However, the potential interference caused by NP aggregation can compromise the determination at the low concentrations required for EOR applications. As demonstrated by Estephan and coworkers[76] and Yousefvand and Jafari[65], turbidimetry was implemented for determining the colloidal stability. Another point to consider is that the sensitivity of turbidity reduces as particle size decreases, as it is dependent on the intensity of nanoparticle scattering.[77] As a result, in the context of EOR, when a porous medium is used, turbidimetry and UV-Vis spectroscopy are not quantitatively selective approaches in complex matrices.

Although there are several research projects involving silica nanoparticles in EOR, the most significant difficulty found in the current literature is a lack of methodologies for evaluated the SiNPs fate as opposed to the already existing methodologies when surfactants are used. As a result, while techniques like electron microscopy allow for qualitative analysis of the process of NP adsorption on the surface of reservoir rocks, they do not yield statistically accurate data from any system.

The use of FSiNPs, which allow the detection and/or quantification of NPs during the transit of the nanofluid through the porous medium, is a potential alternative. The great analytical sensitivity of the equipment used to quantify fluorescence, the low detection limit, the convenience of producing it, and the inexpensive cost are all factors that make the use of fluorescent materials desirable. Developing approaches for determining adsorbed and/or retained NPs during nanofluid transport in porous media can aid in the understanding of the transport processes involved in this process.

3.3.2. Fluorescent SiNPs

The vast majority of published studies on FSiNPs are in the biomedical field, with targets in the application of biological detection such as biosensors and biomarkers[78–80]. Research with FSiNPs applied to EOR is limited, with only studies published by Murugesan[81], Khan et al.[82], and two studies by Singh and Mohanty[74,83].

Murugesan and collaborators synthesized FSiNPs and demonstrated that silica plays a role in the transfer of energy between the donor (FITC) and acceptor (Ru-complex) moieties. The stability of the NPs was assessed in SW at 80°C for 24 h but there are no further details or discussions of the stability test results. The NPs were functionalized with a high level of long-chain hydrocarbons to improve dispersibility in oil and facilitate the reading of the fluorescence in mineral oil, thus they showed distinguishable fluorescence from the emission band of the oil. In this way, according to the authors, these NPs can be used for dual purposes as tracers and EOR agents and the authors claim the modified NPs are environmentally correct. However, the study does not present any research on the toxicity of the synthesized material. Additionally, there is no investigation of the fluorescence intensity response of the NPs synthesized by the authors in a porous medium.

Singh and Mohanty qualitatively evaluated the interaction between FSiNPs obtained from 3M and surfactants in the generation of smart foams for application in EOR. In their 2015[74] article, the authors studied foam drainage behavior, clarifying the imprisonment of NPs at the edges of the plateau and the thickness of the foam lamella by fluorescence microscopy (Figure 12). Confocal laser scanning microscopy was used to confirm the observations of the vertical foam film tests. As the concentration of FSiNPs was relatively high (0.3 wt%), they could be seen around the bubbles surrounding the air-water interface, and dispersed in the continuous liquid phase, as well as on the edge of the plateau. The authors suggest that the formation of NP three-dimensional networks increases the stability of the bubbles.

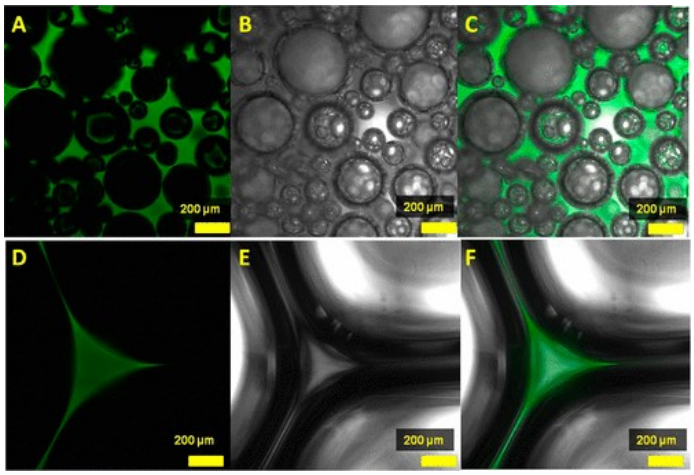

Figure 12: Confocal microscopy of foams stabilized by surfactant and FSiNPs: (A/D) fluorescence images showing NPs (green); (B/E) clear field images; (C/F) mixed images (Singh & Mohanty, 2015)[74].

The authors confirmed that the fluorescence emitted by FSiNPs can be detected by a microscope. Consequently, it can be employed to monitor the location of the NPs within the foam phase. In their 2017[83] article, the efficacy of foam stabilization through the utilization of surfactant-NP mixtures was examined. The researchers conducted a study to demonstrate the dynamics of foam transport in a porous system with a two-layer heterogeneity model. Due to their hydrophilic nature, the aforementioned NPs were observed to be present in the liquid phase and did not adhere to the air-water interface. The results of the foam flow experiments indicated that the incorporation of NPs leads to a notable enhancement in the foam resistance factor, with an increase of 1.95 times observed in comparison to experiments carried out solely with surfactants.

Finally, Khan and collaborators[82] synthesized distinct functionalized SiNPs with partially hydrophobic portions (CH_3, S2), hydrophobic (C_8H_{15}, S3), and hydrophilic (NH_2, S4) on the surface. As illustrated in Figure 13, all synthesized NPs encapsulated zinc oxide. In sample S2, the methyl group on the NP surface reduces hydrogen binding sites in aqueous solutions, making them less hydrophilic. The S3 NPs contain an octyl group that is highly lipophilic and can change the surface of the NPs from hydrophilic to completely hydrophobic. As a result of this functionalization, these NPs (S3) may have the ability to move from the aqueous phase to the oil phase. A

hydrophilic silane with an amino group functionalized sample S4 to make luminescent SiNPs more hydrophilic.

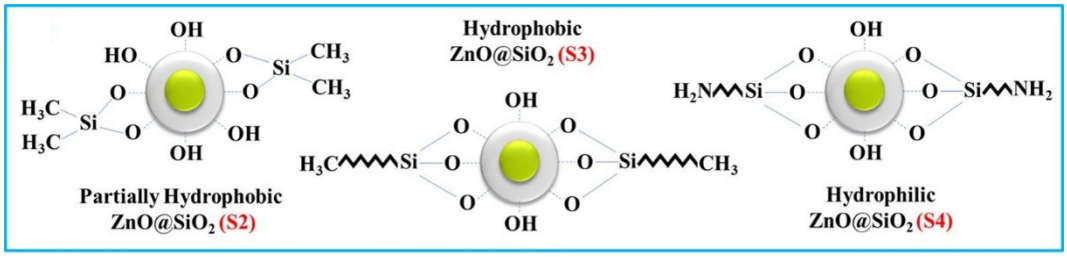

Figure 13: Illustration of the surface structures of the synthesized luminescent NP S2, S3, and S4 (Khan and collaborators, 2022)[82].

Under UV light, the surface chemistry and behavior of photoluminescent NPs in oil (hexadecane) before and after mixing were studied. Before mixing the phases, all three synthesized NPs are in the aqueous phase. After the mixing, the following results were observed: *i*) NPs S2 were shifted toward the interfacial surface between the two phases, with partially hydrophilic and partially hydrophobic characteristics due to the presence of hydroxyl groups (OH) and methyl groups (CH_3), respectively, on their surfaces; *ii*) the S4 remained entirely in the aqueous phase due to NH_2 group (hydrophilic nature); *iii*) NPs S3 moved completely towards the oil phase because of the presence of the octyl group on its surface (see Figure 14).

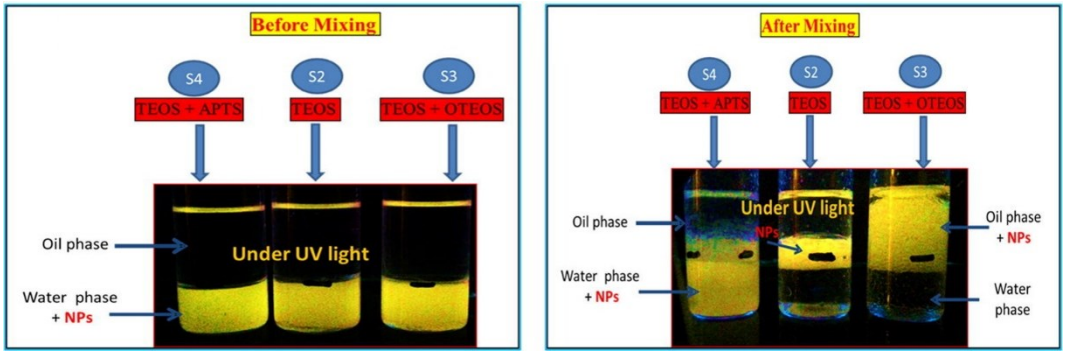

Figure 14: Scheme demonstrating the water/oil systems and NPs before mixing (left) and after mixing (right) (Khan and collaborators, 2022)[82].

The research by Khan et al. aims to apply functionalized NPs in the form of dispersion to investigate their colloidal behavior in the water/oil mixture and at its interface. However, from a colloidal point of view, there

are no data supporting the stability of the NPs in dispersion, traditionally measured by DLS and ζ-potential probably because in tests carried out in the presence of salt, the NPs aggregate, thus influencing the measurements of emission intensity.

As a summary and a quick review of this topic, Table 4 contains a summary of the studies discussed including the principal reagents of the synthesized FSiNP, the type of synthesis, and the applications of this NP.

Table 4: Summary of fluorescent SiNPs used for EOR purposes

Source	Reagents	Synthesis	Application
Murugesan et al., 2017[81]	FITC/APTES/TEOS Ruthenium complex Hexadecyltrimethoxy silane HDTMS	Sol-gel	Sensing materials for oil reservoir applications
Singh & Mohanty, 2015[74]	Commercial Fluorescent SiNPs	-	Fluorescence microscopy to visualize the synergistic stabilization of foams by mixtures of NPs
Singh & Mohanty, 2017[83]	Commercial Fluorescent SiNPs	-	Visualization of foam flow in a two-layered system with a permeability contrast
Khan et al., 2022[82]	ZnO@SiNPs modified with: S2: CH_3; S3: C_8H_{15}; S4: NH_2	Sol-gel	Sensing materials for oil reservoir applications

Fluorescence NPs have shown great potential as tracers for transport and retention studies in porous media for environmental applications,[84] but there are few reports of their use in the petroleum industry[85,86]. Below are some papers that have used FSiNPs in studies with porous medium, but not necessarily in EOR.

Several silica-based NPs (nanobeads) including rare-earth element complexes and organic dyes were synthesized, as shown in Figure 15, by

Agenet et al.[85] for use as “smart” oil field tracers. The authors demonstrated that the close combination (inter-dye distance < 5 nm) of organic molecules and inorganic complexes led to “smart” optical signals of the particles. In addition, the gluconamide surface coating of the nanobeads efficiently minimized rock-NP interactions, leading to a 98% recovery factor in outcrop sandstone. This work validated the concept of fluorescent nanobeads and illustrated their propagation capabilities in porous media, but it cannot be directly applied to understand the transport of SiNPs in nanofluids containing surfactants, in which the stability of the nano tracer depends on specific interactions between the surface functional groups and charges of the NPs and surfactants.

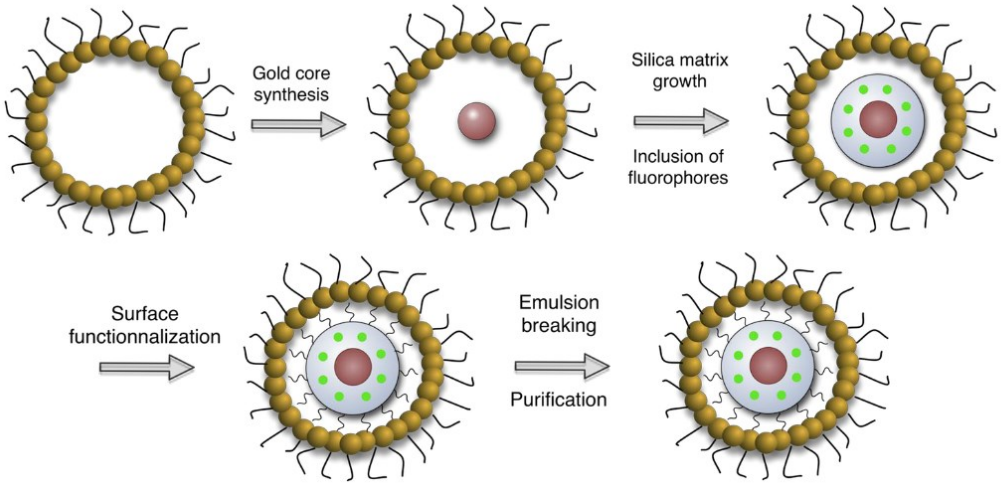

Figure 15: Nanobead synthesis by Agenet et al. 2012[85].

Vitorge et al.[87] synthesized three types of SiNPs using the sol-gel method: fluorescent (FITC) – P1, heavy metal (Ag (0)) – P2, and radioactive (^{110m}Ag) – P3 for a comparative analysis of SiNP transport in porous media using fluorescence, analytical chemistry, and radioactivity for detection, respectively. The authors reported that fluorescent SiNPs are easier to synthesize but their detection concentration is high near the other two. A complementary study by the same authors using the materials[88] conducted breakthrough curves. Sand was used as porous media to simulate the porous environments of aquifers, showing that NP P1 and P3 were completely recovered at the column outlet in DW experiments, indicating no retention (Figure 16). This suggested that particle size and labeling do not

affect behavior under electrostatic attachment. P2 in DW effluents contained only 84% particles. The authors suggested that the electrostatic attraction between colloids and grain surfaces, or physical filtration usually retains nanoparticles in porous media P2 showed a larger particle size than the other two NPs, affecting sand retention, which favors stronger physical filtration. The authors also observed and warned that suspended matter and its natural fluorescence can interfere with the detection of retained P1 NPs in supernatants containing sand fines.

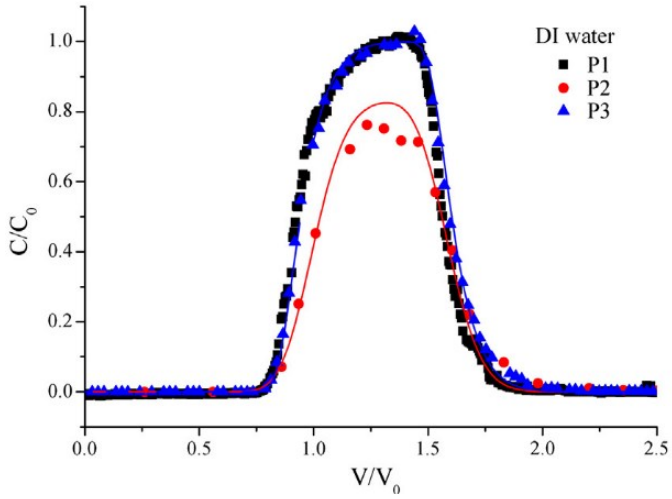

Figure 16: Transport experiments were performed in deionized water using particles P1, P2, and P3 to construct a model (lines) of the breakthrough curves (adapted from Vitorge et al., 2014)[88].

As a conclusion to this topic, Table 5 provides a summary of the works about fluorescent SiNPs that are applicable in porous media. In addition to the previously discussed works (Agenet and Vitorge), there are two more examples of FSiNP in the porous medium in the wastewater treatment area. Industrial and municipal wastewater discharges are recognized as the primary environmental sources of NPs[84] and it is well-established that SiO_2 also facilitates the co-transport of numerous other contaminants, including heavy metals and pesticides.[63] We can conclude that the establishment of a quantification method for SiNP is a result of the widespread use in various aspects of our lives and that this raises concerns about how this impacts water treatment and how SiNPs interact with other substances.

Table 5: Summary of studies of transport in porous media by FSiNPs

	Reagents	Synthesis	Application
Agenet et al., 2012[85]	FITC/APTES Eu-NPs Au APTES/TEOS Si-glucanamide	WORM	Reservoir monitoring
Vitorge et al., 2014[88]	TEOS/APTES/FITC	Sol-gel	Aquifers pollution
Otero-Gonçalez et al., 2015[84]	TEOS/APTES/ Rhodamine B isothiocyanate RITC	WORM	Wastewater treatment
Zeng et al., 2017[89]	TEOS/APTES/RITC	WORM	Wastewater treatment

In this context, the detection and quantification of SiNPs by fluorescence spectroscopy is a promising alternative, as this technique has high selectivity and sensitivity, low detection limit, ease of measurement, low cost, and the potential to be adapted for real-time monitoring.[90] In addition, fluorescent SiNPs with different characteristics can be synthesized using tailored combinations of a silanizing agent, linker, and organic fluorophore.[91]

3.4. Syntheses of silica-based fluorescent SiNPs

A fluorescent tracer is any organic or inorganic compounds that presents fluorescence and can be used to determine the path, transit time, or material dispersion.[92,93] The applicability of a fluorescent tracer is very broad, highlighting its use in the determination of polycyclic aromatic hydrocarbons[94], transport of colloids in porous media in groundwater and soil pollution[95], and the study of coastal rock erosion and morphodynamics[96], among others. One of the factors that make the use of fluorescent tracers advantageous is the high analytical sensitivity of the equipment that measures fluorescence, which has a low detection limit.[93]

Fluorescein isothiocyanate (Figure 17A) is the most popular fluorescent probe available, mainly when applied as biomolecules. This is because it reacts easily with various nucleophiles, such as 3-aminopropyletoxisylane (APTES) (Figure 17B). Compounds generated with primary amines are more stable, such as in the terminal amines in proteins. The reaction involves the attack of the nucleophile (R-NH_2) on the central electrophilic carbon of the isothiocyanate group (N=C=S) with the resulting electron shift creating a thiourea bond between the FITC and the amine without leaving group (Figure 17C). FITC's fluorescent properties include absorption maximum at 495 nm and emission wavelength at 520 nm and can quench at high dye concentrations, the so-called self-quenching, reducing fluorescence emission.[97] The combination of SiNPs with fluorescent materials is a very interesting and important application. Silica acts as a host material of functional materials, for example, if fluorescent molecules are incorporated into a silica matrix, the protective layer formed promoting immobilization of fluorophores may lead to an increase in quantum fluorescence yield.[2]

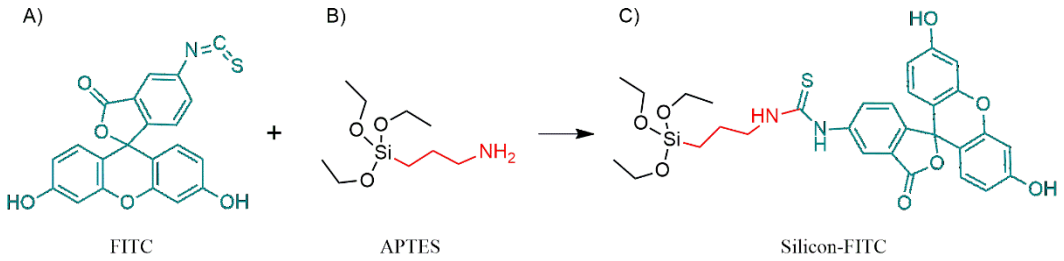

Figure 17: Molecular structure of Fluorescein Isothiocyanate (FITC) (A), APTES (B), and the conjugate dye silicon-FITC (C).

SiNPs can be synthesized with a good degree of control, and the physicochemical properties of silica's surface are among the best known. Furthermore, they can be easily functionalized with different terminal groups ranging from hydrophobic to hydrophilic. There is a vast wealth of literature on the surface functionalization of SiNPs with a variety of materials.[41–46] This type of material can be easily prepared by hydrolyzing and condensing a silica precursor, represented by the general formula $Si(OR)_4$, with the most common compounds being methanol-formed tetramethoxysilane (TMOS) and ethanol-based tetraethoxysilane (TEOS). The most traditional methods

used for the synthesis of SiNPs are via solar gel and the water-to-oil reverse microemulsion method (WORM).[100] Generally, the main differences between them are that the WORM results in the production of more homogeneous NPs, both in shape and size, while the sol-gel method uses fewer reagents, which makes it more viable.[101]

3.4.1.1. Sol-gel

Sol-gel techniques are widely utilized in the production of silica nanoparticles due to their ability to generate monodispersed particles even in the absence of a template using one-pot procedures. It is an ammonia-catalyzed sol-gel reaction where hydrolysis of a silicon source (silica alkoxides) occurs in the presence of water and low molecular weight alcohols like ethanol, followed by subsequent condensation.[102]

When TEOS, NH_4OH, and ethanol synthesis sol-gel are used, it is known as the Stöber method. In this strategy, TEOS hydrolysis and NP formation are promoted by ammonia and water using ethanol as the TEOS co-solvent. The presence of deprotonated Si-OH groups on the surface of the NPs usually generates colloidal suspensions that are strongly stabilized by electrostatic repulsion and are characterized by very large negative ζ-potential values.[103] Figure 18 illustrates a straightforward Stöber method for creating nanoparticles in mild conditions using TEOS, dye, DW, ethanol, and ammonium hydroxide as catalysts typically under moderate conditions such as room temperature.

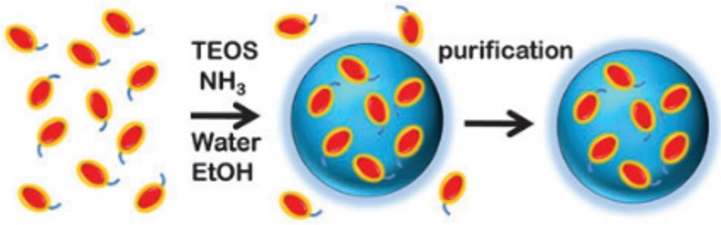

Figure 18: Schematic representation of synthetic strategies for obtaining modified SiNPs with dye through Stöber's method (adapted from Montalti et al., 2014)[103].

Vera et al., (2017)[104] reported the synthesis of fluorescent amino-SiNPs through the co-condensation of APTES and TEOS. Under mild

reaction conditions a one-pot synthesis method has been developed that allows for the simultaneous incorporation of functionalities, namely the fluorescent molecule and the amino group. The synthesis methodology produced NPs of an average nominal size of 110 ± 40 nm that featured amine groups on the surface and FITC confined within the particle interior. The position of the emission maximum of encapsulated FITC is comparable to that of unbound FITC, despite the utilization of an alkoxysilane adduct during the encapsulation process. According to the authors it is noteworthy that the acquisition of hybrid silica nanoparticles with diameters less than 200 nm is challenging in the absence of templates or multi-stage procedures.

SiNPs obtained by the Stöber method are nonporous, therefore introducing porosity requires an extra synthesis step, such as successive treatments with water and ethanol promoting substantial reorganization of the silica creating microchannel within particle; adsorption-based approaches to introduce micropores incorporate by glycerol, which upon mild calcination were evaporated leaving behind micropores in the silica matrix; through co-condensation of TEOS with APTES followed by calcination produces mesopores SiNPs;[102] or when CTAB template was removed to form silica shell with perpendicularly oriented mesopore channels providing highly accessible pore surface (see Figure 19).

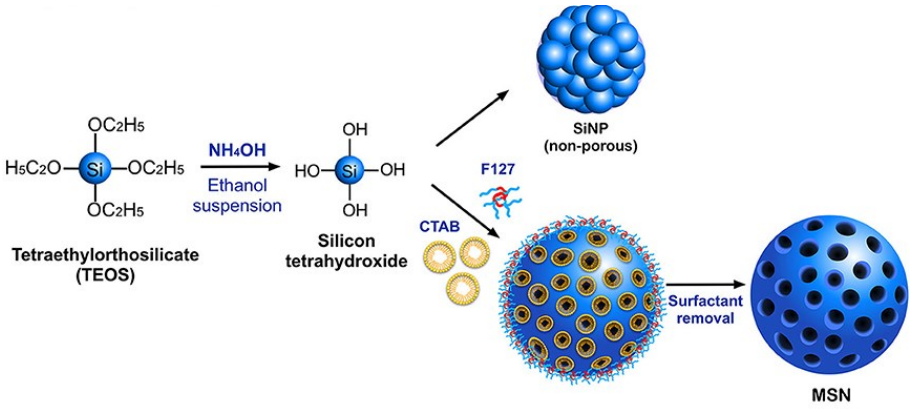

Figure 19: Schematic representation of Stöber's method with different modes of synthesis of SiNPs, non-porous or mesoporous (Selvarajan et al., 2020)[105].

3.4.1.2. Water in oil reverse microemulsion (WORM)

The microemulsion process may be used to synthesize SiNP with a size less than 100 nm in a "nonreactor" made of two incompatible liquids. Inside these nanoreactors, silica precursors undergo hydrolysis and condensation reactions, resulting in the formation of SiNP. Water, silica alkoxide like TEOS, surfactant like alkylphenol ethoxylate, and an organic solvent such as cyclohexane make up the standard formulation. This method has advantages like being thermodynamically stable, exhibiting low viscosity compared to emulsions, do not require any energy contribution, but requiring a large amount of surfactants.[106]

Figure 20 illustrates how the microemulsion process involves the thermodynamically stable dispersion of two immiscible liquids in the presence of an emulsifier or surfactant, with subphases between 10 and 100 nm that serve as nanoreactors in nanoparticle synthesis. Most authors who synthesize SiNPs via WORM use the same reagents and vary only the proportion of one reagent to another. The reagents are dye, cyclohexane, Triton X-100, n-hexanol, DW, TEOS, and ammonium hydroxide. Triton X-100 is used as a neutral surfactant in the reverse microemulsion system, and its concentration is kept much higher than its critical micellar concentration (0.2 to 0.4 mM)[107] to ensure the formation of reverse micelles in the medium.[108]

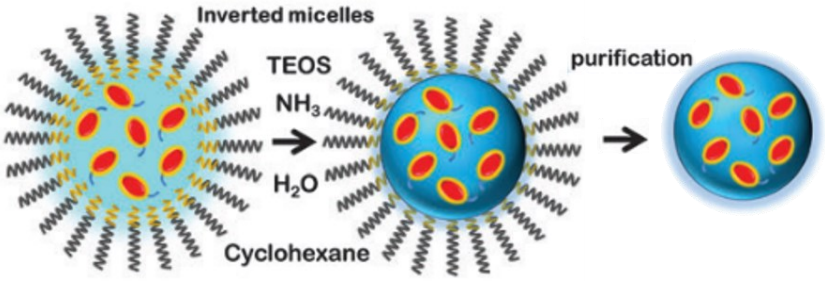

Figure 20: Schematic representation of synthetic strategies to obtain modified SiNPs with dye via the WORM method (adapted from Montalti et al., 2014)[103].

In conclusion, both methods have their pros and cons. Normally, the WORM method produces monodisperse NPs that are smaller (15–50 nm) than traditional Stöber approaches. However, the excessive use of organic solvents and surfactants limits this synthetic approach. The requirement for excessive purification and solvent costs makes upscaling unsuitable (milligram scale), whereas the Stöber method is a surfactant-free method suitable for upscaling (gram scale) but has a higher NP polydispersity than reverse microemulsion making it difficult to produce sub-30 nm NPs.[101,109,110,111]

3.4.1.3. SiNP-NH_2 surface

An unmodified SiNP is inherently negatively charged because of the surface hydroxyls but other more reactive groups are usually added to the NP exterior after synthesis. Alkoxysilane derivatives permit the introduction of functional groups such as thiols, epoxy vinyl, and amines to neutralize or introduce a charge to the surface. The most common, inexpensive, and commercially available reagents for amine surface treatment are aminopropyltrimethoxysilane (APTMS) and APTES. Moreover, the richness of the NP surface chemistry opens a wide range of applications since it can be easily functionalized for further conjugation with fluorescent molecules, as demonstrated in Figure 17. Coatings of SiNP surfaces with amine-reactive moieties can enhance colloidal stability via electrostatic repulsion but it should be noted that such stability is pH-dependent. Amine groups can be protonated ($–NH_3^+$) generating a positively charged group, thereby

reducing the surface charge of the SiNPs (previous negative charge) and reducing NP-NP repulsion causing aggregation.[111,112] Depending on the number of each surface group, the negative or positive charge can be predominant. In the case of the amino-SiNPs, the aminopropyl ($pK_a \approx 9.7$)[113] can be configured on the surface, as demonstrated in Figure 21.

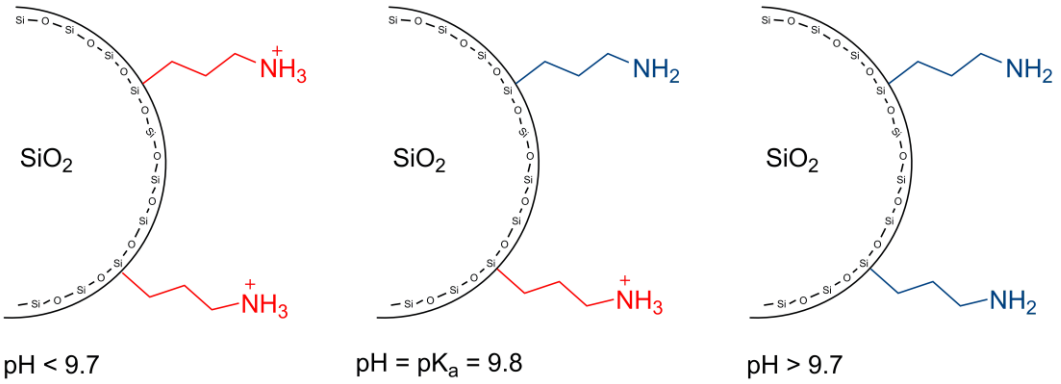

Figure 21: Schematic representation of the silica surface modification by grafting APTES in aqueous suspension.

During the synthesis of SiNPs, the reaction rates of APTES are slower compared to TEOS, resulting in a significant amount of APTES-conjugated dye remaining in the solution even after TEOS has fully reacted and condensed. This leads to a lower efficiency of dye incorporation into the nanoparticles.[101]

In a previous study, SiNPs formed from a mixture of APTES and TEOS were found to have a lower surface charge compared to those formed from TEOS alone.[114] And this fact led to a slightly increased size of NPs when APTES-conjugated dye was added to the synthesis. The authors van Blaaderen and Vrij,[115] assume that in the early stages of the synthesis, siloxane oligomers clump together to form unstable aggregates. As the reaction progresses, these aggregates grow by adding individual molecules. The aggregation process stops when the aggregates reach a size where they become stable NPs. The number of NPs formed depends on the stability of these initial aggregates, and when there are more APTES present, their stability is lower. This allows for more growth space, resulting in the eventual formation of larger particles.[115]

Even in EOR, there are examples of SiNP-NH_2 applications such as “Stabilizing CO_2 foams using APTES surface-modified nano-silica”[116] and “Influence of APTES on SiNP for enhanced oil recovery”[117]. Ngouangna et al.[117] showed that before the modification of the SiNP, the measured ζ–potential was −16.2 mV. With the positive amino groups of APTES attached to the surface of SiNP at a pH of 4.3, APTES neutralized the negative hydroxyl ions and deposited positive amino ions on the surface of unmodified SNP, causing it to become positively charged at +26.4 mV.[117] These and other studies are exemplified in Table 6, emphasizing the main study insights. It is noteworthy that despite the work of Arain et al. (2020)[118] who investigated the colloidal stability and aggregation of the NPs, there is no information about the surface charge of NPs or even of the rocks for studying the adsorption/desorption of the NPs.

Table 6: Studies utilizing amino SiNP nanofluids

Title	Author/year	Highlights
“Stabilizing CO_2 foams using APTES surface-modified nanosilica”	Monjezi et al., 2020[116]	· Surface modification of silica led it to be more gas-wet in the air-water system · The foam half-life was 33% increased in the presence of SiNP-NH_2
“Influence of 3–Aminopropyl triethoxysilane on SiNP for enhanced oil recovery”	Ngouangna et al., 2020[117]	· SiNP-NH_2 exhibited sterling wettability alteration and IFT reduction properties at very low concentrations · Showed greater improve oil displacement compared to the unmodified
“Reversible and irreversible adsorption of bare and hybrid SiNP onto carbonate surface at reservoir condition”	Arain et al., 2020[118]	· Initial hydrophilicity of the NPs and the rock surface influence their adsorption onto the rock · DLS measurement proved the impact of hydrophilicity on the stability and adsorption trend of NPs

“Experimental investigation of enhancement of carbon dioxide foam stability, pore plugging, and oil recovery in the presence of SiNP”	Risal et al., 2019[119]	· SiNP-NH_2 stabilized foam exhibited high stability, and the differential pressure increased in porous media by as much as 3-fold.
“Development of amino-functionalized SiNP for efficient and rapid removal of COD from pre-treated palm oil effluent”	Shafqat et al., 2019[120]	· The maximum removal efficiency >90% of SiNP-NH_2 was found at pH 7, adsorbent dose 0.25 g and 30 ◦C.

3.4.2. Fluorescence stability of the fluorescent SiNPs

One of the most interesting characteristics of these fluorescent molecules bound to SiNPs is their fluorescence stability. The fluorescence intensity response times depend on exposure to air, light, salinity, pH difference and temperatures, even if there is a change in emission after passing through the porous medium. The tests for the stability of fluorescent SiNPs in some conditions have already been described in scientific literature. This short review focuses on modified NPs with the FITC molecule and a connecting agent between the fluorescent and silica molecules.

Photostability tests indicated that the encapsulating dye molecules in the silica matrix increase photostability, reduce solvent effects, and limit exposure to quenchers and oxidizers.[121] The immobilization of dye molecules in a solid silica matrix results in enhanced photostability in contrast to the free dye molecules present in a solution. The observed phenomenon can be explained by a limitation in the movement of dyes within the solid matrix, resulting in a decrease in the pace of nonradiative energy dissipation. The mechanism responsible for the quenching of fluorescence in these systems is attributed to intraparticle energy transfer or other nonradiative pathways. The correlation between the nonradiative rates and the rotational mobility degree of the covalently bound dye within the particle indicates that the fluorescence can be improved and quenching

can be reduced by accurately regulating the architecture within the particle.[91]

In 2010, Zhang[121] and Vera[104] compared the photostability of laboratory-made fluorescent SiNPs to that of free FITC molecules employing APTES and FITC to synthesize fluorescent SiNPs. The photostability evaluation was conducted with the materials in the liquid phase. Vera et al[104] assessed the fluorescence intensity response at pH 2 and 8, and unlike the free behavior of the FITC, the intensity ratio of fluorescence emission between pH 8 and pH 2 was close to one. These observations strongly suggest that most of the embedded fluorophore is confined within the particle and protected from medium changes, while only a small fraction is susceptible to pH changes in the medium.

Zhang et al.[121] synthesized the FSiNP with a layered design by the Stöber method, altering the presence of the fluorescent dye called core-multi shell particle, and performed photostability experiments of free FITC and FSiNP in aqueous solution, as demonstrated in Figure 22. The fluorescence intensity of free FITC decreased by approximately 65% within 30 minutes. In the case of the FSiNP, however, the mean intensity value was reduced by 30% of its initial value during treatment. The FITC molecules were encapsulated into a SiNP matrix using the improved Stöber method, which improved photostability and photoluminescent intensity, increasing the chromophore's stability against photobleaching.

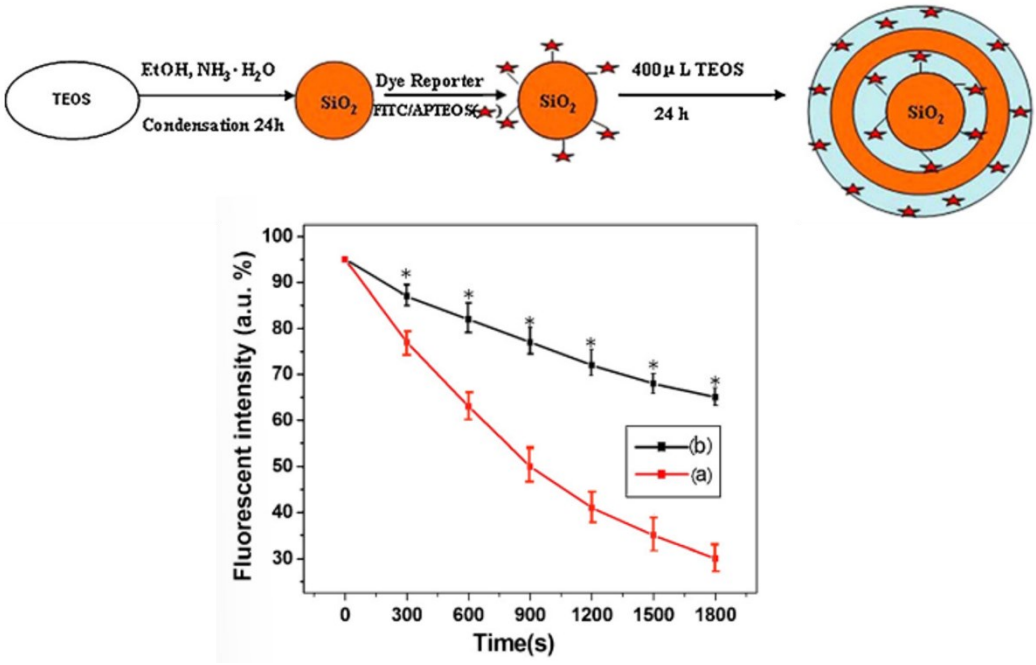

Figure 22: Illustration of the FSiNP structure and procedure. The photostability experiment of free FITC (a) and FSiNPs (b) in an aqueous solution is shown below (Zhang et al., 2012)[121].

Santra et al.[122] assessed the photostability of core-shell SiNPs synthesized by Stöber's method and modified with the APTES/FITC conjugate pair. After 20 minutes, the fluorescence intensity decreased by 10% in an aqueous dispersion but by 80% in the solid state. Oxygen molecules penetrating silica pores photodegrade most solid-state FITC molecules. Time-resolved fluorescence was used to locate the FITC molecules in the FSiNP by observing two lifetimes corresponding to different silica microenvironments. The solvation of molecules closest to the surface and in the pores, where they contact the aqueous phase, accounts for 62% of dye molecules remaining in the solvated silica shell. In a solvent-free, dry environment, 38% of dye molecules remained in the dry silica core, causing the second lifetime. According to the authors, DW may have few dissolved oxygen molecules. Severe photobleaching of FSiNP was observed in air due to the penetration of large amounts of aerial oxygen molecules through the porous silica shell, which photodegraded most FITC molecules. Nevertheless, there is no data on gas adsorption, such as porosity or specific surface area, which would help understand the results.

In conclusion, conventional organic fluorescent dyes are not suitable as they suffer from notorious shortcomings in photostability. Advances in nanoparticle technology have yielded fluorescent probes that are more photostable and sensitive than conventional organic-based fluorescent dyes. Encapsulated FITC emission maximum position is similar to free FITC although the encapsulation procedure involved the formation of an alkoxysilane adduct.[104] Due to dye leakage where dyes are non-covalently bound (via an electrostatic force of attraction) to the silica matrix,[123] dye-doped FSiNP with dye molecules covalently attached to the silica matrix is desired, a feature that improves photostability where dye molecules should be well protected from an oxygenated environment. The fluorophore is shielded from external conditions within the particle, and its primary emission parameters are unaffected by the presence of quenchers. Synthesis of FSiNP is relatively straightforward and does not demand extreme reaction conditions (such as high or low temperatures, pressures, or an inert reaction environment). Nevertheless, core-shell design is one method by which the silica matrix provides a protective encapsulation around the fluorescent dyes, thereby enhancing dye photostability.

3.5. Nanofluid transportation

Nanofluid residue transport in porous media is important due to the potential for their infiltration into aquifers and subsequent entry into groundwater systems posing risks to potable water sources. This highlights the need to comprehend the efficiency of customized filters in water and wastewater treatment for removing these contaminants.[124]

Regarding particles for reservoir application, they must possess the capability to be transported to a desired distance from the injection well. This implies that the particles must demonstrate low retention in sedimentary rock and cause minimal formation damage.[125] However, it is known that once the fluid containing NPs losses may occur due to retention mechanisms during transport and be aware of its extensive use, it is critical to develop methodologies and protocols for quantifying NPs in complex matrices.

When dispersed NPs are injected into a porous media, these main events can cause adsorption, desorption, transport, aggregation, and blockage, depending on the NPs' affinity to the surface, particle size, and particle diameter distribution. Despite its capacity to navigate better in porous media than microparticles, one of the key issues while injecting the nanofluid into the porous medium is the clogging of porous channels.[126] Once adsorption and equilibrium desorption have been achieved, NP transport through the porous medium is governed by diffusion, convection, and hydrodynamics.[29] The mobility of NPs through porous media is heavily influenced by intermolecular interactions, the stability of the NPs, and the rugosity of the porous medium. This implies that NPs with the same surface charge as porous media are more stable against deposition and can be easily transported through the porous medium, while systems with opposite surface charge, will lead to noticeable adsorption in porous media.[23]

When an additive, such as a surfactant agent, is introduced to the system, it can have a significant impact on the stability and transport of NPs in porous media. This is due to the surface-active properties of surfactants, which can adsorb to the NPs and alter their surface chemistry and interactions. The introduction of specific additives can influence the transport and retention of NPs by facilitating chemical interactions between surface groups, as demonstrated in the previous examples.[47,127]

However, sometimes the NPs adsorption in the porous media is the goal of the research. For instance, the potential of different silica nanofluids as surface modifying agents for Berea sandstone, hence reducing fines migration. Abhishek and collaborators[29] provide an example of the interaction between nanofluids and porous media. SiNP/DW, SiNP/DW/stabilizer fluid, and sulfonate-functionalized SiNP/DW were the nanofluids employed to modify the rock surface. The reduction of the fines was indicated by the reduced pressure drop during the post-flush of the NP slug. The change in the ζ-potential measured on the surface of the sandstone indicates the modification by the SiNPs, and the calculation of surface forces showed that the modified sandstone has attractive potential with fine (obtained from water/rock interaction), reducing fine migration, which was desirable.

Another example is the role of NPs in enhancing the surface chemistry of proppant particles, Figure 23. Their incorporation aims to mitigate fines blockage, improve fluid flow pathways, and modify the wettability of proppant packs. This results in increased conductivity for fluid flow and the retention of suspended fine particles. The process of coating proppant particles involves a solid/solid interaction, attracting and coating NPs onto the proppant surface to modify its characteristics. The DLVO theory explains this interaction, and studies have shown that pre-coating the proppant pack yields superior outcomes compared to the simultaneous injection of NPs and proppants.

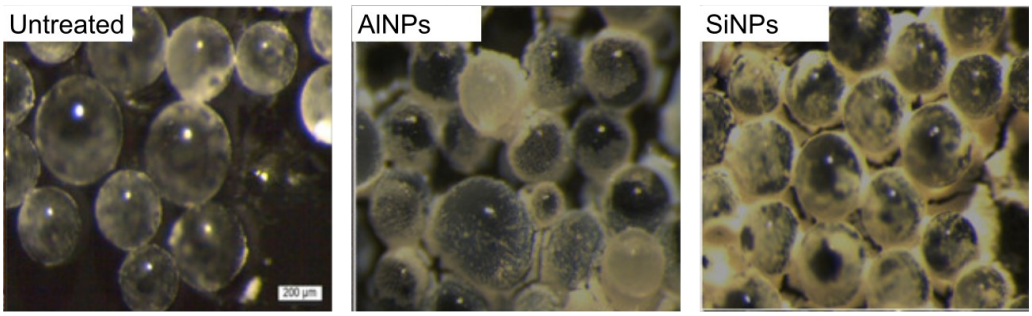

Figure 23: Optical microscopic image of the glass beads untreated, treated with Alumina NPs, and treated with SiNPs (adapted from Awan et al., 2021)[66].

3.6. Overview on bibliography

SiNP quantification is an area of ongoing research, and there is a need for standardized methodologies and improved techniques to detect and quantify SiNPs, especially at low concentrations. Additionally, it is known that further research is necessary to develop reliable and selective approaches for SiNP quantification in complex matrices such as porous media.

The bibliography review discusses the limitations and challenges associated with different techniques used for SiNP quantification. UV-Vis spectroscopy has been used to quantify SiNPs, but discrepancies and lack of information exist in the quantification procedures. Additionally, the sensitivity of UV-Vis spectroscopy decreases at low concentrations, posing

challenges for detecting and quantifying SiNPs at low levels. Despite its limitations, this technique remains commonly used in these studies due to its practicality and non-destructive nature. However, it is important to consider potential interference from other particles and the modification of fluid absorption due to interaction with the porous medium.

The synthesis of silica-based fluorescent SiNPs provides a valuable tool for a wide range of applications, particularly as fluorescent tracers. By combining SiNPs with fluorescent materials like fluorescein isothiocyanate, it becomes possible to achieve high analytical sensitivity and low detection limits. Two commonly used methods for synthesizing SiNPs are the sol-gel and the WORM method. The sol-gel method, specifically the Stöber method, offers a surfactant-free approach that can be easily scaled up. However, it produces a higher degree of polydispersity. On the other hand, the WORM method produces smaller and more uniform NPs but requires a significant amount of organic solvents and surfactants. The core-shell architecture allows for improved fluorescence stability of SiNPs by encapsulating the fluorescent molecules within the silica matrix. As a result, the SiNPs exhibit reduced photodegradation and increased resistance to environmental factors.

SiNPs have a natural tendency to aggregate and settle in aqueous fluids, which can lead to the loss of their intended properties, such as preventing caking in food, altering drug delivery timing and effectiveness, or interfere in the detection of target nanoparticles through fluorescence. To address this challenge, various approaches are employed to enhance colloidal stability, including the use of stabilizing or surface-active fluids and the surface functionalization of NPs. These strategies are particularly relevant in applications related to enhanced oil recovery.

4 Materials and Methods

4.1. Materials

The main reagents used for the synthesis and purification of fluorescent SiNPs were tetraethoxysilane (TEOS), (3-aminopropyl) triethoxysilane (APTES), and fluorescein 5(6)-isothiocyanate (FITC) (Figure 24). Other high-purity grade reagents and solvents used in the experiments included aqueous ammonia solution (25%), ethanol, ethanol anhydrous, n-hexanol, acetone, cyclohexane, ninhydrin, t-octylnonylphenol polyethoxylate ether (Triton X-100), and sodium dodecyl sulfate (SDS). All reagents were obtained from Sigma-Aldrich Brazil and were used without further purification. Deionized water (DW) was used for all experiments. Lithium chloride (99%, ISOFARBrazil) was used to prepare a conservative tracer solution ($c(Li^+)$ = 1 g L^{-1}).

Silica nanopowder (Sigma-Aldrich Brazil, p.n. 718483) with an average particle size of 12 nm and 175–225 m^2/g surface area, was used as a model for commercial nanoparticles. Silica gel powder (Sigma-Aldrich Brazil, p.n. 717185), pore size 60 Å, 230−400 mesh particle size, 40−63 µm particle size was used as a porous material for gas adsorption. SiNP-NH_2, triethoxylpropylaminosilane functionalized (Sigma-Aldrich Brazil, p.n. 791342), <50 nm (DLS) was used as a positive control sample on the ninhydrin test.

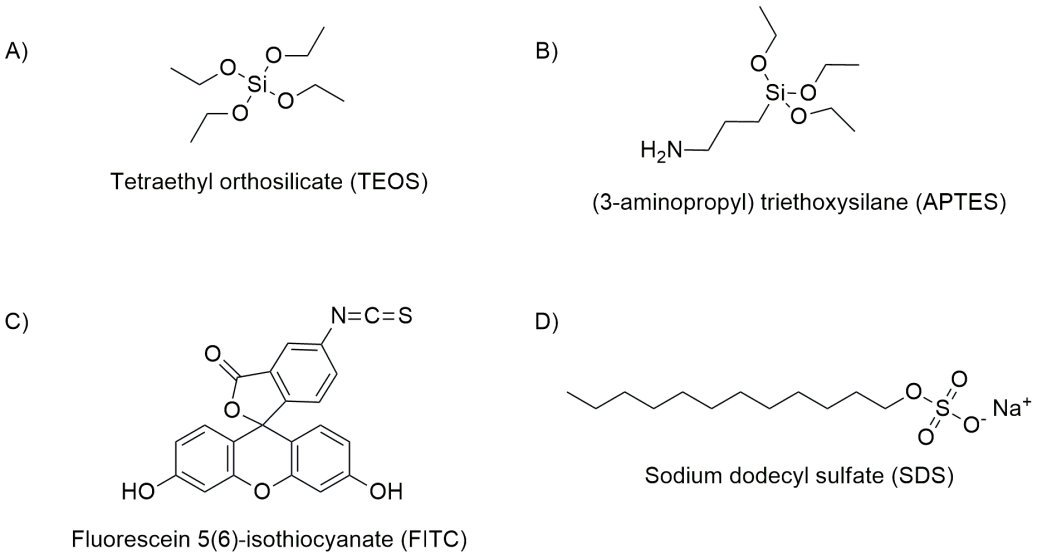

Figure 24: Chemical structure of the main reagents: Tetraethyl orthosilicate (A), (3-aminopropyl) triethoxysilane (B), fluorescein 5(6)-isothiocyanate (C) and sodium dodecyl sulfate (D).

4.2. Nanoparticle synthesis

Four core-shell fluorescent NPs were synthesized in this study, all containing the fluorophore (FITC) in the core and different surface (shell) functional groups through Stöber or WORM procedures. One type of NPs (negative ones) was coated only with silanol and siloxane groups as in commercial SiNP, and the other type (positive ones) was coated with aminopropyl groups. The tailored surface composition aimed to obtain opposite surface charges upon suspension in water owing to protonation/deprotonation of the functional groups, as well as interactions of different strengths with the anionic surfactant in the nanofluids.

The strategies used for the synthesis of fluorescent SiNPs were previously reported in the literature and are based on sol-gel and WORM methods. The methods used to produce positive and negative FSiNP are summarized in Table 7, which correlates the works from which the procedures were derived, the employed method, and the desired surface charge.

Table 7: Summary of the strategic approaches for the synthesis of core-shell fluorescent SiNP

Sample	Method	Surface charge	Adapted from
FSiNP-NH_2 *(S)*	Stöber	Positive	Vitorge et al.[88]
FSiNP *(S)*	Stöber	Negative	Zhang et al.[121]
FSiNP-NH_2 *(W)*	WORM	Positive	Tissandier et al.[128]
FSiNP *(W)*	WORM	Negative	Milleto et al.[100]

4.2.1. Silicon-FITC solution

Initially, a fluorescein-based silane was synthesized in anhydrous ethanol by the reaction of FITC covalently attached to APTES silane by a stable thiourea linkage formation (Figure 17). The synthetic conditions shown in Figure 25A are continuous magnetic stirring for 12 h in the dark to prevent bleaching of the dye, a nitrogen atmosphere, and room temperature (25°C). Finally, the silicon-FITC conjugate was shielded from light during storage to prevent photobleaching and was subsequently employed as a fluorescent silane reagent.

Different proportions of the reagents were used to obtain the fluorescent precursor solutions, as shown in Figure 25B. Silicon-FITC solution B contained a higher concentration of the APTES reagent than

solution A to promote the presence of aminopropyl groups on the silica surface (shell) of the FSiNP-positive particles.

A)

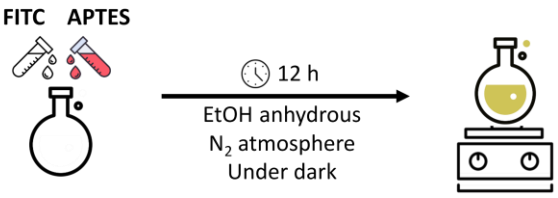

B)

Silicon-FITC solution	FITC (mg)	APTES (mL)	Ethanol anhydrous (mL)
A	6	0.015	3
B	10	0.5	6

Figure 25: Scheme of the reaction between the silane agent (APTES) and the fluorescent molecule (FITC) to form the fluorescent silane (A), and the specifics amounts of the reagents used to produce A and B silicon-FITC solutions (B).

4.2.2. Stöber (Sol-gel)

Both NPs synthesized by Stöber start with the respective amount of the precursor fluorescent silane reagent in the flask. In the case of **FSiNP *(S)*** synthesis, silica polymerization started after the simultaneous addition of NH_4OH (catalyst) and TEOS ethanol solution (5.0 mL of 1.0×10^{-2} mol/L) at a rate of 1.0 mL/h, while in the procedure for **FSiNP-NH_2 *(S)***, the silicon-FITC reacts first with TEOS for 1 h and then the catalyst was added later (see Figure 26 for reaction times in each synthetic procedure). After the reactions were complete, the precipitates were collected by centrifugation (16128 RCF, 10 min) using a 2–16 KL centrifuge (Sigma, Germany) and washed several times with DW and ethanol. The obtained fluorescent SiNPs were dried in a vacuum oven for 8 h at 50°C and 200 mbar and stored in a desiccator at room temperature. Schematics of the two procedures are shown in Figure 26, and detailed information on the reagent quantities can be found in Table 8.

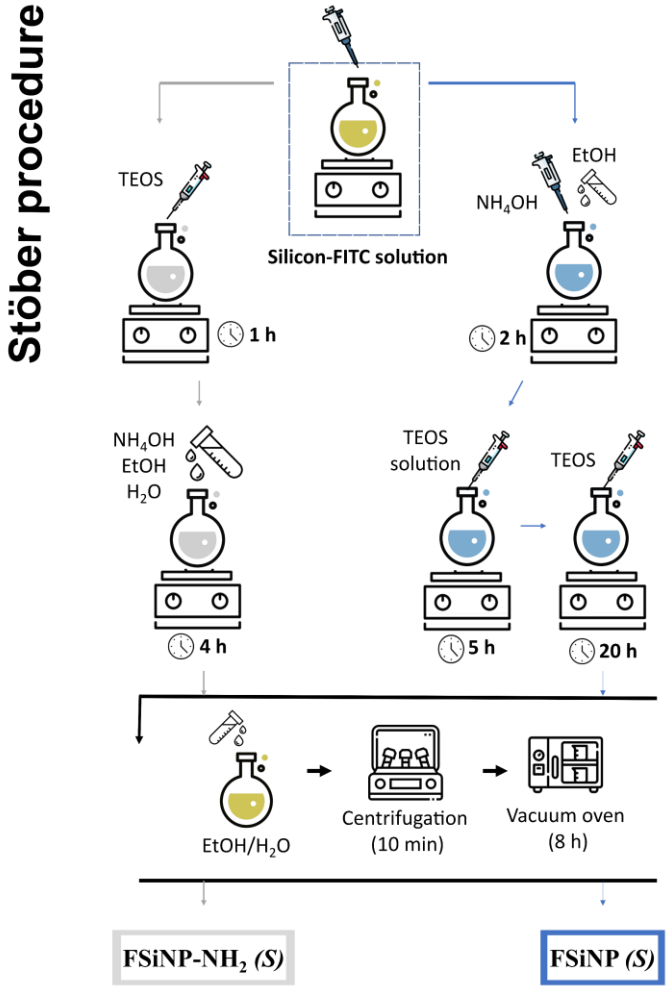

Figure 26: The steps and reagents involved in the synthesis of FSiNP-NH_2 *(S)* and FSiNP *(S)* by the Stöber method at room temperature with magnetic stirring.

Table 8: The amounts of reagents used to synthesize the fluorescent NPs by the Stöber procedure

Stage	Reactants	FSiNP-NH_2 *(S)*	FSiNP *(S)*
Stöber	EtOH (mL)	10	17
	DW (mL)	10	-
Reaction	NH_4OH 25% mL	0.53	1.3
	TEOS (mL)	1	0.14
	Silicon-FITC solution A (mL)	-	0.66
	Silicon-FITC solution B (mL)	2	-

4.2.2.1. FSiNP-fluorescent dye delocalized

The modified Stöber method used for the **FSiNP-NH_2-F *(S)*** synthesis is based on work by Oliveira et al.[129]. To begin, 48 mL of ethanol was added to a mixture containing 1.5 mL of TEOS and 0.5 mL of FITC ethanol solution (1.0×10^{-3} M), then continuously stirred for 30 minutes at room temperature (Figure 27). The mixture was then stirred for an additional 24 hours after 2.3 mL of NH_4OH and 0.8 mL (3.5×10^{-3} mol) of APTES were added. Subsequent the reactions were complete, the precipitates were collected by centrifugation (16128 RCF, 10 min) using a 2–16 KL centrifuge (Sigma, Germany) and washed several times with DW and ethanol. The obtained fluorescent SiNPs were dried in a vacuum oven for 8 h at 50°C and 200 mbar and stored in a desiccator at room temperature.

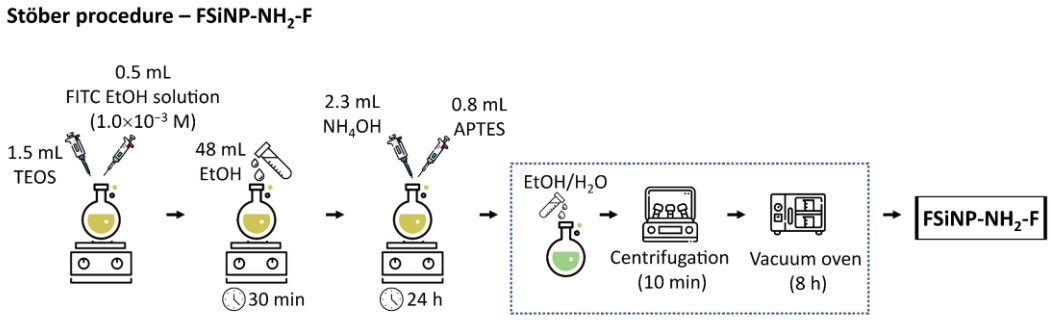

Figure 27: The strategic synthesis utilized to produce FSiNP with the fluorescent dye delocalized on the nanoparticle.

4.2.3. Water in oil reverse microemulsion (WORM)

The solutions containing the precursor fluorescent silane reagent were added dropwise to water-in-oil microemulsions produced by mixing cyclohexane, n-hexanol, Triton X-100, and DW under magnetic stirring at room temperature. In the case of **FSiNP *(W)*** synthesis, silica polymerization started after the simultaneous addition of TEOS and NH_4OH (catalyst) in the reaction mixture, while in the procedure for **FSiNP-NH_2 *(W)***, the catalyst was added later, followed by a reaction with additional APTES (see Figure 28for the reaction times of each synthetic procedure). After the reactions were complete, the microemulsion systems were broken by adding a

solution of DW:acetone (1:1). The precipitates were collected by centrifugation (16128 RCF, 10 min) using a 2–16 KL centrifuge (Sigma, Germany) and washed several times with DW, ethanol, and acetone. The obtained fluorescent SiNPs were dried in a vacuum oven for 8 h at 50 °C and 200 mbar and stored in a desiccator at room temperature. Schematics of the two procedures are shown in Figure 28, and detailed information on the reagent quantities is contained in Table 9.

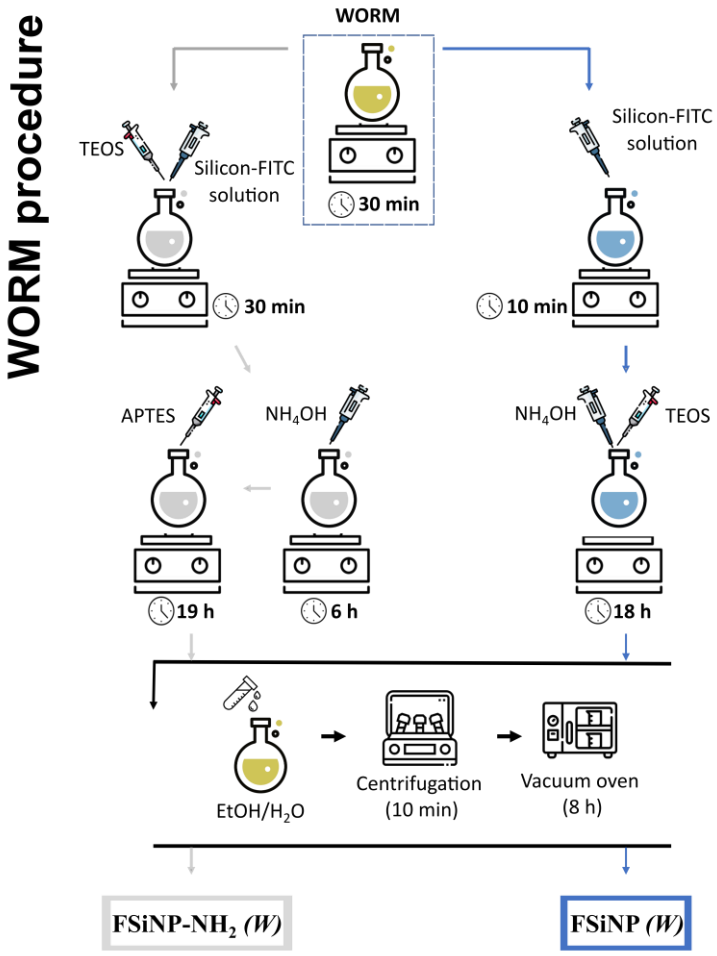

Figure 28: Synthesis of FSiNP-NH_2 *(W)* and FSiNP *(W)* by the WORM method, including the stages and reagents involved.

Table 9: The reagents used to synthesize the fluorescent NPs by WORM

Stage	Reagents	FSiNP-NH_2 *(W)*	FSiNP *(W)*
WORM	Triton x-100 (mL)	2.3	22
	n-Hexanol (mL)	2.3	22
	Ciclohexano mL)	9.6	94

	DW (mL)	0.6	6.7
	NH_4OH 25% mL)	0.08	0.90
	TEOS (mL)	0.13	1.2
Reaction	Silicon-FITC solution A (mL)	0.43	-
	Silicon-FITC solution B (mL)	-	0.25
	APTES (mL)	0.03	-

4.2.4. Evaluation criteria for the NP studies

Assessment criteria that were considered in the FSiNP characterization:

- The structural resemblance to the already-used SiNPs to achieve the same colloidal behavior as the reference NPs.

- FSiNPs' uniformity and size homogeneity and consequently, the transport profiles in the porous medium can be studied without being influenced by possible different retention mechanisms.

4.3. Nanoparticle characterization

The subsequent sections will discuss the process of characterizing silica nanoparticles to confirm that the reaction described above produces the desired material. Various techniques, including elementary (CHN) analysis, ninhydrin qualitative test, spectroscopic infrared by Fourier analysis (FTIR), scanning and transmission electron microscopy, gas adsorption, and the dynamic light scattering technique were employed for this purpose.

4.3.1. Elemental analysis

Elemental analysis (CHN) was performed using a Perkin Elmer-CHN 2400 analyzer to confirm the presence of hydrocarbon chains and amino groups in the obtained NPs. The results are reported as the average of duplicate measurements.

4.3.2. FTIR

Fourier-transform infrared (FTIR) spectroscopy with attenuated total reflection (ATR) was used for the analysis of functional groups on the NP surface. The equipment was an ALPHA II spectrometer (Bruker, Germany) with 32 scans at 4 cm^{-1} resolution in the range of 4000–400 cm^{-1} at room temperature.

4.3.3. Ninhydrin test

A qualitative ninhydrin test was performed to verify the presence of amino groups on the surface of the synthesized fluorescent NPs, considering that the APTES reagent was added to Silicon-FITC solution A and B in different aspect ratios. Commercially available bare SiNPs were also tested, for comparison purposes. Approximately 15 mg of each NP sample was placed on an excavated glass microscope slide, and after heating at 60°C on a heating plate, one drop of ninhydrin solution (1.0 wt% in ethanol) was dripped. Secondary amino groups were detected when the sample showed a final blue coloration (Ruhemann's), characteristic of the ninhydrin-amino complex[130]. The color intensity was proportional to the number of surface amino groups.

4.3.4. Photoluminescence measurements

Fluorescence spectroscopy was used to obtain photophysical data of the NP suspensions (in DW and SDS solutions), including the determination of the maximum excitation and emission wavelengths. Measurements were performed using a Cary Eclipse Fluorescence spectrophotometer (Agilent, USA) with 1 cm optical path quartz cuvettes and excitation and emission slits of 5.0 nm. Fluorescence stability over time was evaluated every 10 min. The first measurement was taken at time zero after placing the cuvette with the sample in the spectrophotometer, while for the other measurements, the cuvette was placed in the equipment at rest.

4.3.5. Electronic microscopy

The size and morphology of the nanoparticles were investigated by scanning electron microscopy (SEM) with the CLARA model from Tescan (Czech Republic) at an acceleration voltage of 10 kV with an E-T detector. The dried powder samples were supported on a conductive double stick carbon tape with Au-coating. In addition, transmission electron microscopy (TEM) was performed using a JEM-2100 model (JEOL Ltd.). For these measurements, NPs samples were dispersed in acetone using a sonicator (Sonics VCX-130 Vibra-Cell Ultrasonic, USA). The average diameter was established by codes written in MATLAB® using functions from MATLAB® Image Processing Toolbox version 2020a. The average nominal diameter was obtained using 100−150 nanoparticles for the calculation.

Notably, the imaging technique for electronic microscopy was chosen based on the size of the particles. TEM was used for imaging commercial SiNP due to their small size, while SEM was used for imaging the synthesized NPs with larger sizes, or a combination of both SEM and TEM was used.

4.3.6. Gas adsorption

The textural properties were evaluated by the surface area and porosity of the material, the N_2 adsorption/desorption isotherm. For comparison of different silica types and to support future discussions, data from N_2 adsorption/desorption for two different types were used. The Brunauer-Emmett-Teller (BET) and Barrett-Joyner-Halenda (BJH) analyses and the textural properties are reported in Figure 29 and Table 10.

The shape of the SiNP isotherm is very similar to that of a type III isotherm (Figure 29A), which is associated with weak interaction with nitrogen. Silica-gel shows typical type IV isotherms that are given by mesoporous adsorbents, with a distinct H1 hysteresis loop in materials with a narrow range of uniform mesopores, like templated silicas.[131] The BET surface area of SiNP and Silica gel samples was 480 and 172 $m^2\ g^{-1}$, respectively. Thus, the porous structure was evaluated through the BJH method. The average pore diameter of the Silica gel sample was centered

at 8 nm as shown in Figure 29B, while SiNP was classified as a non-porous nanoparticle.[132]

Table 10: Silica gel and SiNP nitrogen adsorption-desorption.

	SSA_{BET} $(m^2 g^{-1})$	$Pore\ diameter^{BJH}$ (nm)	$V_{mesopores}^{BJH}$ $(cm^3 g^{-1})$
Silica gel	480	8	0.96
Commercial SiNP	172	-	0.24

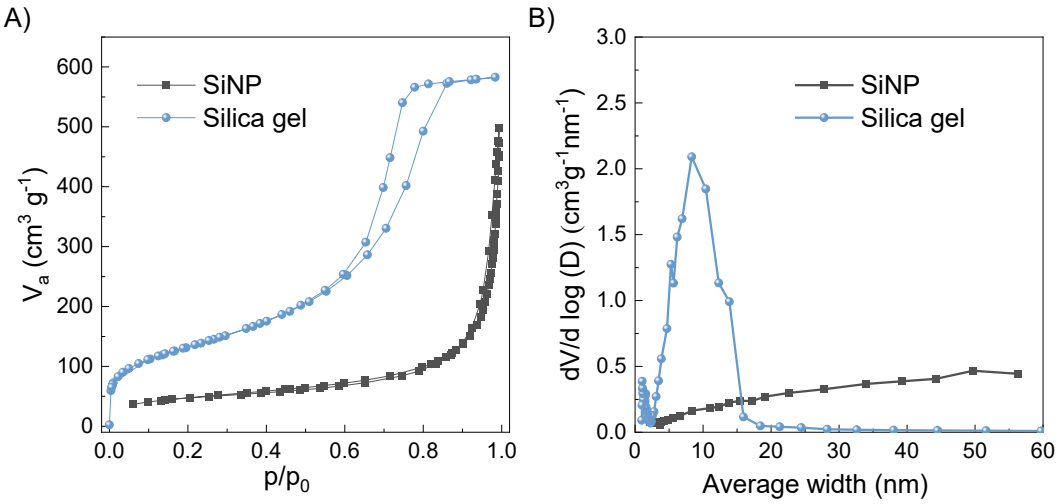

Figure 29: Nitrogen adsorption-desorption isotherms (A) and pore size distribution curves by BJH (B) for non-porous SiNP and mesoporous silica gel.

In this thesis, nitrogen adsorption and desorption isotherms were obtained using a TriStar II 3020 surface area and porosity analyzer. The BET and BJH methods were used to determine the specific surface area and pore size distribution of the NPs. Pore volumes were estimated from the adsorbed gas at a relative pressure of 0.98. Pretreatment of the synthesized fluorescent NPs was performed more mildly than with commercial silica, the former being left for 24 h in a vacuum oven at 65 °C, while the treatment for the latter was performed at 300 °C.

4.3.7. Dispersion proprieties

The hydrodynamic diameter distribution of nanoparticles was determined utilizing the technique of dynamic light scattering (DLS). DLS

analyses are dependent on the intensity of the light scattered by the material over time. The scattered light intensity will oscillate as a result of the study of the particle dynamics, which occurs when scattering particles undergo Brownian motion. Due to the rapid movement of smaller particles, these fluctuations can provide information regarding the decay time via an autocorrelation function. The particle diffusion coefficient and average size were determined by the Stokes-Einstein relation in Equation 1:

$$D = \frac{k_B T}{6\pi\eta R_H} \quad (1)$$

where D is the diffusion coefficient, k_B is the Boltzmann constant, T is the temperature, η is the viscosity of the solvent and R_H is the hydrodynamic radius of the particle.

The colloidal stability of NP suspensions in DW and SDS solutions was evaluated by measuring the hydrodynamic diameter (D_H), polydispersity index (PDI), and ζ-potential using DLS with a Zetasizer NanoSeries (Model Nano-ZS, Malvern Instruments, Malvern, Worcestershire, UK) at 25°C, backscattering configuration (θ = 173°), and 633 nm He-Ne laser. Polystyrene cuvettes with all walls polished (DTS0012) (Figure 30A) were used for size measurements, while a high-concentration cell (model ZEN1010) (Figure 30A) was used for ζ-potential measurements. Electrophoresis mobility was converted to ζ-potential using the Smoluchowski approximation for large ratios of particle radius to Debye screening length. Measurements were performed in triplicate at 25°C (45–300 s) and an average of six measurements were recorded for each point.

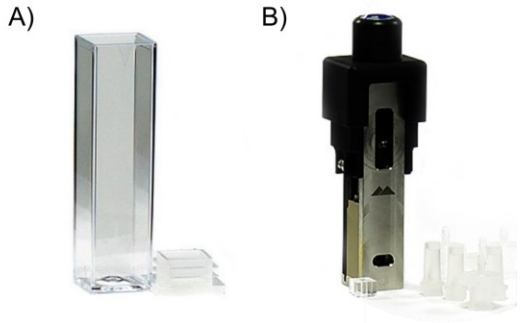

Figure 30: Polystyrene cuvettes with polished walls (DTS0012) were used for size measurements (A) and a high-concentration cell (model

ZEN1010) was used for ζ-potential measurements (B) (images adapted from the Malvern store, malvernstore.com/categories/accessories).

The surface charge of NPs plays a fundamental role in their behavior, particularly in the context of aggregation control. The stability of colloidal dispersions relies on the electrostatic repulsion between particles and this charge can be quantified through the ζ-potential, which measures the potential difference between the electric double layer (EDL) of mobile NPs and the surrounding dispersant layer at the slipping plane as shown in Figure 31. The EDL consists of two distinct regions: the Stern layer characterized by tightly bound ions, and the diffuse layer where ions are less strongly associated. Within the diffuse layer, a boundary exists where ions and particles form a stable entity. As a particle moves, the ions within this boundary contribute to its motion, while the ions beyond the boundary remain within the dispersant. This boundary, referred to as the surface of hydrodynamic shear, serves as the location for measuring the ζ-potential. Understanding the ζ-potential provides valuable insights into the behavior of NPs and their interactions with the surrounding environment.[133,134]

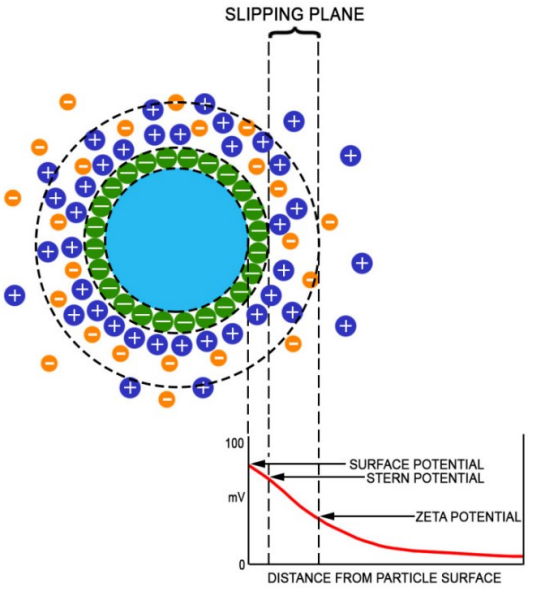

Figure 31: Diagrammatic representation of the electrical double layer. The measurement of electrophoretic mobility, which can be converted to the

zeta potential, is an additional technique for determining the stability of diverse colloidal systems (Matusiak & Grządka, 2017)[135].

The procedure for the measurement of the hydrodynamic diameter and potential is shown in Figure 32. Stock suspensions were prepared by weighing the dry NP powder and suspending it in DW or SDS solution under magnetic stirring, the stock nanoparticle concentration was 0.1 wt%. The NP suspensions were sonicated for 10 min in an ultrasonic bath (Elma Schmidbauer GmbH, Elmasonic Easy model, total power output 100 W, 37 kHz). Dilutions were made from these stock suspensions to obtain the desired NP concentrations for different tests as demonstrated in Figure 32.

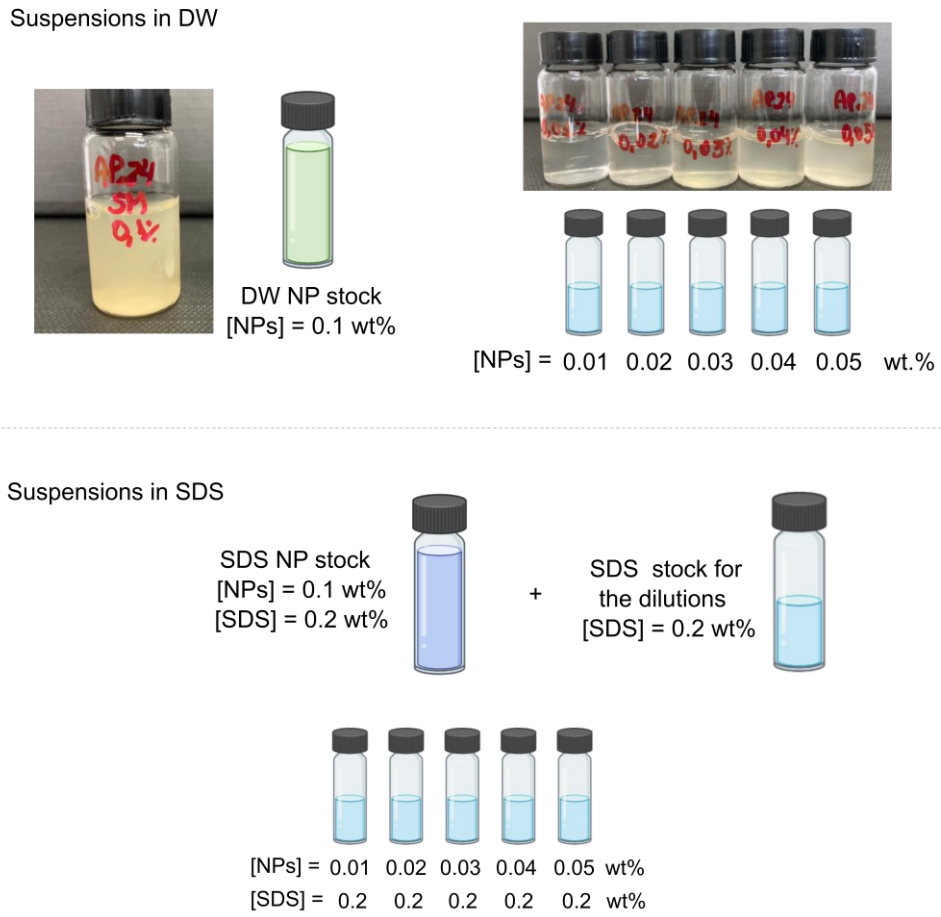

Figure 32: Preparation of the suspensions: an example of FSiNP-NH_2 *(S)* dilutions in DW.

4.3.8. Contact angle

The WORM-FSiNPs were prepared in a stainless-steel cylindrical mold press (Aldrich® macro-micro KBr pellets matrix model, to produce 13

mm diameter pellets) using an automatic hydraulic press (Specac-AtlasTM 8T, Specac Ltd.) under a pressure of 1 ton. The static contact angles were measured using a DSA25 Expert Drop Shape Analyzer (Krüss, Germany) at room temperature. The sessile drop method was used with DW drops with a volume of 6 μL on the surfaces of the tablets (Figure 33). The tablet was placed on the contact angle equipment in the sample port, and the syringe was positioned with a drop generation controller. All measurements were repeated five times and the angles were measured using the mathematical model ellipse (tangent^{-1}).

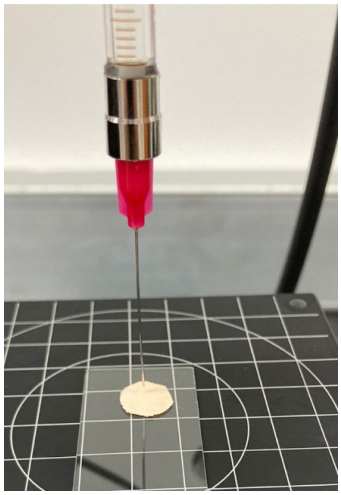

Figure 33: Illustration of how the sessile drop method was used to determine the water contact angle (WCA) on silica pellets.

4.4. Column experiments

Transport experiments were performed using an unconsolidated porous medium prepared by packing glass beads (diameter = 0.4 cm) into a polypropylene column with an internal diameter of 1.37 cm, length of 15.2 cm, and average pore volume (PV) of 10 mL (Figure 34). The unconsolidated porous medium porosity was estimated to be 0.26[136] based on the weight of the dry-packed column and the weight of the column filled with water. The inlet of the packed column was connected to a syringe pump (Pump 11 Plus, EC1 70-2208, Harvard Apparatus, UK), and the outlet was connected to a graduated centrifuge tube to collect the effluent samples. The transport experiment consisted of three stages. First, 100 mL (10 PV)

of DW was injected through the vertically placed packed column at a flow rate of 2 mL/min to displace air bubbles and achieve chemical equilibrium between DW and the glass bead surface. Next, the non-reactive tracer (Li^+) or fluorescent NP suspension was injected through the unconsolidated porous medium at a steady flow rate of 1.0 mL/min, corresponding to a Darcy velocity of 0.17 cm/min (2.8 x 10^{-5} m/s), and effluent samples were collected every 2 mL (0.2 PV). A total of 32 mL (3.2 PV) of each nanofluid was injected during this stage. The final stage consisted of the injection of 4.8 PV to backwash the column and to evaluate the desorption of NPs compared to the non-reactive tracer. All experiments were conducted at ambient temperature (25°C).

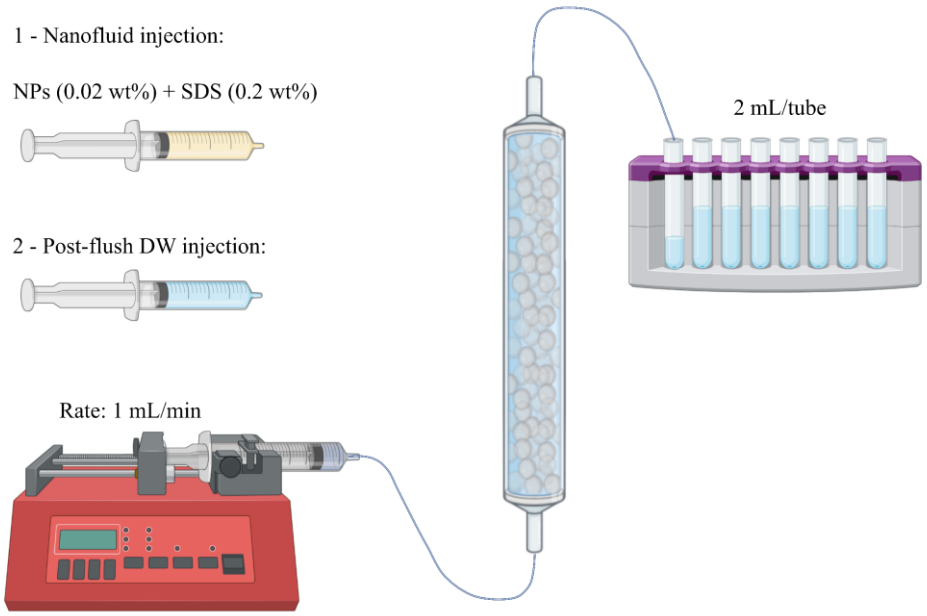

Figure 34: Apparatus set-up and experimental conditions used for the transport study of nanofluids.

Experiments were performed using four nanofluids consisting of 0.02 wt% suspensions of **FSiNP-NH_2** ***(W)*** and **FSiNP** ***(W)*** in SDS solutions (0.2 wt%). The NP concentration was selected to evaluate the suitability of the synthesized fluorescent NPs for quantification and tracer studies at low concentrations, as in typical column transport studies[137], and after the injection of nanofluids in typical reservoir rocks[138]. Quantification of NP concentrations was performed by fluorescence spectroscopy using the response factor (RF) method, RF = I_0/C_0, where I_0 represents the initial

fluorescence intensity of the NP suspension at the working wavelength (517 nm for **FSiNP-NH_2** ***(W)*** and 511 nm for **FSiNP** ***(W)***) and C_0 is the initial NP concentration[139]. The NP concentration in samples collected at different PV was calculated as the sample fluorescence intensity divided by RF, and these values were used to construct the breakthrough curves (BTC) and elution curves (EC). The concentration of the non-reactive tracer was determined by measuring the effluent conductivity (Metrohm 691 pHmeter/conductivimeter) and comparing it with a calibration curve. The values for NP adsorption in the glass bead column were determined by mass balance calculation of the difference between the mass of NP injected into the column (obtained from the initial NP concentration and the injected volume) and the total mass recovered in the effluent stream, considering both breakthrough and elution curves.

5 Results and discussions

The first study objective was to synthesize FSiNPs with structural and colloidal properties and correlating these characteristics to those of commercial SiNP, which would allow the use of these FSiNPs as a representative material for the quantification of SiNP in the form of nanofluid. The chapter is divided into the following sections:

The results and discussion of this first goal are presented in section 5.1.

5.2: Structural assessments such as particle size, surface area, porosity, and colloidal features (hydrodynamic diameter and ζ- potential) in aqueous suspension.

5.3: Testing the core-shell structure and FSiNP aggregation over time through fluorescence emission intensity of the NPs.

5.4: SDS analysis adsorption of positive and negative WORM-FSiNPs.

5.5: Transport experiments using the most promising synthetic FSiNPs to test the hypothesis and evaluate the mobility profile and measure the amount of FSiNPs in the effluent.

5.4: SDS analysis adsorption on positive and negative WORM-FSiNPs.

5.5: Finally, transport experiments were done with the most promising synthetic FSiNPs to test our hypothesis. The mobility profile was looked at, and the amount of FSiNPs in the effluent was measured.

5.1. Synthesis and characterization of surface functional groups of synthesized core-shell nanoparticles

Initially, both the strategic design for the core-shell fluorescent SiNP synthesis and the way that it was structured to accomplish the objective were discussed and explained. Therefore, the chemical and structural characterizations were evaluated, focusing primarily on the surface functional groups using the ninhydrin test, FTIR spectroscopy, and

elemental analysis with commercial SiNP as a reference. Then, the fluorescence properties of the synthesized material were obtained in the aqueous phase, and the results were compared with a FITC solution.

To improve the clarity of this discussion of the results, the following nomenclature was chosen:

FSiNP *(S)*: Silanol coating FSiNPs synthesized via the Stöber method
FSiNP-NH_2 *(S)*: Amino-functionalized FSiNPs synthesized via Stöber
FSiNP *(W)*: Silanol coating FSiNPs synthesized via the WORM method
FSiNP-NH_2 *(W)*: Amino-functionalized FSiNPs synthesized via WORM
Stöber-FSiNPs: FSiNPs pair produced by the Stöber method
WORM-FSiNPs: FSiNPs pair produced by the WORM method

5.1.1. Strategic design for core-shell FSiNPs synthesis

The four fluorescent SiNPs synthesized in this work were designed as core-shell NPs to ensure that the fluorophore remained inside the core, thus protecting the fluorescence signal from possible solvent effects when dispersed in aqueous fluids. Therefore, it was anticipated that the dispersion of these fluorescent NPs in aqueous media would have no impact on their quantification. To obtain the characteristics of non-porous nanoparticles with constant size and shape and targeted surface modification, two FSiNPs were synthesized using the Stöber method and two others using the water-in-oil reverse microemulsion (WORM) approach.

The strategic design for the core-shell shape and surface-targeted groups was the same for both Stöber and WORM:

1) During the FSiNP-negative synthesis, a greater amount of TEOS was employed to produce a coating containing silanol groups and a negative surface charge similar to that of SiNP. As a result, the amount of APTES was reduced and was only intended to serve as a link between the fluorescent moiety and the silica matrix.

2) While the aspect ratio TEOS/APTES was lower for the FSiNP-positive samples, additional APTES was added to the synthesis to graft aminopropyl groups onto the silica surface. Therefore, when dispersed in an aqueous solution, the -NH_2 groups on the surface will be protonated

resulting in a positive charge. The schematic configurations of the four fluorescent NPs synthesized in this study are shown in Figure 35.

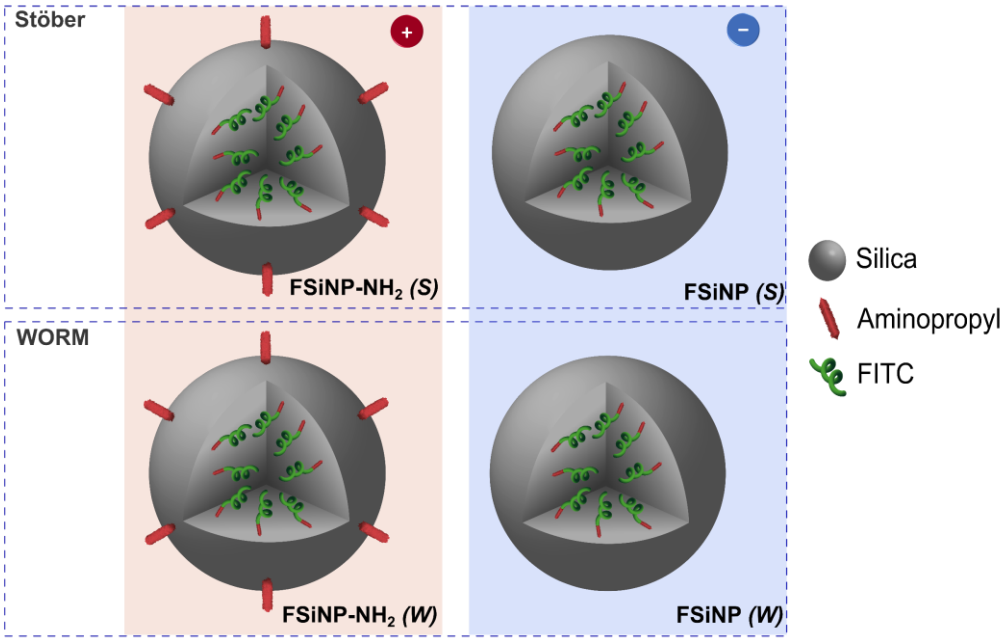

Figure 35: Illustration of the four core-shell structures of the fluorescent NPs synthesized in this study showing the method used to produce FSiNPs, one with a negative surface charge and the other with a positive surface charge.

5.1.2. Chemical and structural characterization

The four fluorescent SiNPs synthesized were first characterized for surface functionalization, which is one of the key features required to evaluate the role of interactions with the anionic surfactant in colloidal stability and transport behavior. The determination of amine content for silica NPs using the ninhydrin test generated a purple color of the ninhydrin-amino complex that is caused by its reaction with amino groups and the quantitative and quantity approaches were reported using this test.[130]

The qualitative results confirmed surface functionalization, indicating the presence of primary amino groups (R-NH_2) on the **FSiNP-NH_2** ***(S)*** and **FSiNP-NH_2** ***(W)*** surfaces (violet color) and the absence of these groups on the **FSiNP** ***(S)*** and **FSiNP** ***(W)*** surfaces (Figure 36). These results indicate that the additional coating of the silanizing agent (TEOS) produced

negative-FSiNP particles, resulting in the absence of amino groups on the surface. As expected, the color of commercial SiNP used as control did not change when exposed to the reagent, while the SiNP-NH_2 used as a positive reference turned violet.

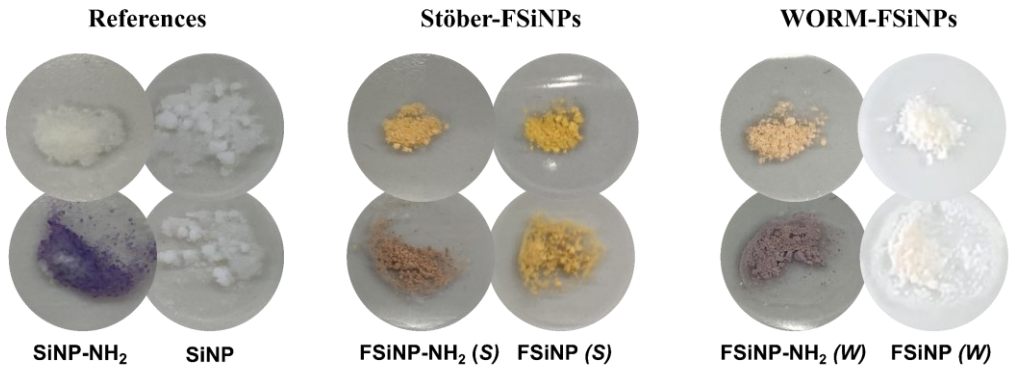

Figure 36: Identification of aminopropyl groups on the silica surface by the ninhydrin test for SiNP-NH_2 (amino-functionalized, as positive control sample), SiNP (unmodified, as negative control sample), and fluorescent nanoparticles synthesized.

Elemental analysis of the samples complemented these results, showing significant amounts of organic matter (C, H) in the synthesized fluorescent NPs compared to commercial samples due to the presence of aminopropyl and FITC groups. Since negative-FSiNPs synthesis uses less dye and is coated by TEOS to create a surface with only silica groups, the lower amount of CHN is more comparable to SiNP. The highest CHN concentrations were found in **FSiNP-NH_2** ***(W)*** and **FSiNP-NH_2** ***(S)***, which is consistent with the strongest N-H and C-H bands found for those NPs in the ATR-FITR analysis as discussed in the next section.

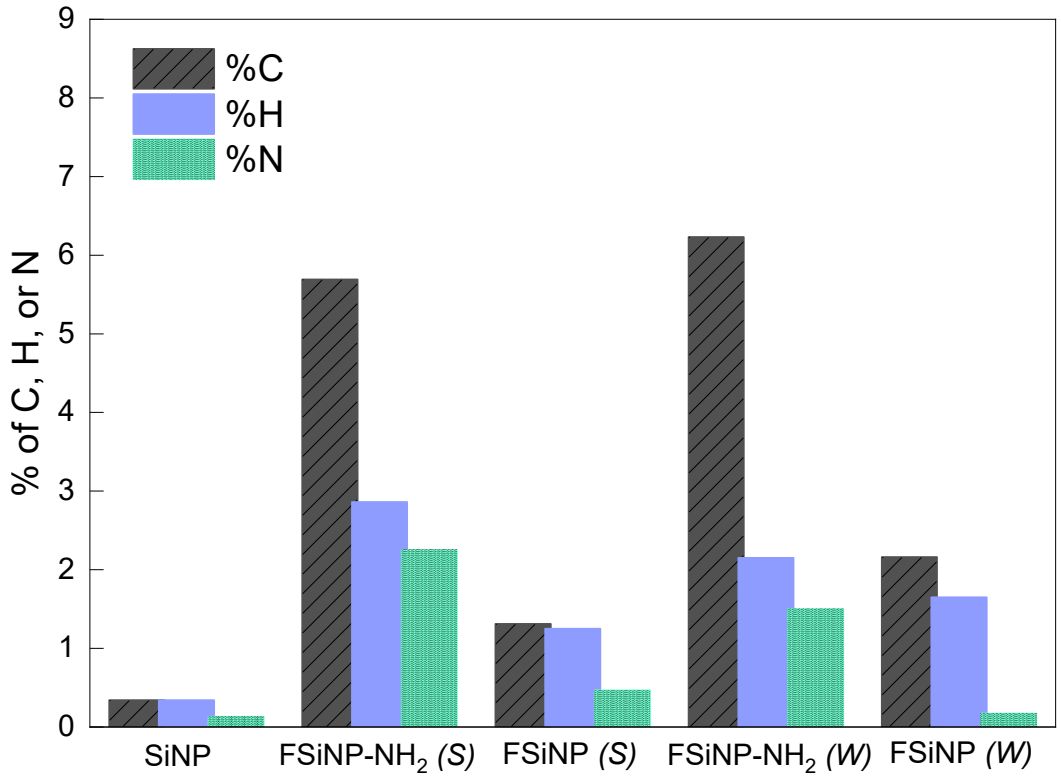

Figure 37: Elemental analysis through CHN of the Stöber and WORM-FSiNPs.

Further characterization of the functional groups present in the fluorescent NPs was performed using ATR-FTIR spectroscopy (Figure 38 and Table 11). All the NPs presented a band related to Si-OH asymmetric bending and a stretching vibration peak at 970 cm^{-1}, confirming the presence of hydroxyl groups on the surface of the silica nanoparticles produced by TEOS hydrolysis. Strong Si-O-Si stretching vibration peaks (ν_{as}~1055 cm^{-1}, ν_{s}~794 cm^{-1}) were observed for all the FSiNPs typical of silica structures. The broad bands at 3700 and 3000 cm^{-1} correspond to O−H stretching and adsorbed water, with a greater proportion in **FSiNP *(W)***, suggesting a greater number of silanol groups on the NP surface. In addition to these silica-characteristic signals, new bands were observed in the **FSiNP-NH₂ *(S)*** and **FSiNP-NH₂ *(W)*** spectra at ~1555 and ~2940 cm^{-1}, attributed to the typical bending vibrations of N-H and C-H stretching, respectively, of the aminopropyl groups from APTES. Notably, these two bands appear only in the infrared spectrum of the positive-FSiNP, which confirms the efficiency of the surface coverage of negative-FSiNP with TEOS, in agreement with the elemental analysis results. Furthermore, none

of the obtained NPs displayed a band between 1787 and 2166 cm^{-1}, which is related to the stretch vibration of the N−C=S group present in the FITC precursor,[140] demonstrating the absence of isothiocyanate groups and excluding the presence of molecular fluorophores not bonded to the APTES groups on the surface of the synthesized NPs.

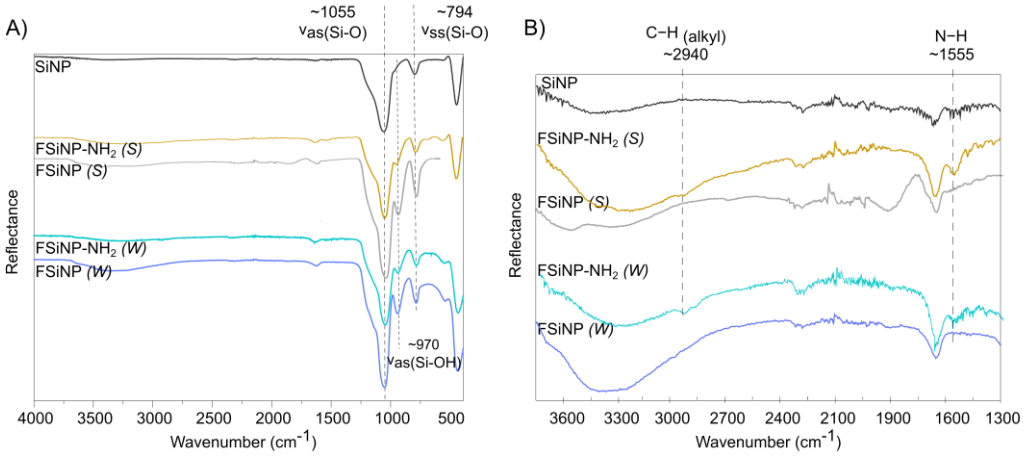

Figure 38: FTIR-ATR spectra of the synthesized FSiNPs (A) highlighting the characteristic bands used for surface functional group identification (B). Bare commercial SiNP were included for comparison.

Table 11: Summary of the molecular attributions of the vibrational bands and their respective bonds of FSiNPs determined by FTIR

		Stöber		WORM	
Wavenumber (cm^{-1})	Molecular attribution	$FSiNP\text{-}NH_2$ *(S)*	FSiNP *(S)*	$FSiNP\text{-}NH_2$ *(W)*	FSiNP *(W)*
970	$\nu_{as(Si-OH)}$	✓	✓	✓	✓
794	$\nu_{ss(Si-O)}$ of Si−O−Si	✓	✓	✓	✓
1055	$\nu_{as(Si-O)}$ of Si−O−Si	✓	✓	✓	✓
1555	N−H	✓		✓	
2940	C−H (alkyl)	✓		✓	
1787/2166	N−C=S				

5.1.3. Partial conclusion

It was confirmed that the strategic design of the core-shell fluorescent SiNP synthesis was successful in producing four different NPs with different surface charges and functional groups using the Stober and WORM methods. The produced NPs' surface functionalization was supported by the ninhydrin test and ATR-FTIR spectroscopy. The presence of primary amino groups was confirmed on the **FSiNP-NH_2** ***(S)*** and **FSiNP-NH_2** ***(W)*** surfaces, while the **FSiNP** ***(W)*** and **FSiNP** ***(S)*** surfaces were found to be free of these groups. The elemental analysis further supported the presence of organic matter in the synthesized fluorescent NPs due to the presence of aminopropyl and FITC groups.

5.2. Size, surface area and colloidal properties

One of the predominant properties of NPs is their tendency to agglomerate.[141] Even if stable in a determined condition, SiNP can quickly lose stability as a colloidal suspension in a new environment, a common scenario in EOR applications. Hence, it is important to evaluate the presence of agglomerates and how the aggregation can impact the interaction of SiNP in the development of a quantitative approach. So, structural assessments such as particle size, surface area, porosity, and colloidal features (hydrodynamic diameter and ζ- potential) in aqueous suspension were performed and correlated with the data from the commercial SiNP.

5.2.1. Electronic microscopy and gas adsorption

The fluorescent NPs were described in terms of physicochemical properties relevant to their transport and possible retention in porous media, such as size and specific surface area, and the results were compared with those of commercial SiNP (Figure 39) with a nominal size of 13 ± 1 nm, typically used in most reports to assess the suitability of the synthesized fluorescent NPs as model tracers for this type of study.

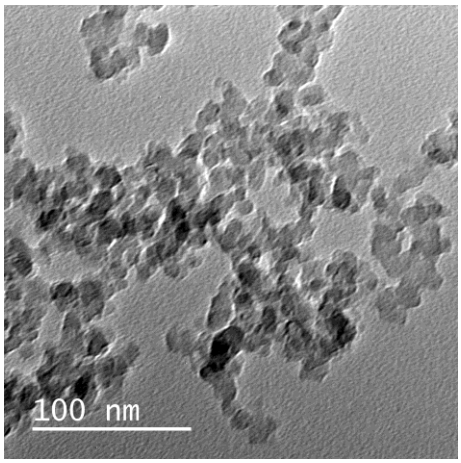

Figure 39: Commercial SiNP TEM image.

The morphology and size distribution of the synthesized NPs were primarily obtained by SEM and the images of the Stöber-FSiNPs are shown in Figure 40. It was observed **FSiNP-NH_2 *(S)*** shows very distinct NP sizes, as well as the presence of irregular *quasi*-spherical silica nanoparticles and a lack of sphericity. The NP size diameter ranged widely from 50 to 500 nm. Also, the NPs formed aggregates of several nanoparticles, which is normal in NP microscopic images. Similarly, **FSiNP *(S)*** had good sphericity, but bimodal populations, with an average diameter of 50 ± 12 and 230 ± 36 nm.

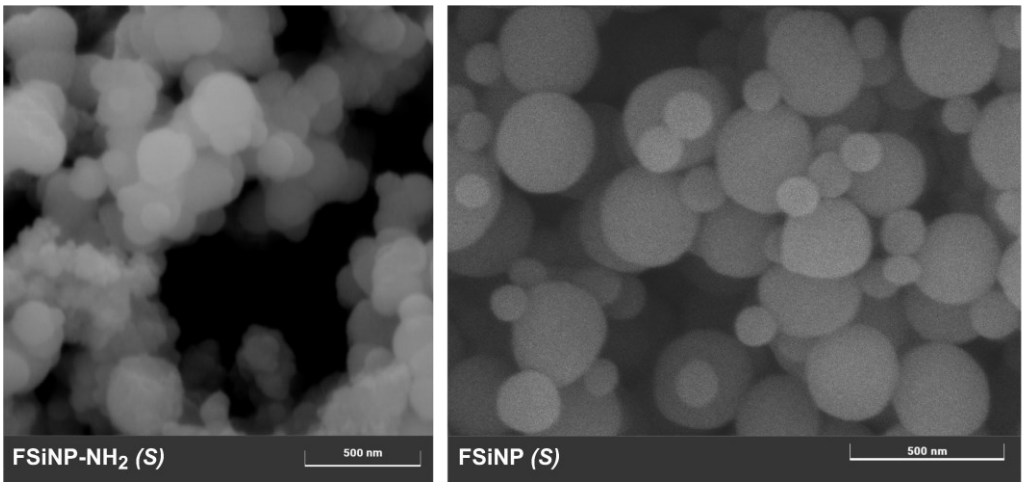

Figure 40: SEM images of FSiNP-NH_2 *(S)* and FSiNP *(S)*, synthesized by the Stöber method.

The prepared WORM-FSiNPs were spherical and monodisperse with an average diameter of 64 ± 9 nm for **FSiNP *(W)*** and 86 ± 23 nm for **FSiNP-NH_2 *(W)*** (Figure 41). Both sizes were below 100 nm, which is consistent

with reported values for core-shell fluorescent nanoparticles[104,142,143] typical use in nanofluid applications[144]. In contrast to the Stöber-FSiNPs results, the WORM method shows an advantage in producing more homogeneous NPs as well as distribution sizes, according to the review of these synthesis methods in section 3.4.1.2. Although the size of **FSiNP *(W)*** and **FSiNP-NH_2 *(W)*** was larger than that of commercial SiNP (13 ± 1 nm), all the values were within the typical range size used in nanofluid applications.[144]

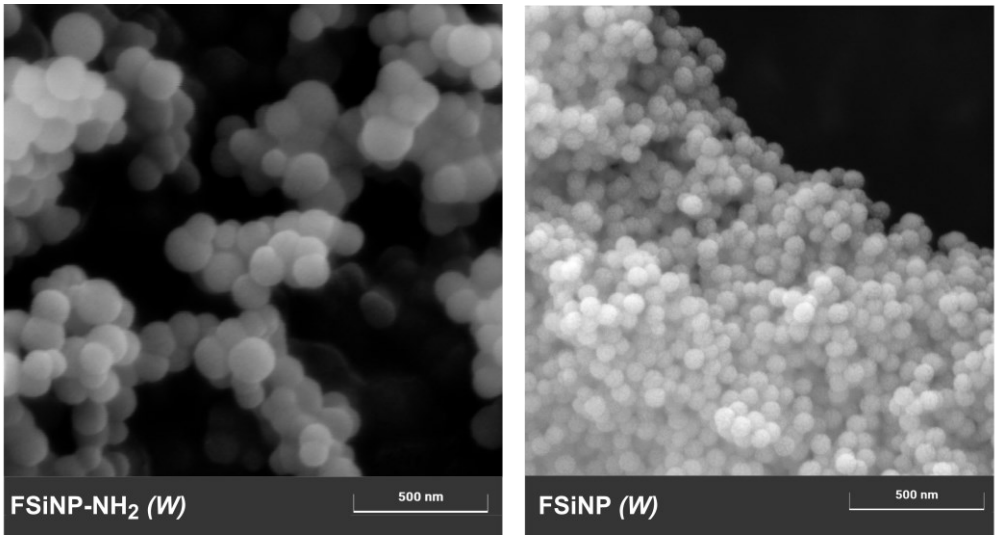

Figure 41: SEM images of FSiNP-NH_2 *(W)* and FSiNP *(W)* synthesized by WORM method.

The surface area and porosity were analyzed using an N_2 adsorption/desorption isotherm, with the BET analysis and the textural properties reported in Figure 42 and Table 12, respectively. The specific surface areas (SSA_{BET}) obtained agreed with the microscopy results, showing the smallest values for **FSiNP-NH_2 *(S)***, **FSiNP *(W),*** and **FSiNP-NH_2 *(W)*** given their larger nominal diameters and smaller areas than the commercial SiNP. The adsorption isotherms exhibited typical type III behavior for all the NPs, with slow adsorption at low pressures, followed by

multilayer formation at higher pressures, indicating weak interactions of the gas with the NP surface as can see in Figure 42A.

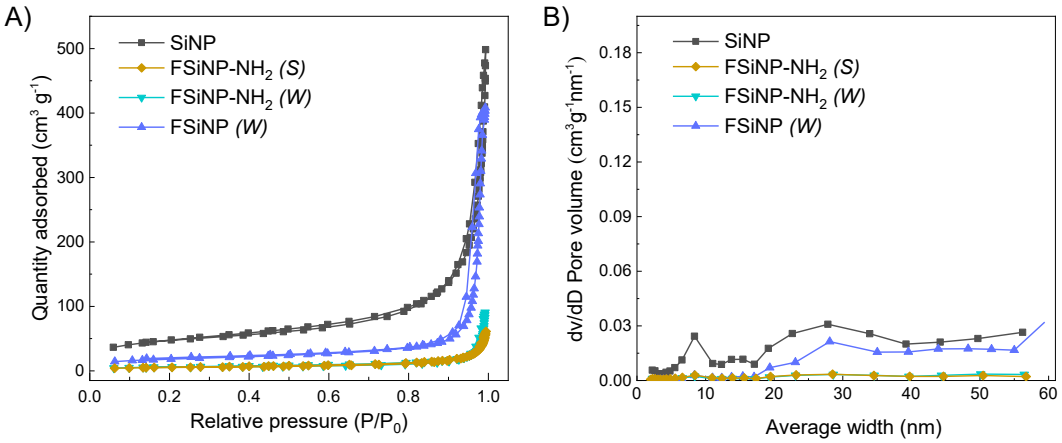

Figure 42: Nitrogen adsorption-desorption isotherm of FSiNPs (A) by BET and, their porosity was evaluated through the BJH method (B).

Furthermore, the analysis of pore size distribution using the BJH method showed no adsorption on specific pore sizes, confirming the non-porous nature of the fluorescent NPs synthesized (Figure 42B). This is important because there is a higher probability of fluorophore leaching when using mesoporous NPs which exhibit an open pore structure that allows water access.[145]

Table 12: Surface area analysis of the synthesized FSiNPs

Samples	SSA_{BET} (m^2g^{-1})	$V^{BET}_{total\ pores}$ (cm^3g^{-1})	$V^{BJH}_{mesopores}$ (cm^3g^{-1})
SiNP	171.9	0.34	0.0086
FSiNP-NH_2 *(S)*	20.22	0.04	0.0038
FSiNP-NH_2 *(W)*	22.77	0.04	0.0000
FSiNP *(W)*	64.37	0.17	0.0058

To complete the characterization and as a complement to the micrography data, the particle size distribution is shown by intensity for the four FSiNPs and the SiNP reference in Figure 43. Even though SiNP has a nominal diameter of 12 nm by the fabricant, DLS demonstrates their hydrodynamic diameter is *ca.* 340 nm and shows a broad profile of the number of nanoparticles. This data indicates that the SiNPs aggregate

resulting in different large-sized nanoparticles. Nanoparticle aggregation is a spontaneous process that occurs with the synthesized NPs and the commercial sample. Furthermore, NP aggregation was observed in suspension in DW in all cases, as evidenced by the larger values of D_H (*ca.* 120–1200 nm). Specifically, the **FSiNP-NH₂ *(S)*** had a bimodal hydrodynamic diameter confirming the heterogeneity obtained in SEM analysis. Although **FSiNP *(S)*** NPs display bimodal primary size distributions in MEV images, the distribution of D_H by DLS appears to be monodispersed. An analysis of three SiNPs was conducted and TEM images provided clear evidence that all samples exhibited a bimodal population. In contrast, the DLS technique was unsuccessful in addressing the discrete size fractions in all three cases.[146]

These results show that synthesized WORM-FSiNPs and the negative Stöber-FSiNP have D_H in the same order as SiNP but with a slightly lower PDI. This means that FSiNPs are scattered in a narrower particle size distribution than commercial SiNP. The direct impact of these findings is that the size distribution of the FSiNPs may not fully represent the size distributions of commercial SiNP, but still represent a similar particle size.

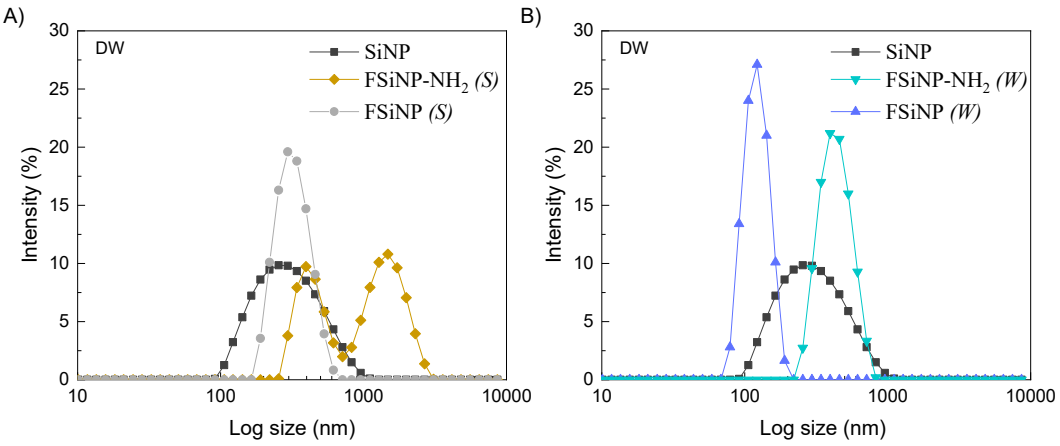

Figure 43: Distribution of the hydrodynamic diameter by intensity for the Stöber-FSiNPs (A) and WORM-FSiNPs (B) in DW. It is notable for its bimodal size distribution in the FSiNP-NH2 *(S)* sample, which correlates with particle size analysis via MEV.

In summary, it is important to highlight that the variations in nominal size and surface area between the FSiNPs do not directly affect the number

of surface groups. This is because different functional groups were intentionally introduced onto the surface of each nanoparticle via distinct synthetic methods. The objective of incorporating these different functional groups was to enable diverse interactions with the anionic surfactant, which was assessed by examining the colloidal stability

The similarity between the synthesized FSiNPs in the adsorption/desorption phenomenon, as studied by BET, is relevant for understanding the results from transport experiments considering only their colloidal behavior in aqueous fluids, and not the possible influence of the size, shape, and porosity of the nanomaterials.[141] In contrast to the remaining samples, **FSiNP-NH_2** ***(S)*** exhibits irregular quasi-spherical silica nanoparticles with varying sizes, as determined by DLS and SEM analyses in aqueous and dry states, respectively. As per the methodology outlined in section 4.2.4 of the Materials and Methods, these FSiNPs were excluded from subsequent evaluations.

5.2.2. Colloidal stability in DW

The near-surface region structure and water molecules determine silica dispersion stability. The interparticle forces are regulated by the equilibrium between attractive (vdW) and repulsive (EDL) forces. Hydrophobic force binding siloxane groups attract and deprotonated silanol groups repel the silica nanoparticle without modifications. Some silanols can form strong hydrogen bonds with water at the water interface, but this cannot guarantee colloidal stability.[147,148]

Therefore, the colloidal stability of the NPs dispersed in DW was evaluated, considering the effect of possible aggregation on fluorescence stability and intensity over time.[149] The hydrodynamic diameter (D_H) and ζ-potential of the negative **FSiNP** ***(S)*** and the WORM-FSiNPs were determined and compared with those of commercial SiNP (Table 13). In 0.01 wt% all the D_H values presented a PDI below 0.4 as well as demonstrated in Figure 44. The reproductivity from the correlation coefficient curves and size distribution of the NPs indicated that the NPs were moderately polydisperse in the solutions, allowing a reliable DLS

analysis.[134] NP aggregation was observed upon suspension in DW in all cases, as evidenced by the larger D_H (*ca.* 120–460 nm) in comparison with the nominal values obtained by TEM/SEM (*ca.* 12–260 nm).

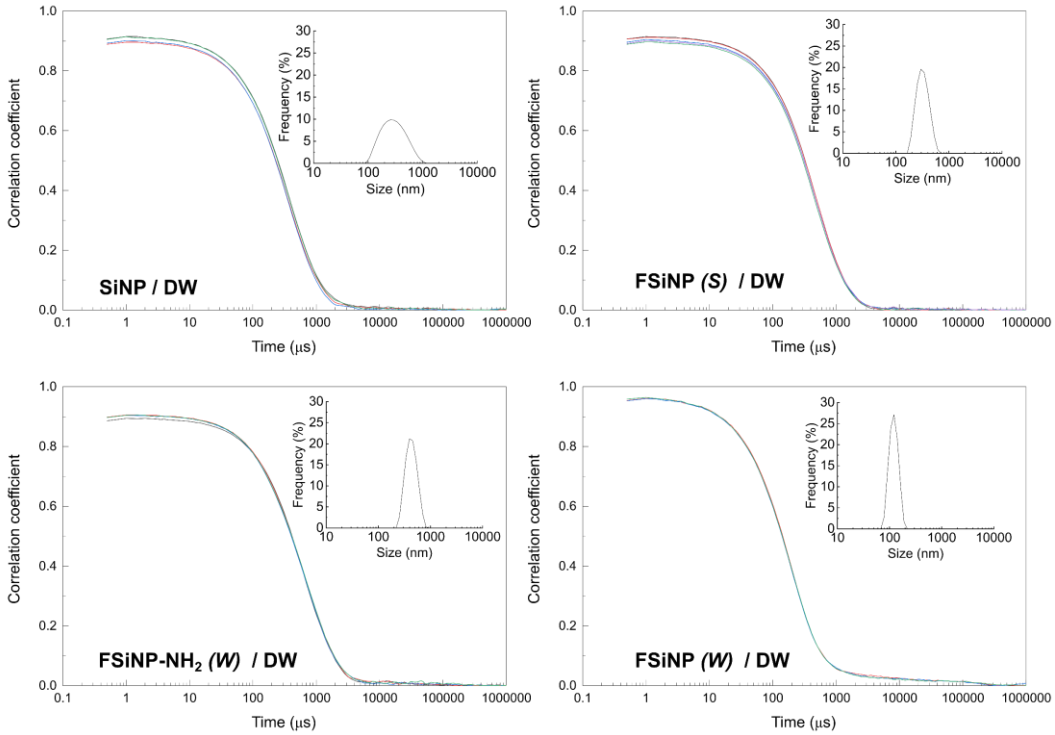

Figure 44: Correlation coefficient and size distribution of the fluorescent NPs (0.01 wt%) in DW.

The highest values were obtained for **FSiNP-NH_2 *(W)***, probably because the presence of aminopropyl groups on the surface increased the hydrophobicity of the NPs, confirmed by the WCA measurements: 32 ± 4° for **FSiNP *(W)*** and 42 ± 5° for **FSiNP-NH_2 *(W)*** (Figure 45) promoting aggregation in polar media, such as DW. This is in accordance with the literature on the data. SiNPs that were amino-functionalized through co-condensation and had surface coverage by $–(CH_2)_3NH_2$ groups exhibited a WCA of 46°, whereas those with Si-OH surface coverage displayed a WCA of 35°, indicating that amino groups result in a more hydrophobic nature of the NPs when compared to the typical silanol of SiNPs.[150] Nevertheless, all the D_H values were within the colloidal range typical for NP suspensions used in EOR[126], and much lower than the average pore throats (6.72 μm) of Berea Sandstones with medium permeability[151].

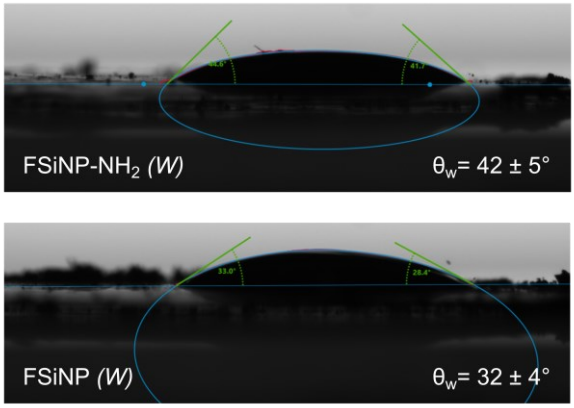

Figure 45: Contact angle measurement of a water drop on a pellet prepared with the WORM-FSiNPs.

Furthermore, it was observed that the positive and negative WORM-FSiNPs maintained good colloidal stability in the aqueous medium, as evidenced by the absence of significant changes in D_H despite a five-fold increase in concentration. Nonetheless, the Stöber-FSiNP exhibits significant instability, as evidenced by both the D_H and PDI values for a concentration of 0.05 wt% which reached 0.743, indicating a high degree of polydispersity.

Table 13: Hydrodynamic diameter (D_H) and ζ-potential of NPs in aqueous suspensions

	D_H (nm)		ζ (mV)	
	0.01 wt% (PDI)	0.05 wt% (PDI)	0.01 wt%	0.05 wt%
SiNP	294 ± 14 (0.340)	292 ± 33 (0.249)	−23 ± 2	−24 ± 1
FSiNP *(S)*	350 ± 7 (0.218)	600 ± 52 (0.743)	−26 ± 1	−29 ± 2
FSiNP-NH_2 *(W)*	458 ± 9 (0.286)	459 ± 9 (0.214)	+20 ± 1	+30 ± 1
FSiNP *(W)*	120 ± 2 (0.293)	109 ± 3 (0.229)	−36 ± 1	−33 ± 2

It was anticipated that the surface loads, represented here by the ζ-potential, of the FSiNPs would vary according to the type of functional group attached to the NPs' surfaces, given that the NPs were modified using different synthesis strategies. The D_H results were complemented by the ζ-potential values, as an indication of the surface charges on the NPs owing to the presence of functional groups (Table 13). The NPs SiNP, **FSiNP *(S)***, and **FSiNP *(W)*** presented negative ζ-potential values typical of silanol groups on silica surfaces[152] as the dispersion solutions were between 6.6 to 7.0. At pH values above the isoelectric point (IEP), which is between pH 2 and 3.5[153], the silanol groups undergo surface deprotonation. The higher value observed for the **FSiNP *(W)*** (−36 mV) can explain the small D_H obtained in comparison with the other NPs because a higher surface charge enhances NP suspension and colloidal stability in the solution.

In the case of **FSiNP-NH_2 *(W)***, positive ζ-potential values were obtained (+20 mV) in agreement with the protonation of the amino groups (pKa ≈ 9.8,[113]) on the silica surface upon suspension in DW. Notably, the positive ζ-potential values also confirmed the large functionalization obtained with the synthetic procedure used because the net surface charge is due to the presence of basic aminopropyl (-NH_3) and acid silanol (-OH) groups on the surface of **FSiNP-NH_2 *(W)***. All NPs schematically illustrated the surface groups' behavior in the aqueous dispersion in Figure 46.

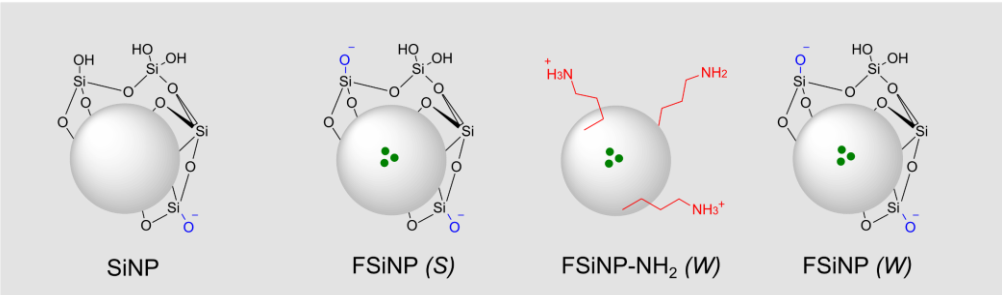

Figure 46: Schematic of FSiNPs based on the ζ-potential data generated by the majority of the surface functional groups.

5.2.3. Partial conclusion

All the materials, except **FSiNP-NH_2 *(S)***, had the same value range of size distribution as SiNP in DW, replicating the colloidal characteristics

exhibited by conventional commercial SiNP regardless of how differently the materials were synthesized to obtain the desired features (core-shell format and different surface groups). The surface charges of the NPs were determined by the presence of the targeted functional groups, -OH or -NH_2, serving as evidence of synthetic strategy validation. **FSiNP** ***(S)*** and ***(W)*** presented negative ζ-potential values, typical of surface silanol groups, while positive ζ-potential values were obtained for **FSiNP-NH_2** ***(W)***, in agreement with the protonation of the amino groups.

Even though the commercial SiNP exhibited a nominal size significantly smaller than that of the synthetic FSiNPs, their hydrodynamic sizes were comparable in aqueous environments. **FSiNP-NH_2** ***(S)*** was an exception, it shows an irregular form and multiple populations, a disadvantage previously reported in literature for the sol-gel method and confirmed for this specific synthesis. In the WORM method, FSiNPs were produced in a controlled ambient environment with surfactant and co-surfactant. In conclusion, the WORM method is superior for FSiNP fabrication, particularly in terms of NP size and shape. Different NP sizes can result in distinct transport and retention characteristics for the same system, making this parameter crucial.

5.3. Fluorescence properties and analysis

The analysis and fluorescence properties of the synthesized FSiNPs are the main subject of investigation in section 5.3. The excitation and emission spectra of the NPs in DW for the Stöber and WORM-FSiNPs are discussed, as well as the synthesis and characterization of a novel nanoparticle, namely **FSiNP-NH_2-F** ***(S)***, by the Stöber method to provide a comparative analysis of **FSiNP** ***(S)*** to assess the efficacy of the synthetic strategy employed. The investigation related to the temporal evolution of fluorescence were obtained and discussed correlated with the colloidal stability as well as the synthetic performance.

5.3.1. Fluorescence properties

The four fluorescent NPs synthesized were designed as core-shell particles to ensure that the fluorophore remained inside the core when the NPs were used as nanofluids. The emission and fluorescence spectra of the NPs suspensions in DW for the Stöber-FSiNPs (Figure 47A) and WORM-FSiNPs (Figure 47B) all exhibited excitation maxima between 487 and 494 nm (related to π-π* transitions in the FITC molecule) and maxima range from 511 to 517 nm (Table 14).

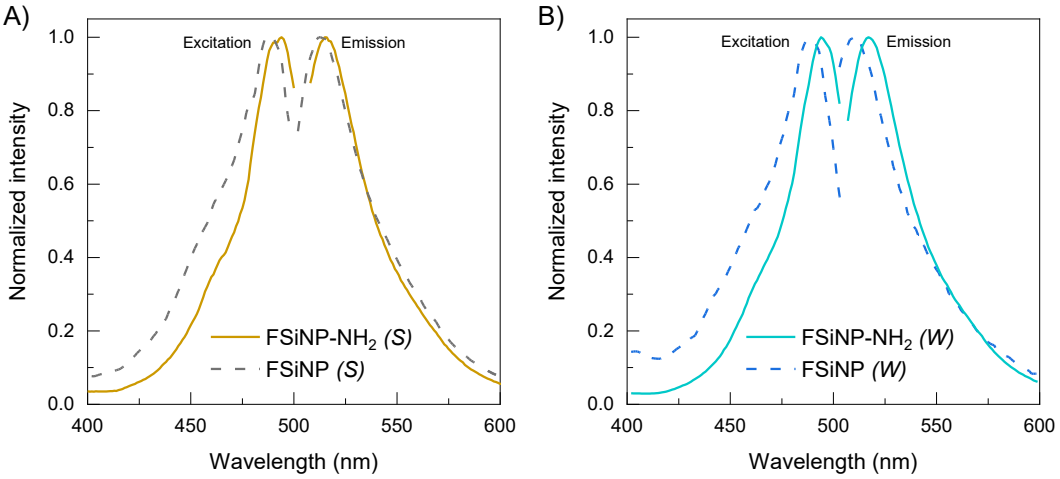

Figure 47: Excitation and emission fluorescence spectra of FSiNP-NH_2 *(S)* and FSiNP *(S)* (A) and FSiNP-NH_2 *(W)* and FSiNP *(W)* (B), normalized by their emission and excitation maxima in aqueous dispersion.

The slight difference in the emission maxima between the NPs (almost constant Stokes shift values) suggests that the presence of different surface groups on the SiNP and the synthesis type did not significantly affect the emission profile of the fluorophore. It was also comparable to that of free FITC which shows excitation and emission at 495 and 510 nm, respectively. Moreover, the similarity of all the emission profiles with that of FITC showed that there was no interference of the solvent, confirming that the suspension of the fluorescent NPs in the nanofluid preparation would not interfere with their quantification. This result is in agreement with other studies reporting that the silica network can act as a protective coating for the fluorophore, thus preventing direct interaction with the medium, and avoiding fluorescence quenching[144].

Table 14: The maxima excitation and emission wavelength of the synthesized FSiNPs in aqueous suspension

	Stöber		WORM	
	FSiNP-NH_2 *(S)*	FSiNP *(S)*	FSiNP-NH_2 *(W)*	FSiNP *(W)*
$\lambda_{exc}^{max}(nm)$	494	487	494	488
$\lambda_{emi}^{max}(nm)$	515	513	517	511

Overall, these results demonstrate the efficiency of the synthetic strategy used in this work to obtain silica-based fluorescent NPs with similar cores but different surface groups, which resemble typical commercial SiNPs used in most nanofluid applications. Therefore, the characterisation of their colloidal and transport behaviours was mainly based on the different properties and interactions in the solution of the functional groups on the silica surface.

5.3.2. FSiNP-NH_2-F *(S)* synthesis and characterization

The location of the fluorophore in the core of the synthesized NPs was designed to protect the fluorescence response from solvent effects in studies of aqueous fluids. Therefore, changes in the intensity of the emission maximum of the fluorescent NPs spectra were expected to be affected only by the colloidal stability of the NPs in solution during the experiment. However, before evaluating these results, **FSiNP-NH_2-F *(S)*** was synthesized via the Stöber method for comparison with **FSiNP *(S)*** to evaluate the strategic synthesis, although **FSiNP-NH_2-F *(S)*** was intentionally prepared in a different form than the core-shell.

Figure 48A is an illustration of the **FSiNP-NH_2-F *(S)*** configuration from a distinct synthetic strategy based on the work of Oliveira et al.[129]. First, FITC and TEOS were added simultaneously, followed by the late addition of APTES. This configuration has an even distribution without the concern of hiding the dye from the surrounding environment. The NP characterization verified the dispersion characteristics, their behavior like that of commercial SiNP, and how exposure of the fluorescent dye can affect the emission response over time.

The ninhydrin test (Figure 48B) of **FSiNP-NH$_2$-F *(S)*** indicated the presence of amines on the nanoparticle surface. In addition, the more intense color development indicated the presence of more amine compared with the previous synthesis. This is in line with the elemental analysis (Table 15A) as **FSiNP-NH$_2$-F *(S)*** shows a higher nitrogen percentage.

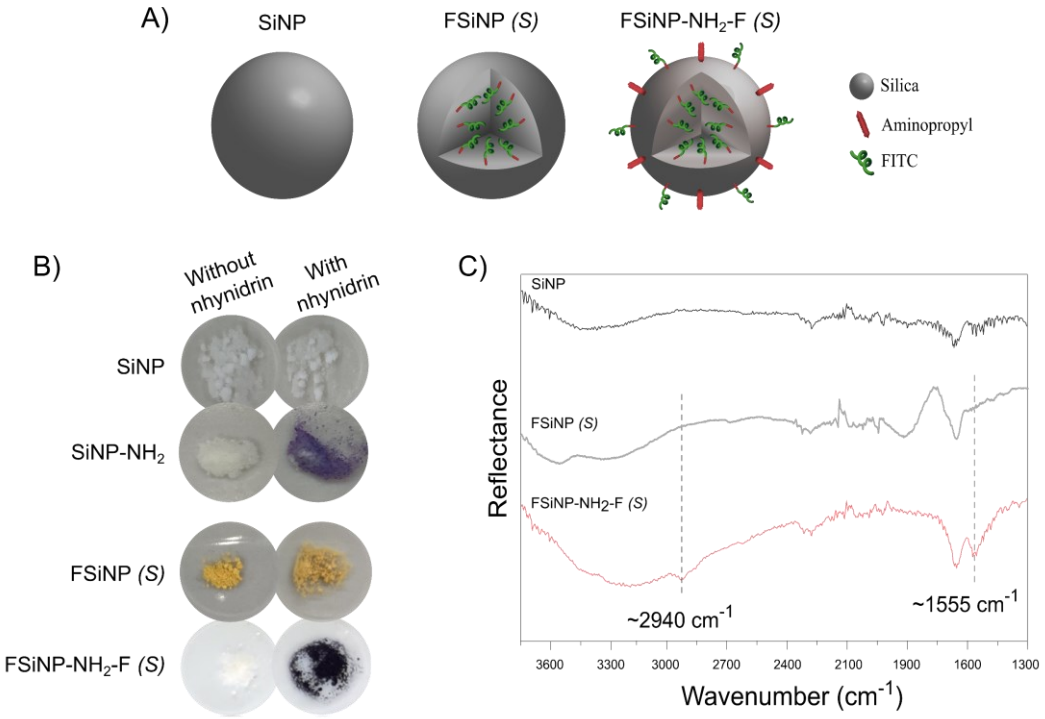

Figure 48: Illustration of the design for FSiNP-NH$_2$-F *(S)* compared to FSiNP *(S)* and SiNP (A). Ninhydrin test with the SiNP and SiNP-NH$_2$ as negative and positive control samples, respectively (B), and FTIR (C).

The FTIR analysis (Figure 48C) also supports the previous results showing that **FSiNP-NH$_2$-F *(S)*** contains the aminopropyl bands (C−H and N−H). The results from the beginning of the analysis (400 – 1300 cm^{-1}) were omitted because they were identical to those of the other silica nanoparticles, emphasizing those that were more significant for the discussion.

Figure 49A of the TEM images for **FSiNP-NH$_2$-F *(S)*** shows that the first image presents a size of 15 ± 2 nm, which is less dense and poorly defined compared to the SiNP image. The second lower zoom image shows larger NPs with sizes up to 200 nm. **FSiNP-NH$_2$-F *(S)*** was the third Stöber-FSiNP to be synthesized and produced NPs of non-uniform size.

Data from the N_2 adsorption and desorption are shown in Table 15B and Figure 49B/C. The SSA_{BET} is similar between SiNP and **FSiNP-NH$_2$-F *(S)*** because they have comparable particle sizes on a certain scale. However, **FSiNP-NH$_2$-F *(S)*** shows a total pore volume by BET of 0.64 $cm^3 g^{-1}$, which may be related to the larger particles observed in TEM images or even fulfill empty spaces between the NP aggregates.

Table 15: Elemental analysis (A) and N_2 adsorption (B) data from the characterization of FSiNP *(S)* and FSiNP-NH$_2$-F *(S)* using SiNP as a reference

A)	Elemental analysis		
	%C	%H	%N
SiNP	0.34	0.34	0.13
FSiNP *(S)*	1.31	1.25	0.46
FSiNP-NH$_2$-F *(S)*	8.14	2.73	2.92
B)	N_2 adsorption/desorption		
	SSA_{BET} $(m^2 g^{-1})$	$V^{BET}_{total\ pores}$ $(cm^3 g^{-1})$	$V^{BJH}_{mesopores}$ $(cm^3 g^{-1})$
SiNP	172	0.34	0.0086
FSiNP-NH$_2$-F *(S)*	167	0.64	0.0000

As discussed in section 4.3.6, the shape of the SiNP isotherm is very similar to that of a type III isotherm showing weak interaction with nitrogen, while for **FSiNP-NH$_2$-F *(S)***, the shape is according to a type V. However, there is a similarity between type V and III at the beginning of the isotherms and as p/p_0 increases, the clustering of molecules is followed by pore filling for type V. Type V isotherms are observed during water adsorption on hydrophobic microporous and mesoporous adsorbents[131]. Figure 49C/D presents the data for the silica gel, showing typical type IV isotherms that are given by mesoporous adsorbents. **FSiNP-NH$_2$-F *(S)*** and silica gel show hysteresis-type H1 loops with a narrow range of uniform mesopores like templated silicas[131].

Another way of acquiring texture information is by the adsorption pore volume versus width diameter graphic (Figure 49C). For **FSiNP-NH$_2$-F *(S)***, a broad distribution centered around 19 nm is observed, while similar behavior occurs with the silica gel with a porous diameter centered at 8 nm, though narrower. This adsorption behavior of **FSiNP-NH$_2$-F *(S)*** may be associated with pores from larger particles shown in TEM images or even fill the voids between the aggregates of small particles. The latter hypothesis has been reported in the literature for several SiNPs, where the adsorption pore volume was ascribed to interparticle pores.[154]

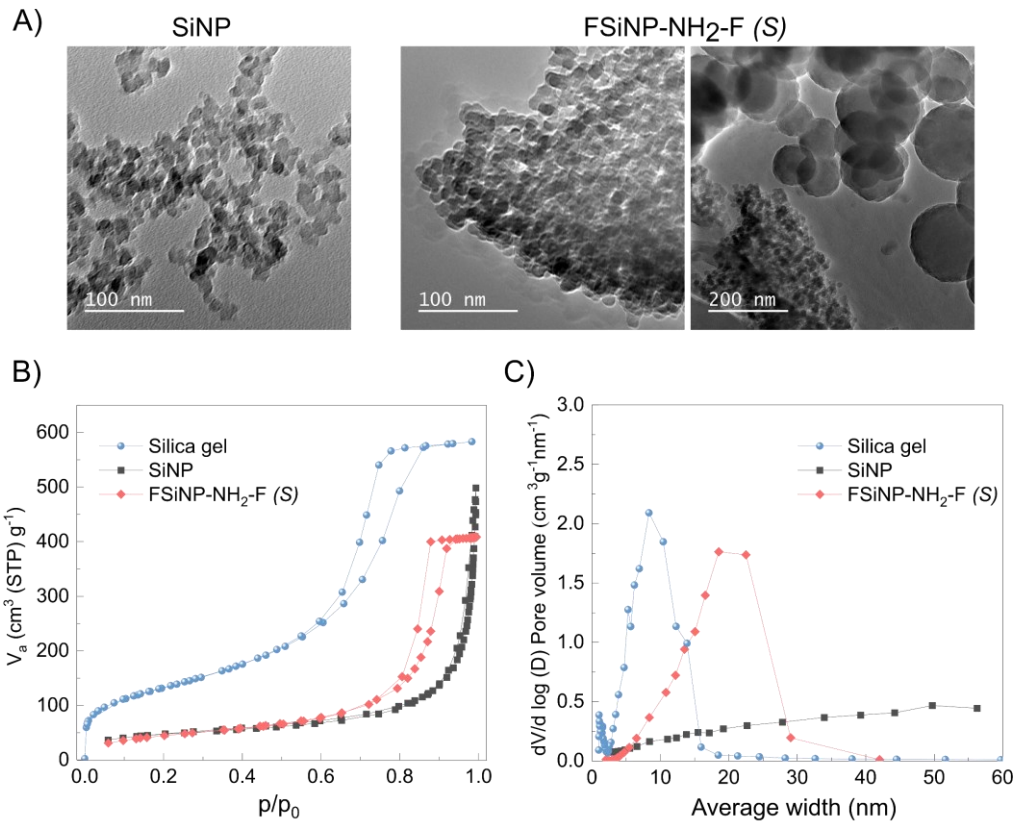

Figure 49: (A) TEM images of SiNP, FSiNP-NH$_2$-F *(S)*, and FSiNP-NH$_2$-F *(S)* with two distinct scale bars (100 nm and 200 nm). (B) N_2 adsorption/desorption to SiNP, silica gel, and FSiNP-NH$_2$-F *(S)*, silica gel as a sample for the hysteresis comparison; and (C) the BJH method to assess porous diameters.

Table 16 presents the colloidal proprieties of this new FSiNPs, as well as for SiNP and **FSiNP *(S)*** for comparison. **FSiNP-NH$_2$-F *(S)*** presents the positive zeta potential value (+20 ± 1 mV), indicating the presence of

protonated amino groups from APTES on the surface. Initially, the higher zeta potential was expected for **FSiNP-NH_2-F *(S)*** due to the higher N content confirmed by the ninhydrin test and supported by CHN because of more R-NH_2 groups on the surface. However, there is a possibility of the dye compensating for the surface charge, by phenoxide and carboxylate group from the fluorescein dye at pH 6.4.[155] According to the pH of the solution, FITC can exist in dianionic, monoanionic, cationic, or neutral forms. The monoanionic and neutral forms are related to the equilibrium with a low quantum yield, while the dianionic form with a large quantum yield[155]; another clue that the core-shell design is preferable. This hypothesis can explain the lower zeta potential because the dye can compensate for the charge from aminopropyl on the surface.

Table 16: Colloidal proprieties of FSiNP *(S)* and FSiNP-NH_2-F *(S)* using SiNP as reference.

	Colloidal proprieties		
	wt%	D_H (nm)	ζ-potential (mV)
SiNP	0.01	294 ± 14	−23 ± 2
	0.05	292 ± 33	−24 ± 1
FSiNP *(S)*	0.01	350 ± 7	−26 ± 1
	0.05	600 ± 52	−29 ± 2
FSiNP-NH_2-F *(S)*	0.01	237 ± 59	+20 ± 1
	0.05	1926 ± 567	+8 ± 1

The response to the increased NPs content in the system had the following D_H and PDI, **FSiNP-NH_2-F *(S)***$_{0.01\ wt\%}$ = 237 ± 59 nm (PDI = 0.372) to **FSiNP-NH_2-F *(S)***$_{0.05\ wt\%}$ = 1926 ± 567 (PDI = 1.000). The high instability can be attributed to hydrophobicity from aminopropyl on their surface, as discussed previously. Also, the phenol and carboxylic acid groups in the dye molecule can become deprotonated as the concentration increased, leading to a further reduction in the ζ-potential (+20 to +8 mV), which may ultimately lead to instability of the nanoparticles in the system. Overall, the reduction in the ζ-potential can decrease the electrostatic repulsion between the NPs

leading to aggregation and instability. This can be particularly problematic at higher concentrations of nanoparticles in the system, where the effect of particle-particle interactions is more pronounced. Figure 50 summarizes the main parameters of **FSiNP *(S)*** and **FSiNP-NH_2-F *(S)*** at a concentration of 0.01 wt%. The same conditions were used for the following experiments to correlate this information with the results of the fluorescence over time.

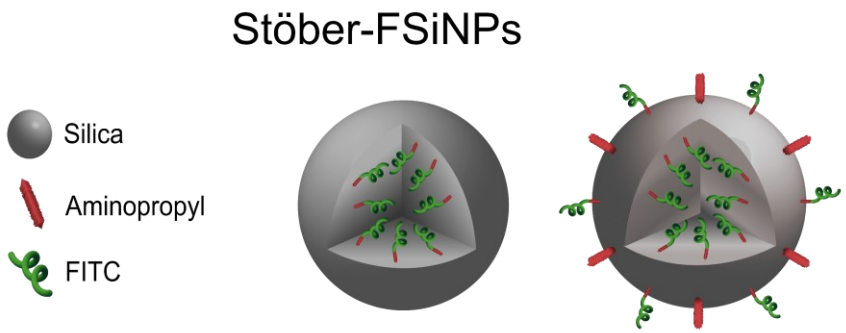

0.01 wt% in DW	FSiNP *(S)*	FSiNP-NH_2-F *(S)*
D_H (nm) / PDI	350 ± 7 (0.218)	237 ± 59 (0.372)
ζ-potential (mV)	-26 ± 1	+20 ± 1
λ_{exc} (nm)	487	494
λ_{emi} (nm)	513	516
Protection of the dye	yes	no
Size by microscopy (nm)	50 ± 12 230 ± 36	15 ± 3 189 ± 34

Figure 50: Summary of the data for comparison and discussion of the fluorescence response over time for FSiNP *(S)* and FSiNP-NH_2-F *(S)*.

5.3.3. Fluorescence response of NPs as a function of time

In this study, the fluorophore was positioned in the core of the FSiNPs to shield the fluorescence response from the solvent effects in experiments involving aqueous fluids. Consequently, changes in the intensity of the emission maxima of the fluorescent NP spectra during the 90-minute experiment were expected to be determined solely by the colloidal stability

of the NPs in solution. However, in general terms, the emission lost for these types of nanomaterials can be associated to:

1) Aggregation: the FSiNPs may aggregate over time leading to a reduction in the effective concentration of fluorophores within each nanoparticle. The colloidal stability of the NPs can also affect the emission over time. If the nanoparticles aggregate or undergo changes in their surface charge or composition, this can lead to a decrease in their colloidal stability, which can in turn affect their fluorescence properties. Similarly, changes in the nanoparticle size or shape can alter the way that light interacts with the fluorophore, which can affect the observed fluorescence properties.

2) Influence of the environment: solvation and O_2 dissolved in the media. Molecular oxygen triggers oxidation (photodegradation) of most organic-based dyes including fluorescein[122] when they are exposed to an excitation source.

3) Photobleaching: the fluorophore may undergo photobleaching over time, resulting in a decrease in the fluorescence intensity. This can occur due to the absorption of photons by the fluorophore which can cause it to degrade or become irreversibly damaged.

4) Fluorescence quenching: in these systems, the fluorescence quenching mechanism is either intraparticle energy transfer or another nonradiative channel (such as free rotation, molecule-molecule interaction, and electron transfer) within the solid matrix. These pathways are likely controlled by the local dye environment within the particle, indicating that precise management of the particle architecture could mitigate fluorescence quenching or possibly lead to its augmentation.[91]

Previous work[122] shows through fluorescent lifetime measurements that even designed core-shell FSiNPs present two different silica micro-environments around the FITC molecules in aqueous environments: (i) FITC molecules that are solvated and close to the nanoparticle surface, so water molecules can penetrate through the porous silica shell and hydrate the referred fluorophore; (ii) FITC molecules that remain away from the solvated region in a non-solvated (dry) microenvironment. However, despite the fact that the authors carried out the coating with TEOS in the final stage

of the synthesis, they did not demonstrate experimentally whether the NPs were fully covered. Therefore, to compare core-shell fluorescent NPS with solvent-accessible fluorescent NPs, **FSiNP-NH_2-F *(S)***, which lacks core-shell characteristics, was synthesized and characterized. This comparison allows us to determine how the dye's lack of protection can affect its fluorescence response.

Figure 51 presents the fluorescence response of the Stöber-FSiNPs over 90 min, showing that **FSiNP *(S)*** has stable emission over time, remaining close to the unit, while **FSiNP-NH_2-F *(S)*** suffers a 30% decrease in the fluorescence intensity over 40 mins, reaching 0.65 in the last read (Appendix A and Table A1). It is known that the core is likely protected from the penetration of oxygen molecules (photostable), whereas the shell is exposed to oxygen molecules, therefore, when porosity is present, as in the case of **FSiNP-NH_2-F *(S)***, the shell remains well hydrated in the aqueous state and the dye molecules are in contact with dissolved oxygen molecules more easily.[122] If the hypothesis formulated by the ζ-potential results is correct, free fluorophores on the surface may waste energy by nonradiative decay, like free rotation. This result shows the importance of hiding the dye, not just for proper emission but for the colloidal instability that the dye gives to the NP.

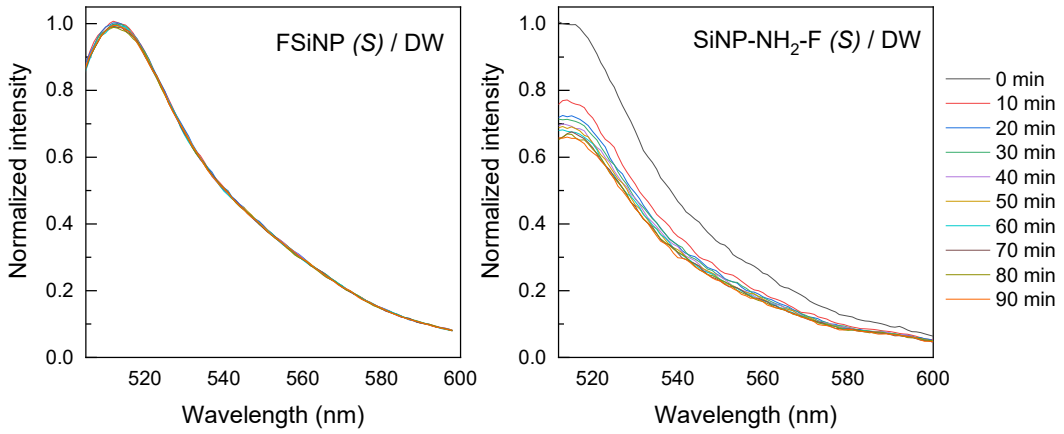

Figure 51: Time stability of the fluorescence response obtained in dispersions (0.01 wt%) of Stöber-FSiNPs FSiNP *(S)* (core-shell) and FSiNP-NH_2-F *(S)* (delocalized dye) in DW, normalized by intensity at time zero.

Despite the **FSiNP *(S)*** showing high emission stability over time, it was not chosen for the following transport experiments due to the lack of size homogeneity.

For WORM-FSiNPs, assuming no contact of the dye with the external environment, the only possibility of fluorescence decrease would be as a result of aggregation. This provides a manner for evaluating the aggregation of nanoparticles through fluorescence, so, the same experiment executed with Stöber-FSiNPs was also performed with WORM-FSiNPs.

Both WORM-FSiNPs showed a change in fluorescence intensity as a function of time (Appendix A and Table A2). A drastic reduction in intensity after the first 10 min was observed for **FSiNP *(W)***, followed by a smooth decrease of the signal that led to a net intensity loss of 52% (Figure 52). The **FSiNP-NH_2 *(W)*** also showed a decrease in the fluorescent intensity over time, although the effect was more gradual, accounting for a total reduction of 18% of the initial value. **FSiNP *(W)*** displays the same negative surface charge as the commercial SiNP and **FSiNP-NH_2 *(W)*** has a positive charge due to aminopropyl groups anchored on the silica surface. Both systems show colloidal instability over time, with a significant decrease in their emission intensity attributed to the aggregation over time due to their relatively low ζ-potential value (−26 and +20 mV).

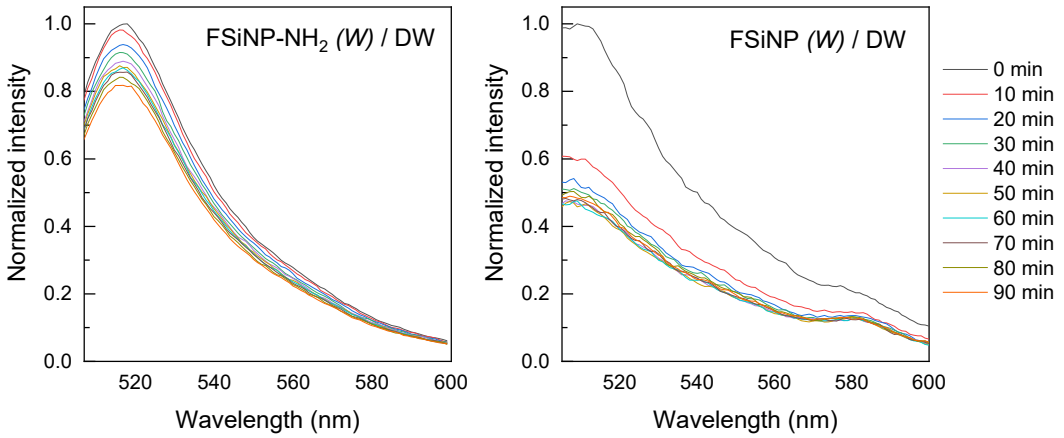

Figure 52: Time stability of the fluorescence response of 0.01 wt% of FSiNP-NH_2 *(W)* and FSiNP *(W)* in DW.

5.3.4. Partial conclusion

The fluorescence response over time of the **FSiNP-NH_2-F *(S)*** showed the importance of hiding the fluorescent dye of the medium, when compared with those of **FSiNP *(S)***. This can be attributed to the lack of colloidal stability as well as the synthetic strategic that expose of the fluorescent moiety on the surface of the **FSiNP-NH_2-F *(S)*** and produced porous NPs. The improved colloidal stability and design of **FSiNP *(S)*** was evident in the high temporal stability of its fluorescence emission maximum.

In the absence of contact between the dye and the external environment, a decrease in fluorescence is assumed to be solely caused by NP aggregation. Both WORM-FSiNPs types displayed decreased fluorescence intensity as time progressed. **FSiNP *(W)*** lost half of its intensity in the first minutes, followed by a progressive drop. The fluorescence intensity of the **FSiNP-NH_2 *(W)*** also decreased over time, albeit more slowly, by 18%. These results are attributed to the occurrence of aggregation due to their relatively low ζ-potential values (−36 and +20 mV, respectively), leading to a reduction in the apparent concentration of FSiNPs.

5.4. Nanofluid: WORM-FSiNPs in surfactant dispersion

5.4.1. SDS adsorption analysis

Considering the synergistic potential with surfactants and the fact that EOR applications are the focus of this research, it was necessary to evaluate the presence of a surfactant in the aqueous environment of the NPs. SiNPs and SDS are the most studied surface-active and nanoparticle combinations in EOR applications, and numerous researchers have evaluated their positive effects.[20,38,51,68] Therefore, the D_H and ζ-potential of the NPs in SDS dispersion were evaluated. Consideration must be given to a comprehensive understanding of the mechanism stabilizing interactions between surfaces and nanoparticles at the molecular level. Due to the electrostatic attraction or repulsive force that SDS can provide, it is anticipated that the dispersion of WORM-FSiNPs with surfactant will exhibit increased colloidal stability.

Thus, the colloidal properties of NPs dispersed in SDS were assessed, focusing on the impact of potential aggregation on the stability and intensity of fluorescence over time, as previously discussed in the context of DW suspension. As expected, the NPs were better dispersed in SDS solutions (smaller D_H) because of further stabilization mediated by the adsorption of surfactant molecules on the NP surface.[47,156] The decrease in D_H was more pronounced for **FSiNP-NH$_2$** ***(W)***, likely owing to the strong attractive interactions between the positively charged NP surface and anionic surfactant head groups (Figure 53A). This effect was also evidenced in the charge inversion of the ζ-potential from +20 mV in DW to −44 mV in SDS (Figure 53B), indicating large surfactant adsorption on the **FSiNP-NH$_2$** ***(W)*** surface. The negative sign of the ζ-potential is a consequence of the formation of local surfactant aggregates on the NP surface, known as admicelles.[157] In this case, the adsorbed SDS molecules facing the aqueous medium were responsible for the large negative ζ-potential values (−44 mV) obtained in the **FSiNP-NH$_2$** ***(W)*** suspension. In contrast, the fluorescent NPs containing only silanol groups on the surface (**FSiNP** ***(W)***) did not show

significant changes in ζ-potential, similar to SiNP, owing to weaker interactions with the polar heads of the anionic surfactant.

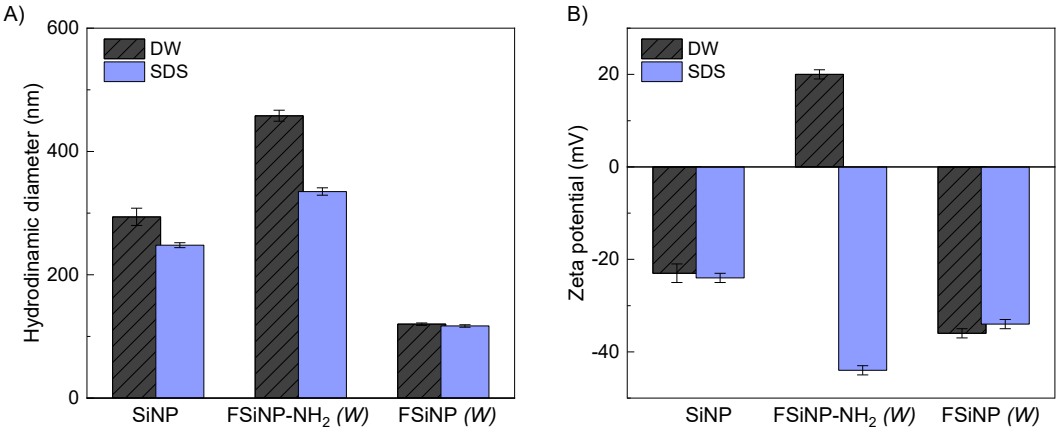

Figure 53: Comparison of the colloidal properties of 0.01 wt% WORM-FSiNPs suspensions in DW and in SDS (0.2 wt%) D_H data (A) and ζ-potential (B).

With a five-fold increase in concentration, the D_H and ζ-potential of positive and negative WORM-FSiNPs were measured and compared to those of commercial SiNP (Table 17). Figure 54 demonstrates the reproductivity of the correlation coefficient curves and size distribution of the NPs, indicating that the nanoparticles were moderately polydisperse in the solutions, thereby enabling reliable DLS analysis.

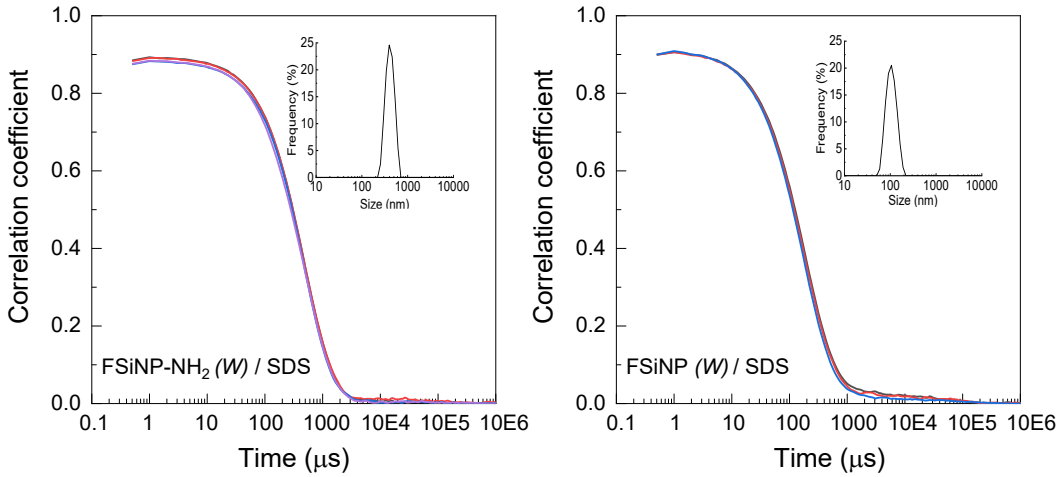

Figure 54: Correlation coefficient and distribution of hydrodynamic diameter by the intensity in an SDS solution of WORM-FSiNPs.

Table 17: Hydrodynamic diameter (D_H) and ζ-potential of NPs in aqueous suspensions in the presence of the anionic surfactant SDS

	D_H (nm)		ζ (mV)	
	0.01 wt% (PDI)	0.05 wt% (PDI)	0.01 wt%	0.05 wt%
SiNP / SDS	248 ± 4 (0.188)	231 ± 1 (0.218)	−24 ± 1	−24 ± 1
FSiNP-NH_2 *(W)* / SDS	335 ± 6 (0.207)	384 ± 4 (0.219)	−44 ± 1	−47 ± 1
FSiNP *(W)* / SDS	117 ± 2 (0.229)	150 ± 1 (0.348)	−34 ± 1	−31 ± 1

The differences in specific surface area between the WORM-FSiNPs did not influence the results regarding the interactions with the surfactant. This is because the dominant interactions were electrostatic, which were mediated by the signal of the surface potential rather than the number of functional groups. As discussed previously, the analysis of the zeta potential revealed that there was a strong attraction between the opposite surface charges of **FSiNP-NH_2 *(W)*** and SDS, which promoted high adsorption of the surfactant molecules on the nanoparticle surface, leading to the inversion and change of zeta potential by nearly 60 mV (as shown in Figure 53B). Notably, this was observed for the largest-sized NP (86 nm) and

smallest surface area. Therefore, we can conclude that the key factor for the observed interaction with the surfactant is the surface group charge rather than the surface area.

5.4.2. Fluorescence proprieties in SDS solution

Figure 55 shows the emission and fluorescence spectra of the NPs suspensions in DW and SDS solutions for comparison. The NPs exhibited excitation maxima at 494 and 489 nm and emission maxima at 517 and 511 nm for **FSiNP-NH₂** ***(W)*** and **FSiNP** ***(W)*** in SDS, respectively. The slight difference in the emission maxima suggests that the presence of surfactant molecules did not significantly affect the emission profile of the fluorophore, which is comparable to that of free FITC.

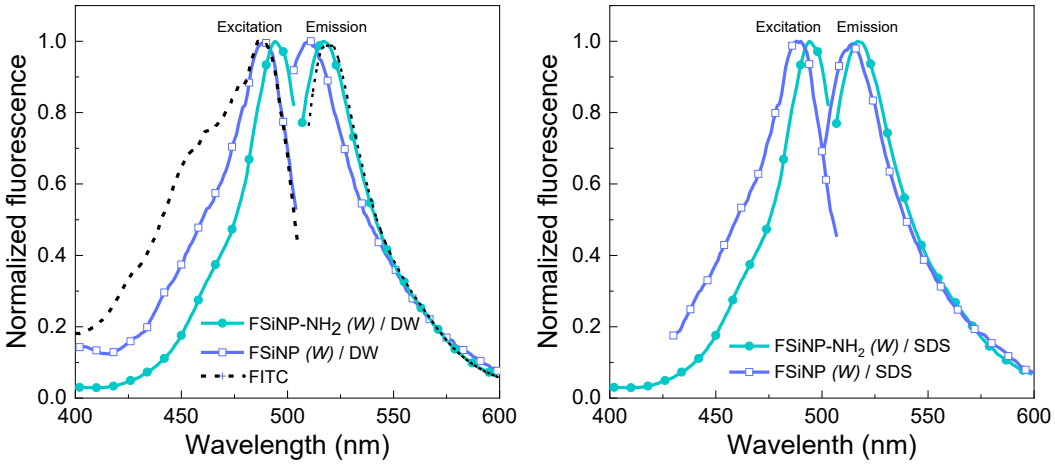

Figure 55: Fluorescence excitation and emission spectra of FITC and the fluorescent SiNP in aqueous suspensions (left panel) and in SDS solution (right panel).

The improved colloidal stability of **FSiNP-NH₂** ***(W)*** in SDS solutions compared to the effect on **FSiNP** ***(W)*** reflected the stability of the fluorescence emission maximum at different times (Figure 56). The comparison of the fluorescence intensities of **FSiNP-NH₂** ***(W)*** and **FSiNP** ***(W)*** without any form of normalization (Figure 56A) shows a difference in the spectra of the two nanoparticles attributed to the higher concentration of APTES used in the synthesis of **FSiNP-NH₂** ***(W)*** compared to that used in the synthesis of **FSiNP** ***(W)***, which was necessary to obtain the aminopropyl functionalization on the NP surface. This higher APTES

concentration increased the likelihood of APTES/FITC binding in the core, thereby increasing the fluorescence intensity.

The fluorescence spectra of **FSiNP-NH₂ *(W)*** showed remarkable stability (Figure 56B), as the signal variation was only 3% after 90 min, which can be considered negligible (Appendix A and Table A3). This agrees with the high ζ-potential values measured for NPs in the SDS solution. It was hypothesized that the strong surfactant adsorption on the NP surface mediated by the aminopropyl groups present on the surface of **FSiNP-NH₂ *(W)*** was responsible for the high stability of the fluorescent signal in solution, which is a desirable characteristic of fluorescent tracers for evaluating the transport and adsorption behavior in porous media.

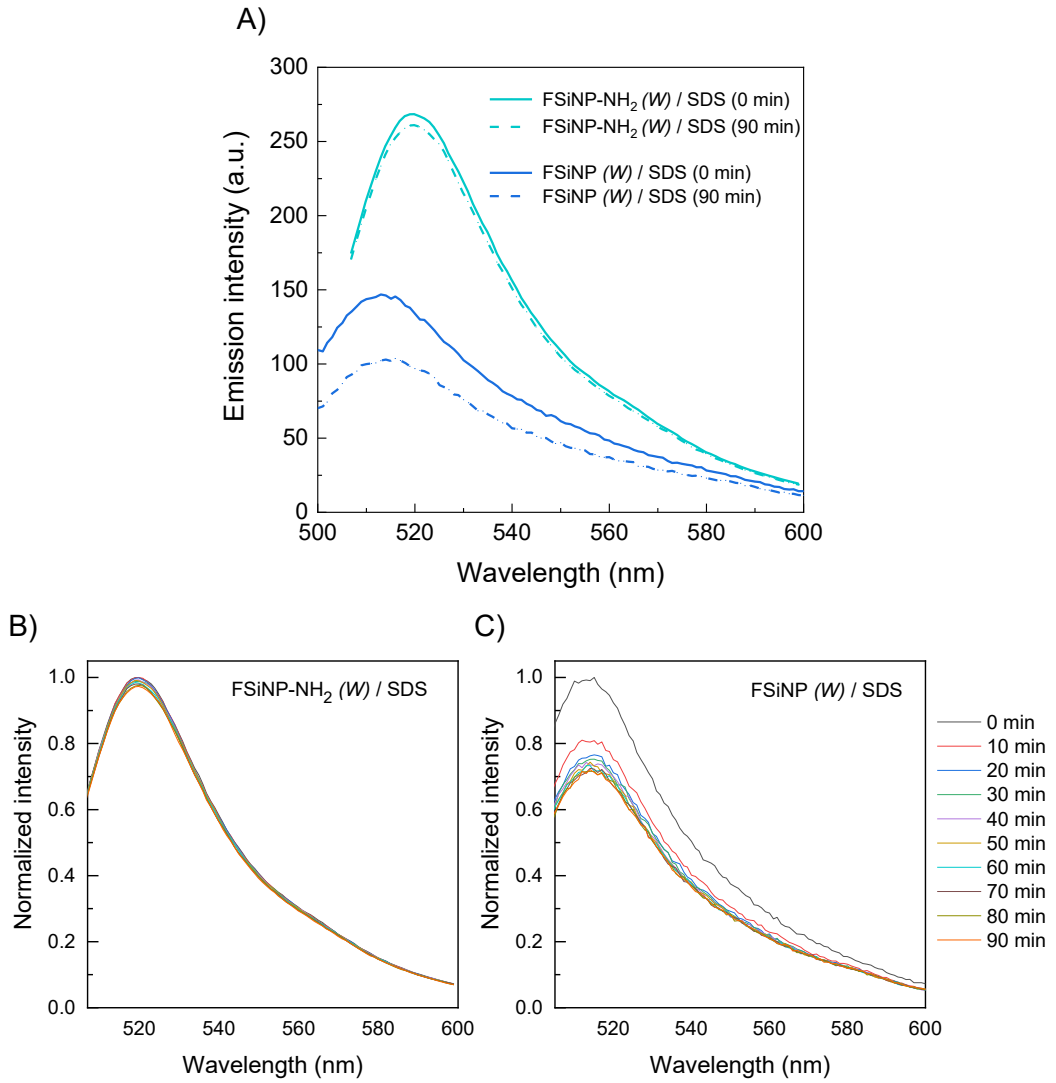

Figure 56: Fluorescence spectra at time zero and after 90 min without normalization for both synthesized NPs (A), time stability of the fluorescence

response obtained for FSiNP *(W)* (B) and FSiNP-NH_2 *(W)* (C), in 0.2 wt% SDS suspension at an NP concentration of 0.01 wt%.

In the case of **FSiNP *(W),*** the spectra showed a reduction in the initial intensity after the first 10 min of the experiment, followed by a less intense decrease with a tendency to stabilize after ~20 min (Figure 56C). This behavior was attributed to possible NP aggregation due to ζ-potential values smaller than those obtained for **FSiNP-NH_2 *(W)***, combined with fewer adsorbed SDS molecules on the NP surface. Nevertheless, the dispersed **FSiNP *(W)*** still showed a significant fluorescence response in SDS, which qualifies for NP quantification in transport studies.

5.4.3. Partial conclusion

It was observed that the excitation and emission of the FSiNPs didn't change, suggesting the core-shell architecture protected the fluorophore group from SDS interactions, ensuring that NP quantification was not affected by the external medium.

Large SDS adsorption occurred on the **FSiNP-NH_2 *(W)*** surface, due to attractive interactions between the protonated aminopropyl groups present on the NP surface and the anionic head groups of the surfactant. As a result, there was a significant charge inversion of the ζ-potential and an increase in surface charge that led to an improvement in colloidal stability. Conversely, there was almost no change in the negative values of ζ-potential obtained for **FSiNP *(W)*** upon dispersion in SDS since the negatively-charged silanol groups on the NP surface did not favor strong interactions with the surfactant molecules (Figura 57).

The improved colloidal stability of the **FSiNP-NH_2 *(W)*** in SDS solutions was reflected in the stability of the fluorescence emission maximum over time, while the signal stabilized only after 20 min for **FSiNP *(W)*** dispersions. However, when compared to the fluorescence results over time in water, we can affirm that the reason for the more drastic decrease was indeed colloidal instability, to the point that both WORM-FSiNPs showed an improvement in SDS.

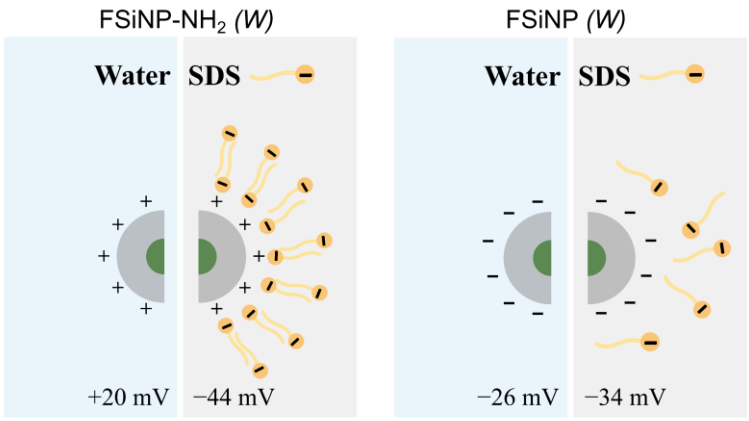

Figure 57: Adsorption behavior through ζ-potential analysis of SDS in the presence of WORM-FSiNPs.

5.5. Transport behavior of WORM-FSiNPs in a packed glass bead column

5.5.1. Transport

It is time to test the hypothesis that synthesized modified NPs can be quantified in the effluent by fluorescence spectroscopy after transport through a porous medium. Different fluorescent NP surface functionalizations allowed for different anionic surfactant interactions in nanofluids, which affected colloidal stability and transport in porous media. Transport experiments were performed comparing the breakthrough and elution curves of a non-reactive tracer with those of two types of WORM-FSiNPs in SDS nanofluids.

The NFs were injected through a glass bead column to evaluate the suitability of fluorescent NPs as tracers in porous media. The suspensions were injected into an unconsolidated porous medium and quantified in the effluents by fluorescence spectroscopy. Both NPs (**FSiNP-NH_2 *(W)*** and **FSiNP *(W)***) were detected in the effluent, allowing the construction of BTC and EC as a function of the injected volume. The BTC and EC for nanofluids had a similar profile to that of the non-reactive tracer (lithium-Li^+), indicating that all systems traveled the pore space of the homogeneous and unconsolidated media at the same velocity and that the fluorescent NPs could access all pores, advection being the dominant mechanism of

transport (as expected due to the homogeneity of the pore network generated by the packing of glass beads).[52]

Furthermore, the similarity observed in the shape of the curves suggested that the attractive interactions between **FSiNP-NH_2** ***(W)*** and the surfactant molecules were maintained during the flow through the column, protecting the NPs from strong adsorption on the negatively charged glass bead surface. Consequently, there was no significant difference between the transport mechanisms of the two fluorescent NPs in the porous medium. This highlights the relevance of tailored surfactant-NP interactions for the transport behavior of nanofluids, as it has been reported that functionalization of NP surfaces with surfactants can reduce the effect of surface charges on NP retention compared to bare surfaces.[127]

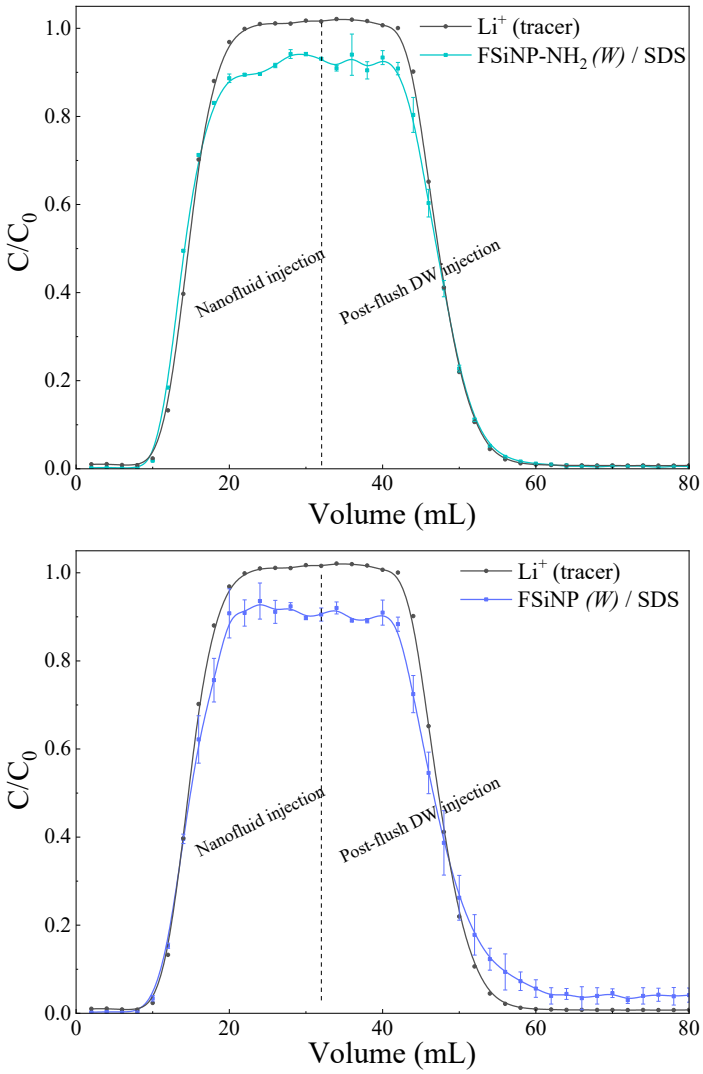

Figure 58: Breakthrough curves of fluorescent nanoparticles, FSiNP-NH_2 *(W)* and FSiNP *(W)*, in SDS solution, obtained by dynamic adsorption test in a glass bead column, at 25°C.

The values for steady-state relative effluent concentration, obtained at the BTC plateau, were 0.91 and 0.92 for **FSiNP *(W)*** and **FSiNP-NH_2 *(W)***, respectively. These values were smaller than those obtained using the tracer, suggesting that NP transport was slightly disturbed. This can be explained by considering the microscopic exclusion of the NPs while passing through the porous medium. In this mechanism, colloids are prevented from freely flowing through pore throats due to charge exclusion, assuming there are repulsive forces between the walls and colloidal particles, and/or due to large colloidal sizes (chromatographic effect).[158] This can be applied to our results because both NPs showed negative ζ-

potential when dispersed in SDS (Table 17), which is the same charge sign as glass beads. Electrostatic repulsive forces could thus slow down the transport of some of the dispersed NPs, destabilize the suspension, and retain the NPs in pore space. These results are in line with the work of Agenet et al.[85], in which recoveries of up to 0.95 were observed for fluorescent nanobeads injected through a Bentheimer sandstone core. In that study, the fluorescent NPs were stabilized in solutions by a gluconamide coating instead of by non-covalent interactions with an anionic surfactant, as in the present study.

Furthermore, unlike the **FSiNP-NH$_2$** ***(W)*** curve, the BTC of **FSiNP** ***(W)*** showed a small delay between 1.5 and 2.0 PV (corresponding to an injected volume of 15 and 20 mL, respectively) compared to the tracer profile. The EC for both NPs showed a sharp drop in concentration following the same profile as that of the lithium tracer. There was no tailing in the EC profile of **FSiNP-NH$_2$** ***(W)***, while some tailing was observed for **FSiNP** ***(W)*** (compared to that of the lithium tracer). This indicates that the nanofluid containing **FSiNP-NH$_2$** ***(W)*** was more effectively displaced by the injected DW than the **FSiNP** ***(W)*****/SDS** system where DW could not quickly remove all NPs retained in the pore space. A possible reason for the tailing observed in the elution of **FSiNP** ***(W)*****/SDS** is its lower ζ-potential (−34 mV) compared to that of the **FSiNP-NH$_2$** ***(W)*****/SDS** system (−44 mV), which can lead to some agglomeration of the **FSiNP** ***(W)*** and posterior deposition in the column. These differences accounted for more adsorbed **FSiNP** ***(W)*** (0.034 mg/g-beads), whereas much less adsorption was obtained for the nanofluid containing **FSiNP-NH$_2$** ***(W)*** (0.004 mg/g-beads) (Table 18). The result obtained with the **FSiNP** ***(W)*** nanofluid was attributed to the weak interactions of the functional groups on the silica surface with SDS molecules, possibly leading to lower colloidal stability in solution (as also observed in the decay of the fluorescence intensity as a function of time). Nevertheless, the NP adsorption values were very low in both cases, which indicates that the fluorescent NPs developed in this work are good candidates for transport studies in porous media of nanofluids containing combinations of SiNP and anionic surfactants.

Table 18: Mass balance analysis of the adsorption of fluorescent WORM-FSiNPs in the glass bead column

	FSiNP-NH_2 *(W)* / SDS	FSiNP *(W)* / SDS
Injected mass (mg)	6.4	6.4
Recovered mass (mg)	6.2 ± 0.2	5.1 ± 0.7
Adsorbed mass (mg)	0.1 ± 0.1	1.3 ± 0.7
Adsorption (mg/g-beads)	0.004 ± 0.002	0.034 ± 0.018

5.5.2. Partial conclusion

Even though the difference in fluorescence emission over time for **FSiNP-NH_2 *(W)*** and **FSiNP *(W)*** was very stable in SDS solutions for the first 20 minutes, column transport experiments showed that both fluorescent NPs could be used to measure concentrations as low as 0.02 wt%. The quantification in the effluent allowed the construction of the BTC and EC as a function of the injected volume, which is key for evaluating the mechanisms of NP adsorption and transport in porous media. The NFs showed a similar profile to that of the non-reactive tracer, indicating that both systems traveled the pore space at the same velocity, and that the fluorescent NPs were able to access all pores, with advection being the dominant transport mechanism in this type of porous media. These conclusions support the importance of gas adsorption and desorption similarity between the NP for transport experiment findings based only on colloidal behavior.

In addition, it is possible that the surfactant molecules are most likely retained on the **FSiNP-NH_2 *(W)*** surface during the flow through the column, acting as a protective coating from strongly adsorbing on the negatively-charged glass beads surface, as illustrated in Figure 59. This approach directly confirmed NP-surfactant interactions during column transport, unlike the traditional method of only quantifying surfactant behavior in nanofluid studies.

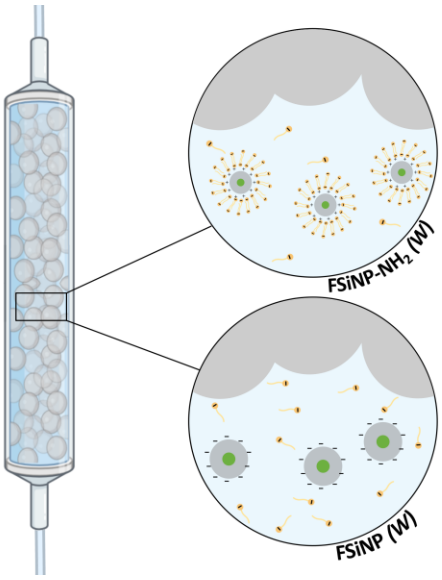

Figure 59: Illustration of the theoretically interact of FSiNP-NH_2 *(W)* and FSiNP *(W)* with SDS molecules during transportation.

The effluent maximum NPs concentration values were slightly smaller than those of the tracer, possibly due to the exclusion of negatively-charged NP/surfactant colloids at the microscopic level while passing through the glass bead packing. The electrostatic repulsive forces between the walls and colloidal particles could slow down the transport of some dispersed nanoparticles, destabilize the suspension, and retain the NPs in the pore space. The higher adsorption (~8 times) of **FSiNP *(W)*** compared to **FSiNP-NH_2 *(W)*** due to weaker interactions of SDS with the surface functional groups contributed to this behavior. This is in line with the results of the time stability study of fluorescence response. However, the adsorption from both nanofluids was relatively low in both cases, indicating the potential of the fluorescent NPs developed in this study for transport and adsorption studies in nanofluids containing surfactants.

6 Conclusions

Four core-shell silica-based fluorescent nanoparticles (FSiNPs) were synthesized with similar cores but different surface groups using two synthesis methods, namely Stöber ***(S)*** and WORM ***(W)***, designed to obtain nanomaterials with similar behavior than commercial SiNP commonly used in nanofluid applications. The core-shell structure was tested when **FSiNP** ***(S)*** resulted in improved fluorescence stability over time, while **FSiNP-NH_2-F** ***(S)***, with exposed fluorescent moieties showed decreased stability. This result supported the hypothesis that protection of the fluorophore group is one factor which makes them suitable for adsorption and transport studies in porous media.

The presence of primary amino groups was confirmed on the surfaces of positive-FSiNPs, while negative-FSiNPs were found to be free of these groups. Comparative analyses using DLS and SEM techniques revealed that the WORM method produced more uniform and homogeneous NPs, compared to the Stöber method. The N_2 adsorption/desorption analysis ruled out the influence of size, shape, and porosity, showing similarities with commercial SiNPs. This ensured that the subsequent transport experiments focused solely on their colloidal behavior.

The FSiNPs exhibited good colloidal stability, as supported by ζ-potential measurements, which varied based on surface functional groups. Negative ζ-potential values confirmed silanol groups on **FSiNP** ***(S)*** and **FSiNP** ***(W)*** surfaces in aqueous suspension, while positive ζ-potential indicated aminopropyl functionalization on **FSiNP-NH_2** ***(W)***. Evaluation of fluorescence stability emphasized the importance of colloidal stability in detecting and quantifying FSiNPs since WORM-FSiNPs/SDS nanofluid explicitly shows the dependence of fluorescence over time on colloidal stability. **FSiNP-NH_2** ***(W)*** exhibited significant attraction to SDS, resulting in charge inversion and increased surface charge, while **FSiNP** ***(W)*** showed weak interactions with SDS due to their negative charges.

Column transport experiments in an unconsolidated porous media provided insights into the adsorption and transport behavior. It was observed that **FSiNP *(W)*** had higher adsorption and exhibited minor delays in BTC and tailing in EC compared to its positively charged counterparts, indicating the influence of surface charge on adsorption phenomena, and supporting the high colloidal stability of **FSiNP-NH_2 *(W)*** as observed in SDS emission stability studies. Surfactant retention on **FSiNP-NH_2 *(W)*** protected against strong adsorption of the NPs on negatively charged glass beads. Overall, the NP adsorption remained relatively low, highlighting the potential of the fluorescent NPs synthesized in this work for transport and adsorption studies in surfactant-containing nanofluids.

6.1. Perspectives

- Studied the adsorption of a positive surfactant.
- Time-resolved fluorescence to assess the microenvironments around the fluorophore.
- Further testing using different media and consolidated porous media will provide more realistic information.

7 References

1. Gomes L, Furtado A, Souza M. Silica and its Peculiarities. *Rev Virtual Química*. 2018;10(4):1018-1038. doi:10.21577/1984-6835.20180072
2. Schärtl W. Current directions in core–shell nanoparticle design. *Nanoscale*. 2010;2(6):829. doi:10.1039/c0nr00028k
3. Sreejith S, Ma X, Zhao Y. Graphene Oxide Wrapping on Squaraine-Loaded Mesoporous Silica Nanoparticles for Bioimaging. *J Am Chem Soc*. 2012;134(42):17346-17349. doi:10.1021/ja305352d
4. Lu J, Liong M, Zink JI, Tamanoi F. Mesoporous Silica Nanoparticles as a Delivery System for Hydrophobic Anticancer Drugs. *Small*. 2007;3(8):1341-1346. doi:10.1002/smll.200700005
5. Samart C, Sreetongkittikul P, Sookman C. Heterogeneous catalysis of transesterification of soybean oil using KI/mesoporous silica. *Fuel Process Technol*. 2009;90(7-8):922-925. doi:10.1016/j.fuproc.2009.03.017
6. Karimi B, Mirzaei HM, Mobaraki A. Periodic mesoporous organosilica functionalized sulfonic acids as highly efficient and recyclable catalysts in biodiesel production. *Catal Sci Technol*. 2012;2(4):828. doi:10.1039/c2cy00444e
7. Shang J, Gao X. Nanoparticle counting: Towards accurate determination of the molar concentration. *Chem Soc Rev*. 2014;43(21):7267-7278. doi:10.1039/c4cs00128a
8. Auras F, Li Y, Löbermann F, et al. A Zinc Phthalocyanine Based Periodic Mesoporous Organosilica Exhibiting Charge Transfer to Fullerenes. *Chem - A Eur J*. 2014;20(46):14971-14975. doi:10.1002/chem.201404169
9. Yamamoto Y, Takeda H, Yui T, et al. Efficient light harvesting via sequential two-step energy accumulation using a Ru–Re5 multinuclear complex incorporated into periodic mesoporous organosilica. *Chem Sci*. 2014;5(2):639-648. doi:10.1039/C3SC51959G
10. Yu J, Kim YH, Kim HM, Oh JM, Kim YR, Choi SJ. Determination of the fate and biological responses of food additive silica particles in commercial foods. *Food Chem*. 2020;331:127304. doi:10.1016/j.foodchem.2020.127304
11. Zhang W, Ahari H, Zhang Z, Jafari SM. Role of silica (SiO2) nano/micro-particles in the functionality of degradable packaging films/coatings and their application in food preservation. *Trends Food Sci Technol*. 2023;133(September 2022):75-86. doi:10.1016/j.tifs.2023.01.009
12. Medina-Reyes EI, Rodríguez-Ibarra C, Déciga-Alcaraz A, Díaz-Urbina D, Chirino YI, Pedraza-Chaverri J. Food additives containing nanoparticles induce

gastrotoxicity, hepatotoxicity and alterations in animal behavior: The unknown role of oxidative stress. *Food Chem Toxicol*. 2020;146(September). doi:10.1016/j.fct.2020.111814

13. Kearns P, Gonzalez M, OKI N, Lee K, Rodriguez F. The Safety of Nanotechnologies at the Oecd. In: Linkov I, Steevens J, eds. *Nanomaterials: Risks and Benefits*. NATO Science for Peace and Security Series C: Environmental Security. Springer; 2009:351-358. doi:10.1007/978-1-4020-9491-0_27
14. Yadav M, Dwibedi V, Sharma S, George N. Biogenic silica nanoparticles from agro-waste: Properties, mechanism of extraction and applications in environmental sustainability. *J Environ Chem Eng*. 2022;10(6):108550. doi:10.1016/j.jece.2022.108550
15. Jadhav SA, Garud HB, Patil AH, et al. Recent advancements in silica nanoparticles based technologies for removal of dyes from water. *Colloids Interface Sci Commun*. 2019;30(February):100181. doi:10.1016/j.colcom.2019.100181
16. Rosa AJ, Carvalho R de S, Xavier JAD. *Engenharia de Reservatórios de Petróleo*. Interciência; 2006.
17. Tzimas E, Georgakaki A, Cortes G, Peteves SD. *Enhanced Oil Recovery Using Carbon Dioxide in the European Energy System*.; 2005.
18. Thomas JE. *Fundamentos de Engenharia de Petróleo*. 2nd ed. (Thomas JE, ed.). Interciência; 2001.
19. Introduction. In: *Geology of Carbonate Reservoirs*. John Wiley & Sons, Inc.; :1-12. doi:10.1002/9780470370650.ch1
20. Olayiwola SO, Dejam M. A comprehensive review on interaction of nanoparticles with low salinity water and surfactant for enhanced oil recovery in sandstone and carbonate reservoirs. *Fuel*. 2019;241(October 2018):1045-1057. doi:10.1016/j.fuel.2018.12.122
21. AlHammadi M, Mahzari P, Sohrabi M. Fundamental investigation of underlying mechanisms behind improved oil recovery by low salinity water injection in carbonate rocks. *Fuel*. 2018;220(February):345-357. doi:10.1016/j.fuel.2018.01.136
22. Khaledialidusti R, Kleppe J, Enayatpour S. Evaluation of surfactant flooding using interwell tracer analysis. *J Pet Explor Prod Technol*. 2017;7(3):853-872. doi:10.1007/s13202-016-0288-9
23. Agi A, Junin R, Gbadamosi A. Mechanism governing nanoparticle flow behaviour in porous media: insight for enhanced oil recovery applications. *Int Nano Lett*. 2018;8(2):49-77. doi:10.1007/s40089-018-0237-3
24. Naik S, You Z, Bedrikovetsky P. Rate enhancement in unconventional gas reservoirs by wettability alteration. *J Nat Gas Sci Eng*. 2015;26:1573-1584. doi:10.1016/j.jngse.2015.06.016
25. Zargartalebi M, Kharrat R, Barati N. Enhancement of surfactant flooding

performance by the use of silica nanoparticles. *Fuel*. 2015;143:21-27. doi:10.1016/j.fuel.2014.11.040

26. Nguyen P, Fadaei H, Sinton D. Pore-Scale Assessment of Nanoparticle-Stabilized CO 2 Foam for Enhanced Oil Recovery. *Energy & Fuels*. 2014;28(10):6221-6227. doi:10.1021/ef5011995
27. Ogolo NA, Olafuyi OA, Onyekonwu MO. Enhanced Oil Recovery Using Nanoparticles. In: *All Days*. SPE; 2012:1-9. doi:10.2118/160847-MS
28. Keykhosravi A, Simjoo M. Insights into stability of silica nanofluids in brine solution coupled with rock wettability alteration: An enhanced oil recovery study in oil-wet carbonates. *Colloids Surfaces A Physicochem Eng Asp*. 2019;583:124008. doi:10.1016/j.colsurfa.2019.124008
29. Abhishek R, Hamouda AA. Effect of Various Silica Nanofluids: Reduction of Fines Migrations and Surface Modification of Berea Sandstone. *Appl Sci*. 2017;7(12):1216. doi:10.3390/app7121216
30. Hadia NJ, Ng YH, Stubbs LP, Torsæter O. High Salinity and High Temperature Stable Colloidal Silica Nanoparticles with Wettability Alteration Ability for EOR Applications. *Nanomaterials*. 2021;11(3):707. doi:10.3390/nano11030707
31. Hurtado Y, Beltrán C, Zabala RD, et al. Effects of Surface Acidity and Polarity of SiO 2 Nanoparticles on the Foam Stabilization Applied to Natural Gas Flooding in Tight Gas-Condensate Reservoirs. *Energy & Fuels*. 2018;32(5):5824-5833. doi:10.1021/acs.energyfuels.8b00665
32. Li Y, Dai C, Zhou H, et al. A Novel Nanofluid Based on Fluorescent Carbon Nanoparticles for Enhanced Oil Recovery. *Ind Eng Chem Res*. 2017;56(44):12464-12470. doi:10.1021/acs.iecr.7b03617
33. Maaref S, Kantzas A, Bryant SL. The effect of silanization assisted nanoparticle hydrophobicity on emulsion stability through droplet size distribution analysis. *Chem Eng Sci*. 2019;201:175-190. doi:10.1016/j.ces.2019.02.034
34. Rattanaudom P, Alimin AA, Shiau B jier Ben, Harwell JH, Suriyapraphadilok U, Charoensaeng A. Experimental investigation of hydrophobic and hydrophilic silica nanoparticles on extended surfactant properties: Micro-emulsion, viscosity, and adsorption behaviors. *Geoenergy Sci Eng*. 2023;223(February):211582. doi:10.1016/j.geoen.2023.211582
35. Tang W, Wu P, Da C, et al. Synergy of surface modified nanoparticles and surfactant in wettability alteration of calcite at high salinity and temperature. *Fuel*. 2023;331(P2):125752. doi:10.1016/j.fuel.2022.125752
36. Ma L, Zhu M, Liu T. Effects of chain length of surfactants and their adsorption on nanoparticles on stability of CO2-in-water emulsions. *Colloids Surfaces A Physicochem Eng Asp*. 2022;644(March):128877. doi:10.1016/j.colsurfa.2022.128877
37. Li S, Sng A, Daniel D, Lau HC, Torsæter O, Stubbs LP. Visualizing and Quantifying

Wettability Alteration by Silica Nanofluids. *ACS Appl Mater Interfaces*. 2021;13(34):41182-41189. doi:10.1021/acsami.1c08445

38. Zhou Y, Wu X, Zhong X, Sun W, Pu H, Zhao JX. Surfactant-Augmented Functional Silica Nanoparticle Based Nanofluid for Enhanced Oil Recovery at High Temperature and Salinity. *ACS Appl Mater Interfaces*. 2019;11(49):45763-45775. doi:10.1021/acsami.9b16960
39. Du D, Zhang X, Yu K, et al. Parameter Screening Study for Optimizing the Static Properties of Nanoparticle-Stabilized CO2 Foam Based on Orthogonal Experimental Design. *ACS Omega*. 2020;5(8):4014-4023. doi:10.1021/acsomega.9b03543
40. Ortega DJS, Kim HB, James LA, Johansen TE, Zhang Y. The Effectiveness of Silicon Dioxide SiO_2 Nanoparticle as an Enhanced Oil Recovery Agent in Ben Nevis Formation, Hebron Field, Offshore Eastern Canada. In: *Abu Dhabi International Petroleum Exhibition & Conference*. Society of Petroleum Engineers; 2016. doi:10.2118/183546-MS
41. Hendraningrat L, Torsæter O. A Stabilizer that Enhances the Oil Recovery Process Using Silica-Based Nanofluids. *Transp Porous Media*. 2015;108(3):679-696. doi:10.1007/s11242-015-0495-8
42. Faure B, Salazar-Alvarez G, Bergström L. Hamaker constants of iron oxide nanoparticles. *Langmuir*. 2011;27(14):8659-8664. doi:10.1021/la201387d
43. Gregory J. *Particles in Water*.; 2005. doi:10.1201/9780203508459
44. Peukert W, Romeis S. Nanoparticle handling and formulation. In: Higashitani, K. Makino, H. & Matsusaka S, ed. *Powder Technology Handbook*. 4th ed. CRC Press Taylor & Francis Group; 2020:521-532.
45. Morozova TI, Lee VE, Panagiotopoulos AZ, Prud'homme RK, Priestley RD, Nikoubashman A. On the Stability of Polymeric Nanoparticles Fabricated through Rapid Solvent Mixing. *Langmuir*. 2019;35(3):709-717. doi:10.1021/acs.langmuir.8b03399
46. Metin CO, Lake LW, Miranda CR, Nguyen QP. Stability of aqueous silica nanoparticle dispersions. *J Nanoparticle Res*. 2011;13(2):839-850. doi:10.1007/s11051-010-0085-1
47. Almahfood M, Bai B. The synergistic effects of nanoparticle-surfactant nanofluids in EOR applications. *J Pet Sci Eng*. 2018;171(July):196-210. doi:10.1016/j.petrol.2018.07.030
48. Vatanparast H, Javadi A, Bahramian A. Silica nanoparticles cationic surfactants interaction in water-oil system. *Colloids Surfaces A Physicochem Eng Asp*. 2017;521:221-230. doi:10.1016/j.colsurfa.2016.10.004
49. Yekeen N, Manan MA, Idris AK, et al. A comprehensive review of experimental studies of nanoparticles-stabilized foam for enhanced oil recovery. *J Pet Sci Eng*. 2018;164:43-74. doi:10.1016/j.petrol.2018.01.035

50. Wu Y, Chen W, Dai C, et al. Reducing surfactant adsorption on rock by silica nanoparticles for enhanced oil recovery. *J Pet Sci Eng*. 2017;153(2016):283-287. doi:10.1016/j.petrol.2017.04.015
51. Venancio JCC, Nascimento RSV, Pérez-Gramatges A. Colloidal stability and dynamic adsorption behavior of nanofluids containing alkyl-modified silica nanoparticles and anionic surfactant. *J Mol Liq*. 2020;308:113079. doi:10.1016/j.molliq.2020.113079
52. Sun Q, Liu W, Li S, Zhang N, Li Z. Interfacial Rheology of Foam Stabilized by Nanoparticles and Their Retention in Porous Media. *Energy and Fuels*. 2021;35(8):6541-6552. doi:10.1021/acs.energyfuels.0c03680
53. Negin C, Ali S, Xie Q. Most common surfactants employed in chemical enhanced oil recovery. *Petroleum*. 2017;3(2):197-211. doi:10.1016/j.petlm.2016.11.007
54. Li B, Chua SL, Ch'ng AL, et al. An effective approach for size characterization and mass quantification of silica nanoparticles in coffee creamer by AF4-ICP-MS. *Anal Bioanal Chem*. 2020;412(22):5499-5512. doi:10.1007/s00216-020-02770-x
55. Yu J, An C, Mo D, Liu N, Lee R. Study of Adsorption and Transportation Behavior of Nanoparticles in Three Different Porous Media. In: *All Days*. Vol 1. SPE; 2012:311-323. doi:10.2118/153337-MS
56. Abhishek R, Hamouda A, Ayoub A. Effect of Silica Nanoparticles on Fluid/Rock Interactions during Low Salinity Water Flooding of Chalk Reservoirs. *Appl Sci*. 2018;8(7):1093. doi:10.3390/app8071093
57. Esfandyari Bayat A, Junin R, Shamshirband S, Tong Chong W. Transport and retention of engineered Al2O3, TiO2 and SiO2 nanoparticles through various sedimentary rocks. *Sci Rep*. 2015;5(1):14264. doi:10.1038/srep14264
58. Zhang T, Murphy MJ, Yu H, et al. Investigation of Nanoparticle Adsorption During Transport in Porous Media. *SPE J*. 2015;20(04):667-677. doi:10.2118/166346-PA
59. Dehghan Monfared A, Ghazanfari MHH, Jamialahmadi M, Helalizadeh A. Adsorption of silica nanoparticles onto calcite: Equilibrium, kinetic, thermodynamic and DLVO analysis. *Chem Eng J*. 2015;281:334-344. doi:10.1016/j.cej.2015.06.104
60. Iqbal M, Lyon BA, Ureña-Benavides EE, et al. High temperature stability and low adsorption of sub-100 nm magnetite nanoparticles grafted with sulfonated copolymers on Berea sandstone in high salinity brine. *Colloids Surfaces A Physicochem Eng Asp*. 2017;520:257-267. doi:10.1016/j.colsurfa.2017.01.080
61. Li S, Torsæter O, Lau HC, Hadia NJ, Stubbs LP. The Impact of Nanoparticle Adsorption on Transport and Wettability Alteration in Water-Wet Berea Sandstone: An Experimental Study. *Front Phys*. 2019;7(May). doi:10.3389/fphy.2019.00074
62. Hamouda AA, Abhishek R. Effect of salinity on silica nanoparticle adsorption kinetics and mechanisms for fluid/rock interaction with calcite. *Nanomaterials*. 2019;9(2):19-23. doi:10.3390/nano9020213
63. Ghosh D, Das S, Gahlot VK, et al. Nano-SiO2 transport and retention in saturated

porous medium: Influence of pH, ionic strength, and natural organics. *J Contam Hydrol*. 2022;248(April):104029. doi:10.1016/j.jconhyd.2022.104029

64. Keykhosravi A, Bedrikovetsky P, Simjoo M. Experimental insight into the silica nanoparticle transport in dolomite rocks: Spotlight on DLVO theory and permeability impairment. *J Pet Sci Eng*. 2022;209(November 2021):109830. doi:10.1016/j.petrol.2021.109830
65. Yousefvand HA, Jafari A. Stability and flooding analysis of nanosilica/ NaCl /HPAM/SDS solution for enhanced heavy oil recovery. *J Pet Sci Eng*. 2018;162:283-291. doi:10.1016/j.petrol.2017.09.078
66. Awan FUR, Keshavarz A, Azhar MR, et al. Adsorption of nanoparticles on glass bead surface for enhancing proppant performance: A systematic experimental study. *J Mol Liq*. 2021;328:115398. doi:10.1016/j.molliq.2021.115398
67. Khlebtsov BN, Khanadeev VA, Khlebtsov NG. Determination of the Size, Concentration, and Refractive Index of Silica Nanoparticles from Turbidity Spectra. *Langmuir*. 2008;24(16):8964-8970. doi:10.1021/la8010053
68. Suresh R, Kuznetsov O, Agrawal D, Darugar Q, Khabashesku V. Reduction of Surfactant Adsorption in Porous Media Using Silica Nanoparticles. In: Vol 2. OTC; 2018:984-992. doi:10.4043/28879-MS
69. Peuschel H, Ruckelshausen T, Cavelius C, Kraegeloh A. Quantification of Internalized Silica Nanoparticles via STED Microscopy. *Biomed Res Int*. 2015;2015:1-16. doi:10.1155/2015/961208
70. Li X, Yang Q, Ye Y, et al. Quantifying 3D-nanosized dispersion of SiO2 in elastomer nanocomposites by 3D-scanning transmission electron microscope (STEM). *Compos Part A Appl Sci Manuf*. 2020;131(January):2-7. doi:10.1016/j.compositesa.2020.105778
71. Aureli F, D'Amato M, Raggi A, Cubadda F. Quantitative characterization of silica nanoparticles by asymmetric flow field flow fractionation coupled with online multiangle light scattering and ICP-MS/MS detection. *J Anal At Spectrom*. 2015;30(6):1266-1273. doi:10.1039/c4ja00478g
72. Bolea-Fernandez E, Leite D, Rua-Ibarz A, et al. Characterization of SiO2 nanoparticles by single particle-inductively coupled plasma-tandem mass spectrometry (SP-ICP-MS/MS). *J Anal At Spectrom*. 2017;32(11):2140-2152. doi:10.1039/c7ja00138j
73. Barahona F, Geiss O, Urbán P, Ojea-Jimenez I, Gilliland D, Barrero-Moreno J. Simultaneous determination of size and quantification of silica nanoparticles by asymmetric flow field-flow fractionation coupled to ICPMS using silica nanoparticles standards. *Anal Chem*. 2015;87(5):3039-3047. doi:10.1021/ac504698j
74. Singh R, Mohanty KK. Synergy between Nanoparticles and Surfactants in Stabilizing Foams for Oil Recovery. *Energy & Fuels*. 2015;29(2):467-479. doi:10.1021/ef5015007

75. Håkanson L. The relationship between salinity, suspended particulate matter and water clarity in aquatic systems. *Ecol Res*. 2006;21(1):75-90. doi:10.1007/s11284-005-0098-x

76. Estephan ZG, Jaber JA, Schlenoff JB. Zwitterion-Stabilized Silica Nanoparticles: Toward Nonstick Nano. *Langmuir*. 2010;26(22):16884-16889. doi:10.1021/la103095d

77. Irache JM, Durrer C, Ponchel G, Duchêne D. Determination of particle concentration in latexes by turbidimetry. *Int J Pharm*. 1993;90(3):93-96. doi:10.1016/0378-5173(93)90203-R

78. Lian W, Litherland SA, Badrane H, et al. Ultrasensitive detection of biomolecules with fluorescent dye-doped nanoparticles. *Anal Biochem*. 2004;334(1):135-144. doi:10.1016/j.ab.2004.08.005

79. Halamoda-Kenzaoui B, Ceridono M, Urbán P, et al. The agglomeration state of nanoparticles can influence the mechanism of their cellular internalisation. *J Nanobiotechnology*. 2017;15(1):48. doi:10.1186/s12951-017-0281-6

80. Ha SW, Camalier CE, Beck Jr. GR, Lee JK. New method to prepare very stable and biocompatible fluorescent silica nanoparticles. *Chem Commun*. 2009;(20):2881. doi:10.1039/b902195g

81. Murugesan S, Suresh R, Kuznetsov O, Khabashesku VN, Darugar Q. Multicolor Fluorescent Silica Nanoparticles as Tracers for Production and Well Monitoring. In: *Day 1 Mon, October 09, 2017*. SPE; 2017. doi:10.2118/187207-MS

82. Khan SA, Al-Jabari MH, Mansha M, Ali S, Yamani ZH. Hydrophobic, partially hydrophobic, and hydrophilic ZnO@SiO2 nanoparticles as fluorescent partitioning tracers for oil sensing applications. *J Mol Liq*. 2022;360:119505. doi:10.1016/j.molliq.2022.119505

83. Singh R, Mohanty KK. Foam flow in a layered, heterogeneous porous medium: A visualization study. *Fuel*. 2017;197:58-69. doi:10.1016/j.fuel.2017.02.019

84. Otero-González L, Field JA, Calderon IAC, et al. Fate of fluorescent core-shell silica nanoparticles during simulated secondary wastewater treatment. *Water Res*. 2015;77:170-178. doi:10.1016/j.watres.2015.03.021

85. Agenet N, Perriat P, Brichart T, Crowther N, Martini M, Tillement O. Fluorescent Nanobeads: a First Step Toward Intelligent Water Tracers. In: *All Days*. SPE; 2012. doi:10.2118/157019-MS

86. Pedersen T. Properly designed temperature history nanoparticles may improve residual oil saturation estimates from SWCT tests. *J Pet Sci Eng*. 2018;170(2017):383-391. doi:10.1016/j.petrol.2018.06.069

87. Vitorge E, Szenknect S, Martins JMF, et al. Comparison of three labeled silica nanoparticles used as tracers in transport experiments in porous media. Part I: Syntheses and characterizations. *Environ Pollut*. 2014;184:605-612. doi:10.1016/j.envpol.2013.07.031

88. Vitorge E, Szenknect S, Martins JMF, Barthès V, Gaudet JP. Comparison of three labeled silica nanoparticles used as tracers in transport experiments in porous media. Part II: Transport experiments and modeling. *Environ Pollut*. 2014;184:613-619. doi:10.1016/j.envpol.2013.08.016

89. Zeng C, Shadman F, Sierra-Alvarez R. Transport and abatement of fluorescent silica nanoparticle (SiO2 NP) in granular filtration: effect of porous media and ionic strength. *J Nanoparticle Res*. 2017;19(3):105. doi:10.1007/s11051-017-3808-8

90. Resch-Genger U, Hoffmann K, Nietfeld W, et al. How to improve quality assurance in fluorometry: Fluorescence-inherent sources of error and suited fluorescence standards. *J Fluoresc*. 2005;15(3):337-362. doi:10.1007/s10895-005-2630-3

91. Larson DR, Ow H, Vishwasrao HD, Heikal AA, Wiesner U, Webb WW. Silica Nanoparticle Architecture Determines Radiative Properties of Encapsulated Fluorophores. *Chem Mater*. 2008;20(8):2677-2684. doi:10.1021/cm7026866

92. E. F. Hubbard, F. A. Kitpatrick LAM, and J. F. Wilson J. MEASUREMENT OF TIME OF TRAVEL AND DISPERSION IN STREAMS BY DYE TRACING. In: *Techniques of Water-Resources Investigations of the United States Geological Survey*. ; 1986.

93. Silva, L.; Donnici, C.; Ayala J. Tracers: the use of chemical agents for hydrological, environmental, petrochemical and biological studies. *Quim Nova*. 2009;32(6):1576-1585.

94. Yu Goryacheva I, Eremin SA, Shutaleva EA, Suchanek M, Niessner R, Knopp D. Development of a Fluorescence Polarization Immunoassay for Polycyclic Aromatic Hydrocarbons. *Anal Lett*. 2007;40(7):1445-1460. doi:10.1080/00032710701297034

95. Klauth P, Bauer R, Ralfs C, et al. Fluorescence macrophotography as a tool to visualise and quantify spatial distribution of deposited colloid tracers in porous media. *Colloids Surfaces A Physicochem Eng Asp*. 2007;306(1-3):118-125. doi:10.1016/j.colsurfa.2007.03.058

96. Ciavola P, Taborda R, Ferreira Ó, Dias JA. Field observations of sand-mixing depths on steep beaches. *Mar Geol*. 1997;141(1-4):147-156. doi:10.1016/S0025-3227(97)00054-6

97. Hermanson GT. Fluorescent Probes. In: *Bioconjugate Techniques*. Elsevier; 2013:395-463. doi:10.1016/B978-0-12-382239-0.00010-8

98. Vazquez NI, Gonzalez Z, Ferrari B, Castro Y. Synthesis of mesoporous silica nanoparticles by sol–gel as nanocontainer for future drug delivery applications. *Boletín la Soc Española Cerámica y Vidr*. 2017;56(3):139-145. doi:10.1016/j.bsecv.2017.03.002

99. Penelas MJ, Soler-Illia GJAA, Levi V, Bordoni A V., Wolosiuk A. Click-based thiol-ene photografting of COOH groups to SiO2 nanoparticles: Strategies comparison. *Colloids Surfaces A Physicochem Eng Asp*. 2019;562:61-70. doi:10.1016/j.colsurfa.2018.11.023

100. Miletto I, Gilardino A, Zamburlin P, et al. Highly bright and photostable cyanine dye-

doped silica nanoparticles for optical imaging: Photophysical characterization and cell tests. *Dye Pigment*. 2010;84(1):121-127. doi:10.1016/j.dyepig.2009.07.004

101. Shahabi S, Treccani L, Rezwan K. A comparative study of three different synthesis routes for hydrophilic fluorophore-doped silica nanoparticles. *J Nanoparticle Res*. 2016;18(1):28. doi:10.1007/s11051-016-3334-0
102. Ghimire PP, Jaroniec M. Renaissance of Stöber method for synthesis of colloidal particles: New developments and opportunities. *J Colloid Interface Sci*. 2021;584:838-865. doi:10.1016/j.jcis.2020.10.014
103. Montalti M, Prodi L, Rampazzo E, Zaccheroni N. Dye-doped silica nanoparticles as luminescent organized systems for nanomedicine. *Chem Soc Rev*. 2014;43(12):4243-4268. doi:10.1039/C3CS60433K
104. Vera ML, Cánneva A, Huck-Iriart C, et al. Fluorescent silica nanoparticles with chemically reactive surface: Controlling spatial distribution in one-step synthesis. *J Colloid Interface Sci*. 2017;496:456-464. doi:10.1016/j.jcis.2017.02.040
105. Selvarajan V, Obuobi S, Ee PLR. Silica Nanoparticles—A Versatile Tool for the Treatment of Bacterial Infections. *Front Chem*. 2020;8(July):1-16. doi:10.3389/fchem.2020.00602
106. Pallavi P, Harini K, Alshehri S, et al. From Synthetic Route of Silica Nanoparticles to Theranostic Applications. *Processes*. 2022;10(12):2595. doi:10.3390/pr10122595
107. Li M, Rharbi Y, Huang X, Winnik M. Small Variations in the Composition and Properties of Triton X-100. *J Colloid Interface Sci*. 2000;230:135-139. doi:10.1006/jcis.2000.7050
108. Boonsin R, Chadeyron G, Roblin JP, Boyer D, Mahiou R. Silica encapsulated fluorescein as a hybrid dye for blue-LED based lighting devices. *J Mater Chem C*. 2016;4(27):6562-6569. doi:10.1039/C6TC01039C
109. Gonçalves MC. Sol-gel Silica Nanoparticles in Medicine: A Natural Choice. Design, Synthesis and Products. *Molecules*. 2018;23(8):2021. doi:10.3390/molecules23082021
110. Yokoi T, Wakabayashi J, Otsuka Y, et al. Mechanism of Formation of Uniform-Sized Silica Nanospheres Catalyzed by Basic Amino Acids. *Chem Mater*. 2009;21(15):3719-3729. doi:10.1021/cm900993b
111. Gubala V, Giovannini G, Kunc F, Monopoli MP, Moore CJ. Dye-doped silica nanoparticles: synthesis, surface chemistry and bioapplications. *Cancer Nanotechnol*. 2020;11(1):1. doi:10.1186/s12645-019-0056-x
112. Cabañas MV, Lozano D, Torres-Pardo A, et al. Features of aminopropyl modified mesoporous silica nanoparticles. Implications on the active targeting capability. *Mater Chem Phys*. 2018;220(September):260-269. doi:10.1016/j.matchemphys.2018.09.005
113. Bondarenko L, Illés E, Tombácz E, et al. Fabrication, Microstructure and Colloidal

Stability of Humic Acids Loaded Fe3O4/APTES Nanosorbents for Environmental Applications. *Nanomaterials*. 2021;11(6):1418. doi:10.3390/nano11061418

114. Vrij A, Introduction I. Synthesis and Characterization of Monodisperse Spheres Colloidal. *J Colloid Interface Sci*. 1993;156:1-18.
115. Imhof A, Megens M, Engelberts JJ, de Lang DTN, Sprik R, Vos WL. Spectroscopy of Fluorescein (FITC) Dyed Colloidal Silica Spheres. *J Phys Chem B*. 1999;103(9):1408-1415. doi:10.1021/jp983241q
116. Monjezi K, Mohammadi M, Khaz'ali AR. Stabilizing CO2 foams using APTES surface-modified nanosilica: Foamability, foaminess, foam stability, and transport in oil-wet fractured porous media. *J Mol Liq*. 2020;311:113043. doi:10.1016/j.molliq.2020.113043
117. Ngouangna EN, Manan MA, Oseh JO, Norddin MNAM, Agi A, Gbadamosi AO. Influence of (3–Aminopropyl) triethoxysilane on silica nanoparticle for enhanced oil recovery. *J Mol Liq*. 2020;315:113740. doi:10.1016/j.molliq.2020.113740
118. Arain Z ul abedin, Al-anssari S, Ali M, et al. Reversible and irreversible adsorption of bare and hybrid silica nanoparticles onto carbonate surface at reservoir condition. *Petroleum*. 2020;6(3):277-285. doi:10.1016/j.petlm.2019.09.001
119. Risal AR, Manan MA, Yekeen N, Azli NB, Samin AM, Tan XK. Experimental investigation of enhancement of carbon dioxide foam stability, pore plugging, and oil recovery in the presence of silica nanoparticles. *Pet Sci*. 2019;16(2):344-356. doi:10.1007/s12182-018-0280-8
120. Shafqat SS, Khan AA, Zafar MN, et al. Development of amino-functionalized silica nanoparticles for efficient and rapid removal of COD from pre-treated palm oil effluent. *J Mater Res Technol*. 2019;8(1):385-395. doi:10.1016/j.jmrt.2018.03.002
121. Zhang N, Ding E, Feng X, Xu Y, Cai H. Synthesis, characterizations of dye-doped silica nanoparticles and their application in labeling cells. *Colloids Surfaces B Biointerfaces*. 2012;89(1):133-138. doi:10.1016/j.colsurfb.2011.09.017
122. Santra S, Liesenfeld B, Bertolino C, et al. Fluorescence lifetime measurements to determine the core–shell nanostructure of FITC-doped silica nanoparticles: An optical approach to evaluate nanoparticle photostability. *J Lumin*. 2006;117(1):75-82. doi:10.1016/j.jlumin.2005.04.008
123. Chandra A, Prasad S, Gigli G, del Mercato LL. Fluorescent nanoparticles for sensing. In: *Frontiers of Nanoscience*. Vol 16. 1st ed. Elsevier Ltd.; 2020:117-149. doi:10.1016/B978-0-08-102828-5.00006-1
124. Hennebert P, Avellan A, Yan J, Aguerre-Chariol O. Experimental evidence of colloids and nanoparticles presence from 25 waste leachates. *Waste Manag*. 2013;33(9):1870-1881. doi:10.1016/j.wasman.2013.04.014
125. Solovitch N, Labille J, Rose J, et al. Concurrent aggregation and deposition of TiO2 nanoparticles in a sandy porous media. *Environ Sci Technol*. 2010;44(13):4897-4902. doi:10.1021/es1000819

126. Alnarabiji MS, Husein MM. Application of bare nanoparticle-based nanofluids in enhanced oil recovery. *Fuel*. 2020;267(January):117262. doi:10.1016/j.fuel.2020.117262
127. Nourafkan E, Hu Z, Garum M, Esmaeili H, Wen D. Nanomaterials for subsurface application: study of particles retention in porous media. *Appl Nanosci*. 2021;11(6):1847-1856. doi:10.1007/s13204-021-01843-2
128. Tissandier C, Diop N, Martini M, Roux S, Tillement O, Hamaide T. One-Pot Synthesis of Hybrid Multifunctional Silica Nanoparticles with Tunable Coating by Click Chemistry in Reverse W/O Microemulsion. *Langmuir*. 2012;28(1):209-218. doi:10.1021/la203580q
129. de Oliveira L, Bouchmella K, Picco A, et al. Tailored Silica Nanoparticles Surface to Increase Drug Load and Enhance Bactericidal Response. *J Braz Chem Soc*. 2017;28(9):1715-1724. doi:10.21577/0103-5053.20170017
130. Sun Y, Kunc F, Balhara V, et al. Quantification of amine functional groups on silica nanoparticles: a multi-method approach. *Nanoscale Adv*. 2019;1(4):1598-1607. doi:10.1039/C9NA00016J
131. Thommes M, Kaneko K, Neimark A V., et al. Physisorption of gases, with special reference to the evaluation of surface area and pore size distribution (IUPAC Technical Report). *Pure Appl Chem*. 2015;87(9-10):1051-1069. doi:10.1515/pac-2014-1117
132. Shin WK, Cho J, Kannan AG, Lee YS, Kim DW. Cross-linked Composite Gel Polymer Electrolyte using Mesoporous Methacrylate-Functionalized SiO2 Nanoparticles for Lithium-Ion Polymer Batteries. *Sci Rep*. 2016;6(1):26332. doi:10.1038/srep26332
133. Modena MM, Rühle B, Burg TP, Wuttke S. Nanoparticle Characterization: What to Measure? *Adv Mater*. 2019;31(32):1-26. doi:10.1002/adma.201901556
134. Bhattacharjee S. DLS and zeta potential - What they are and what they are not? *J Control Release*. 2016;235:337-351. doi:10.1016/j.jconrel.2016.06.017
135. Matusiak J, Grządka E. Stability of colloidal systems - a review of the stability measurements methods. *Ann Univ Mariae Curie-Sklodowska, Sect AA – Chem*. 2017;72(1):33. doi:10.17951/aa.2017.72.1.33
136. Hales T. A proof of the Kepler conjecture. *Ann Math*. 2005;162(3):1065-1185. doi:10.4007/annals.2005.162.1065
137. Bueno V, Bosi A, Tosco T, Ghoshal S. Mobility of solid and porous hollow SiO2 nanoparticles in saturated porous media: Impacts of surface and particle structure. *J Colloid Interface Sci*. 2022;606:480-490. doi:10.1016/j.jcis.2021.07.142
138. Liu Q, Sun Z, Santamarina JC. Transport and Adsorption of Silica Nanoparticles in Carbonate Reservoirs: A Sand Column Study. *Energy & Fuels*. 2019;33(5):4009-4016. doi:10.1021/acs.energyfuels.9b00057
139. Inczédy J, Lengyel T, Ure AM, International Union of Pure and Applied Chemistry.

Compendium of analytical nomenclature : definitive rules 1997. Published online 1998.

140. Yang Q, Pan X. A facile approach for fabricating fluorescent cellulose. *J Appl Polym Sci*. 2010;116(5):n/a-n/a. doi:10.1002/app.32287
141. Scheurer C, Hincapie RE, Neubauer E, Metz A, Ness D. Sorption of Nanomaterials to Sandstone Rock. *Nanomaterials*. 2022;12(2):200. doi:10.3390/nano12020200
142. Yang HH, Qu HY, Lin P, Li SH, Ding MT, Xu JG. Nanometer fluorescent hybrid silica particle as ultrasensitive and photostable biological labels. *Analyst*. 2003;128(5):462-466. doi:10.1039/b210192k
143. Kotsuchibashi Y, Zhang Y, Ahmed M, Ebara M, Aoyagi T, Narain R. Fabrication of FITC-doped silica nanoparticles and study of their cellular uptake in the presence of lectins. *J Biomed Mater Res Part A*. 2013;101A(7):2090-2096. doi:10.1002/jbm.a.34498
144. Kazemzadeh Y, Shojaei S, Riazi M, Sharifi M. Review on application of nanoparticles for EOR purposes: A critical review of the opportunities and challenges. *Chinese J Chem Eng*. 2019;27(2):237-246. doi:10.1016/j.cjche.2018.05.022
145. Rosenholm J, Näreoja T. *Handbook of Materials for Nanomedicine*. (Torchilin V, ed.). Jenny Stanford Publishing; 2020. doi:10.1201/9781003045076
146. Al-Khafaji MA, Gaál A, Wacha A, Bóta A, Varga Z. Particle size distribution of bimodal silica nanoparticles: A comparison of different measurement techniques. *Materials (Basel)*. 2020;13(14). doi:10.3390/ma13143101
147. Schrader AM, Monroe JI, Sheil R, et al. Surface chemical heterogeneity modulates silica surface hydration. *Proc Natl Acad Sci U S A*. 2018;115(12):2890-2895. doi:10.1073/pnas.1722263115
148. Pfeiffer-Laplaud M, Costa D, Tielens F, Gaigeot MP, Sulpizi M. Bimodal Acidity at the Amorphous Silica/Water Interface. *J Phys Chem C*. 2015;119(49):27354-27362. doi:10.1021/acs.jpcc.5b02854
149. Tsyalkovsky V, Burtovyy R, Klep V, et al. Fluorescent Nanoparticles Stabilized by Poly(ethylene glycol) Containing Shell for pH-Triggered Tunable Aggregation in Aqueous Environment. *Langmuir*. 2010;26(13):10684-10692. doi:10.1021/la101021t
150. Calvo A, Joselevich M, Soler-Illia GJAA, Williams FJ. Chemical reactivity of amino-functionalized mesoporous silica thin films obtained by co-condensation and post-grafting routes. *Microporous Mesoporous Mater*. 2009;121(1-3):67-72. doi:10.1016/j.micromeso.2009.01.005
151. Shi JQ, Xue Z, Durucan S. Supercritical CO2 core flooding and imbibition in Berea sandstone — CT imaging and numerical simulation. *Energy Procedia*. 2011;4:5001-5008. doi:10.1016/j.egypro.2011.02.471
152. Marchioro A, Bischoff M, Lütgebaucks C, Biriukov D, Předota M, Roke S. Surface

Characterization of Colloidal Silica Nanoparticles by Second Harmonic Scattering: Quantifying the Surface Potential and Interfacial Water Order. *J Phys Chem C*. 2019;123(33):20393-20404. doi:10.1021/acs.jpcc.9b05482

153. Daberkow T, Meder F, Treccani L, Schowalter M, Rosenauer A, Rezwan K. Fluorescence labeling of colloidal core-shell particles with defined isoelectric points for in vitro studies. *Acta Biomater*. 2012;8(2):720-727. doi:10.1016/j.actbio.2011.11.007
154. Koike N, Ikuno T, Okubo T, Shimojima A. Synthesis of monodisperse organosilica nanoparticles with hollow interiors and porous shells using silica nanospheres as templates. *Chem Commun*. 2013;49(44):4998. doi:10.1039/c3cc41904e
155. Xu J, Sun L, Li J, Liang J, Zhang H, Yang W. Fitc and Ru(phen) 3spi_sup2+spii_sup co-doped silica particles as visualized ratiometric pH indicator. *Nanoscale Res Lett*. 2011;6(li):1-7. doi:10.1186/1556-276X-6-561
156. Li P, Ishiguro M. Adsorption of anionic surfactant (sodium dodecyl sulfate) on silica. *Soil Sci Plant Nutr*. 2016;62(3):223-229. doi:10.1080/00380768.2016.1191969
157. Sharma R. Small-Molecule Surfactant Adsorption, Polymer Surfactant Adsorption, and Surface Solubilization: An Overview. In: ; 1996:1-20. doi:10.1021/bk-1995-0615.ch001
158. Zhang P, Šimůnek J, Bowman RS. Nonideal transport of solute and colloidal tracers through reactive zeolite/iron pellets. *Water Resour Res*. 2004;40(4):1-11. doi:10.1029/2003WR002445

Appendix A: Additional information

Table A1: Normalized emission intensity over time for FSiNP-NH_2-F *(S)* and negative Stöber-FSiNP in DW.

FSiNP-NH_2-F *(S)* / DW										
Wavelength (nm)	0 min	10 min	20 min	30 min	40 min	50 min	60 min	70 min	80 min	90 min
516	1.00	0.77	0.73	0.71	0.70	0.69	0.68	0.66	0.66	0.66
FSiNP *(S)* / DW										
Wavelength (nm)	0 min	10 min	20 min	30 min	40 min	50 min	60 min	70 min	80 min	90 min
513	1.00	1.00	1.00	1.00	1.00	0.99	0.99	0.99	0.99	1.00

Table A2: Normalized emission intensity over time for WORM-FSiNPs in DW.

FSiNP-NH_2 *(W)* / DW										
Wavelength (nm)	0 min	10 min	20 min	30 min	40 min	50 min	60 min	70 min	80 min	90 min
515	1.00	0.97	0.94	0.91	0.89	0.87	0.86	0.86	0.83	0.81
FSiNP *(W)* / DW										
Wavelength (nm)	0 min	10 min	20 min	30 min	40 min	50 min	60 min	70 min	80 min	90 min
520	1.00	0.59	0.53	0.51	0.50	0.48	0.48	0.47	0.48	0.45

Table A3: Normalized emission intensity over time for FSiNP-NH2 (W) and FSiNP (W) in SDS solution.

FSiNP-NH_2 *(W)* / SDS										
Wavelength (nm)	0 min	10 min	20 min	30 min	40 min	50 min	60 min	70 min	80 min	90 min
520	1.00	1.00	0.99	0.98	0.99	0.99	0.98	0.98	0.98	0.97
FSiNP *(W)* / SDS										
Wavelength (nm)	0 min	10 min	20 min	30 min	40 min	50 min	60 min	70 min	80 min	90 min
515	1.00	0.81	0.77	0.75	0.73	0.73	0.72	0.72	0.71	0.71

Appendix B: Academic production

- **Published articles related to doctoral thesis:**

A. Pazini, L. Maqueira, J.M.F. Façanha, A. Pérez-Gramatges, Colloids Surfaces A Physicochem. Eng. Asp. 670 **(2023)** 131586. https://doi.org/10.1016/j.colsurfa.2023.131586

- **Published articles not related to doctoral thesis:**

R. da Costa, R. de Queiroz Garcia, R.M. da R. Fiuza, L. Maqueira, A. Pazini, L. de Boni, J. Limberger, J. Lumin. 239 **(2021)** 118367.

A. Pazini, L. Maqueira, F. da Silveira S, A.R. Jardim Barreto, R. Carvalho, F. Valente, D. Back, R. Aucélio, M. Cremona, F.S. Rodembusch, J. Limberger, Dye & Pigment. 178 **(2020)** 108377.

G. Matiello, A. Pazini, K. da Silva, R. da Costa, G. Ebeling, J. Dupont, J. Limberger, J.D. Scholten, Tetrahedron Lett. 60 **(2019)** 780–784.

- **Awards:**

2022: Has been awarded a RSC joint journal poster prize at the AutoOrg-7th Meeting on Self-Assembly Structures in Solution and at Interfaces Bento Gonçalves-Brazil, 2nd to 4th November, Royal Society of Chemistry.

2022: Received 1st place in the category of "Best Poster Presentation" with the work "Synthesis of Fluorescent Silica Nanoparticles for Quantification in EOR Applications." Department of Chemistry, PUC-Rio